EXPERIMENTAL AND NUMERICAL ANALYSES OF DYNAMIC DEFORMATION AND FAILURE IN MARINE STRUCTURES SUBJECTED TO UNDERWATER IMPULSIVE LOADS

A Thesis

Presented to

The Academic Faculty

By

Siddharth Avachat

In Partial Fulfillment

Of the Requirements for the Degree

Master of Science in the

School of Materials Science and Engineering

Georgia Institute of Technology

August 2012

EXPERIMENTAL AND NUMERICAL ANALYSES OF DYNAMIC DEFORMATION AND FAILURE IN MARINE STRUCTURES SUBJECTED TO UNDERWATER IMPULSIVE LOADS

Approved by:

Dr. Min Zhou, Advisor
School of Mechanical Engineering
Georgia Institute of Technology

Dr. Naresh Thadhani
School of Materials Science and Engineering
Georgia Institute of Technology

Dr. George Kardomateas
School of Aerospace Engineering
Georgia Institute of Technology

Date Approved: May 01, 2012

PREFACE

The research work reported in this thesis was performed at the Georgia Institute of Technology. Research funding was provided by the Office of Naval Research through grant numbers N00014-09-1-0808 and N00014-09-1-0618 (program manager: Dr. Yapa D. S. Rajapakse). Calculations were carried out on the High-Performance Computing cluster of the Dynamic Properties Research Laboratory at Georgia Institute of Technology.

The purpose of this thesis is to present in a comprehensive manner, the research carried out to assess and improve the blast resistance of composite structures. The research topics discussed here involve experimental and computational techniques, and optimization and scaling. This thesis is divided into 8 chapters and includes a literature review, details about manufacturing techniques and material constitutive models and analysis of the dynamic response of composite structures subjected to underwater impulsive loads in different environmental conditions.

The work is original and has not been submitted for any other degree.

Siddharth Avachat

Atlanta, GA

May 01, 2012

ACKNOWLEDGEMENTS

I would like to take this opportunity to thank all the people who have made my stay at Georgia Tech a unique and enriching experience. First and foremost, I would like to thank my adviser Dr. Min Zhou for his invaluable guidance and advice. I thank the members of my thesis committee Dr. Naresh Thadhani and Dr. George Kardomateas for their comments and suggestions. I would also like to thank Dr. Ashish K. Lele of the National Chemical Laboratory, Pune for an opportunity to work in the CFPE lab. I would like to thank Dr. Mukund Y. Gokhale, Dr. Giridhar M. Joshi and Anil M. Datar for their advice and support regarding research as well as academic issues. I gratefully acknowledge the support and guidance of Dr. Yapa D. S. Rajapakse of the Office of Naval Research (ONR).

I am thankful to my fellow graduate students for their helpfulness and memorable discussions over endless cups of coffee. I would like to thank my lab members Ananda Barua, Nathan Bailey, Yifan Gao, Barett Hardin, Seokpum Kim, Christopher Lammi and Yan Li for their support. I would also like to thank Peter Marshall, Michael Kirka, William Musinki, Patxi Fernandez-Zelaia, Shreevant Tiwari, George Mathai, Matthias Seher, Anirban Patra, Jeffery Lloyd and Brett Ellis for their friendship and interactions.

Last but not the least, I am indebted to my family for the support, guidance and encouragement I have received and will continue to receive.

DEDICATION

Dedicated to my parents Suchitra and Sudhir Avachat.

TABLE OF CONTENTS

LIST OF TABLES

Page

LIST OF FIGURES

Page

SUMMARY

Marine structures are designed to operate in hostile environments consisting of corrosive sea-water, hot and cold temperature extremes, transient dynamic loads like hull-slamming and complex three-dimensional hydrostatic loads. Additionally, naval structures are required to withstand weapons impacts and blast loads resulting from surface and underwater explosions. Recent assessments of marine structures have demonstrated that sandwich structures and composite materials can provide high strength-to-weight ratios and good blast mitigation.

This thesis is focused on the dynamic response of composite materials and structures to underwater impulsive loading. This research work seeks to establish structure-material-property relationships for marine structures based on different materials, loading intensities and novel structural design concepts to enhance the blast-resistance of naval structures. Of particular interest are experimental and computational evaluations of the physical processes involved in the dynamic response of fiber-reinforced composite materials and composite sandwich. This research work encompasses blast/shock loading; rupture and penetration; Fluid Structure Interaction (FSI) effects; dynamic constitutive relations and strain-rate effects; damage-modeling; and concepts for damage mitigation.

A novel experimental technique is developed allowing the generation of high-intensity underwater impulsive loads in a controlled environment based on a projectile impact mechanism. This experimental setup, called the Underwater Shock Loading

Simulator (USLS), can generate peak pressures up to 300 MPa and evaluate different boundary-conditions and loading configurations. In-situ high-speed digital imaging enables the tracking of deformation mechanisms including core-face debonding, facesheet-wrinkling, core-indentation, core-cracking and fragmentation.

Fully detailed finite-element simulations are carried out, explicitly accounting for the different deformation mechanisms in constituent materials. Energy-based damage criteria are used to model fracture and fragmentation in PVC foam cores and glass-fiber facesheets. A Lagrangian simulation scheme is implemented for water; this scheme captures the effects of Fluid-Structure Interaction (FSI) at the water-structure interface. Finite-element simulations are shown to be in good agreement with experimental results. The finite-element simulations are then extended to 3-dimensional, fully dynamic numerical calculations to account for the effects of water-backed/submerged loading conditions; and the effect of facesheet stiffness on the dynamic response of composite structures.

Composite structures with different core-materials and identical total mass are subjected to underwater impulsive loads of varying intensities. It is demonstrated that polymer foam cores exhibit significant strain-rate effects and undergo considerable dynamic cracking and fragmentation when they are subjected to complex, multi-axial dynamic transient loads. Low-density core materials consistently out-perform high-density core materials; undergoing lesser deflections and transmitting smaller impulses. The damage mechanisms in low-density cores are primarily in the form of face-wrinkling under compressive loads, core-crushing and cracking due to bending-stresses. Damage

mechanisms in high-density cores are primarily in the form of face-rupture, core-cracking and fragmentation and core-crushing, in that order. Finite-element simulations are in good agreement with experimental results. A phenomenological damage criterion allows the explicit tracking of core-cracking and fragmentation. The reaction forces measured at the supports show that low-density cores transmit the lowest impulses.

To analyze the effect of a submerged environment, simulations are carried out with water on both impulse-side and back-side of the structure. Results show that the blast-resistance of sandwich-structures in water-backed conditions is influenced by the core-density and the stiffness in the front-face and back-face has very little effect on blast-resistance.

The effects of face-stiffness on the dynamic response of sandwich composites are evaluated in a set of simulations in which the core-density and thickness are kept constant, while the front and back-face stiffness are varied. Results show that there exists an optimum facesheet stiffness to minimize deflection and maximize energy dissipation in the core.

Results are presented in the form of non-dimensional design-maps to establish material-structure-property relationships and enable scaling and materials-selection for marine structures with enhanced blast-mitigation.

Finally, the objectives of this work are restated, the results and conclusions of each section are evaluated and the novel contributions and recommendations for future work are stated.

1. INTRODUCTION

1.1 Background and objectives

Marine structures are subjected to dynamic loading from underwater explosions, projectile impact and hull slamming resulting from high-speed motion. The dynamic response of materials under such conditions is complicated by many factors, including fluid-structure interactions, superposition of dynamic and static pressures, a range of load triaxiality and varying impulsive loading conditions. Consequently, analysis of the dynamic response of marine structures to underwater loads presents significant challenges. There is a need for research in a number of areas pertaining to experimental diagnostics, structural mechanics, materials science, material-structure-property relations, computational modeling and scaling.

The objectives of the research work presented here are:

i. develop an experimental technique to accurately characterize the dynamic response of composite and metallic structures to underwater blasts;
ii. develop high-speed digital diagnostics for in-situ characterization of deformation mechanisms in heterogeneous materials;
iii. develop a numerical framework for modeling the dynamic deformation and failure of composite laminates that accounts for damage in the form of matrix-

cracking and rupture in composite materials, and cracking and fragmentation in polymeric foam cores;

iv. characterize time and space-resolved evolution response and failure of composite structures under impulsive underwater loading;

v. develop scaling methodologies and structure-performance relations to reveal underlying trends in material response and aid in material and structural design; and

vi. evaluate the blast-resistance of fiber-reinforced composite/PVC foam sandwich structures to develop material-structure-property relations and enhance blast-mitigation of naval structures.

The focus of this thesis will be on the underwater blast response of composite structures. While the advantages of sandwich composites are well established, the dynamic behavior of composite structures remains to be fully explored, owing to the complex and competing dynamic deformations in heterogeneous marine structures. The following section gives an outline of the thesis.

1.2 Thesis outline

Chapter 1 states the objectives of proposed research work and the outline of the thesis.

Chapter 2 provides a detailed literature review of previous research work in underwater blasts. This review is divided into four distinct sections: (1) underwater explosions; (2) dynamic response of thin plates; (3) dynamic response of metallic

sandwich structures and (4) dynamic response of composite sandwich structures. Literature on both experimental and computational research is reported.

Chapter 3 outlines the materials used in experiments and manufacturing methods for composite sandwich structures. The Vacuum Assisted Resin Transfer Molding (VARTM) process is explained. All constitutive and damage models implemented in this thesis are provided here. This includes the Hashin model for composites, Mie-Grüneisen equation-of-state for water, and Deshpande-Fleck model for compressible foams.

Chapter 4 covers the design and development of an experimental setup to generate underwater impulsive loads sans explosives. The different diagnostics envisioned and developed for the Underwater Shock Loading Simulator (USLS) are explained including laser-interferometry, high-speed photography, and pressure and force transducers. An elastic solution is derived for the USLS to show that theoretical and experimental observations are in agreement. Finite element studies are carried out to study the effects of projectile velocities, flyer plate thicknesses and material properties.

Chapter 5 deals with composite sandwich structures, manufactured from E-glass/epoxy facesheets and Divinycell foam (HP200, HP100, HP60) cores. These composite sandwich structures are then impulsively loaded in the USLS. A set of 16 experiments is carried out and the pressure and displacement are measured at the end of 1000 μs. Finite element simulations are carried out accounting for different material properties and loading intensities. The main purpose of this set of experiments is to understand the failure mechanisms in composite sandwich structures, to capture the

different damage-modes in-situ using high-speed imaging and laser interferometry and develop material-structure-property relationships. Experiments and finite-element calculations are compared and a monolithic composite-plate is used as a benchmark.

Chapter 6 deals with finite element simulations involving water-backed or submerged structures - sandwich structures with water on both sides. The dynamic responses of composites to underwater impulsive loads are then compared.

Chapter 7 covers a set of simulations to examine the effect of the ratio between facesheet thickness and core thickness on the dynamic response of composite sandwich structures. To this end, the core thickness and core density are kept constant and the thickness of the facesheets is varied. The dynamic behavior of composite structures is quantified using fiber and matrix damage, facesheet deflections and energy-dissipation. The results are analyzed in both normalized and non-normalized forms to gain insight into underlying trends that can be explored in the design of materials and structures.

Chapter 8 provides a summary of research work and the conclusions in each section and a discussion on future work.

2. LITERATURE REVIEW

2.1 Review of underwater explosions

R.H. Cole, in his book Underwater Explosions [1], gives a detailed account of the shock waves generated during an explosions and the effect of these waves on structures. Explosive materials are inherently unstable compounds which undergo chemical reactions to form stable products. Explosive reactions are triggered by imparting sufficient energy to the compound. Heated fuses or frictional heat from impact by a firing pin are most commonly used to initiate these reactions. Once initiated, the explosive material is rapidly converted into a gas at very high temperatures and pressures. This process is called "detonation" and it creates a shock front which advances at the speed of several thousand meters per second. This shock front is termed "detonation wave" and chemical transformation resulting from detonation occurs simultaneously with the progression of this wave. When this wave reaches the boundary of the explosive material and surrounding medium, there is an impedance mismatch and the wave is transmitted through the boundary at a lower pressure and particle velocity. In the case of underwater explosions, the surrounding medium is water which can be regarded as a homogeneous fluid incapable of sustaining shear stresses. A shock wave travelling through water has two distinct physical characteristics - shock-wave velocity and local particle velocity. At the pressures considered here, the speed of sound wave in water is independent of peak

pressure and is ~1440 m/s. The speed of sound waves in water changes at extreme pressures and temperatures; that phenomenon is not discussed here.

Trinitrotoluene (TNT) is often used to generate, characterize and study underwater explosions. TNT has a specific energy of 4500 kJ/kg and the specific energy released by other explosive compounds is often expressed in the form of equivalent mass of TNT for the purpose of calibration. Upon detonation, TNT forms nitrogen, water, carbon- monoxide and solid carbon and generates a large amount of pressure - on the order of 14000 MPa [2]. This pressure compresses the surrounding medium and radiates a high-pressure disturbance which falls off rapidly and is called "explosive decay." The velocities commonly observed for TNT are several times the limiting value of ~1440 m/s in water. The maximum pressure in this wave falls off rapidly with distance and approaches steady state behavior at large distances. The temporal profile of the wave broadens gradually as the wave radiates outward. This behavior of the blast wave is illustrated in Figure 2.1 showing blast attenuation as a function of distance from source.

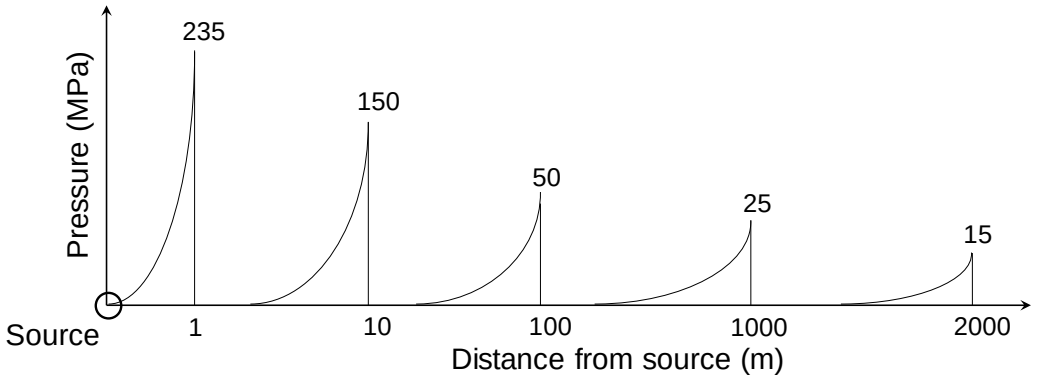

Figure 2.1 Spatial evolution of blast pulse for a TNT explosion. Figure not to scale. [1]

As the gas expands, it forms a bubble by displacing the water surrounding it. After reaching a maximum radius, the bubble contracts. The cyclical expansion and contraction of this gas-bubble is called "bubble oscillation." Bubble oscillations generate secondary pressure waves with ~10% initial blast overpressure and the peak pressure reduces with increasing number of oscillations. The gas-bubble simultaneously travels to the surface and once it reaches the surface, creates the characteristic plumes observed after an underwater explosion (shown in Figure 2.2). Of the total energy generated during a detonation event, ~40% is available for damage creation in marine structures while the rest is expended on bubble oscillations.

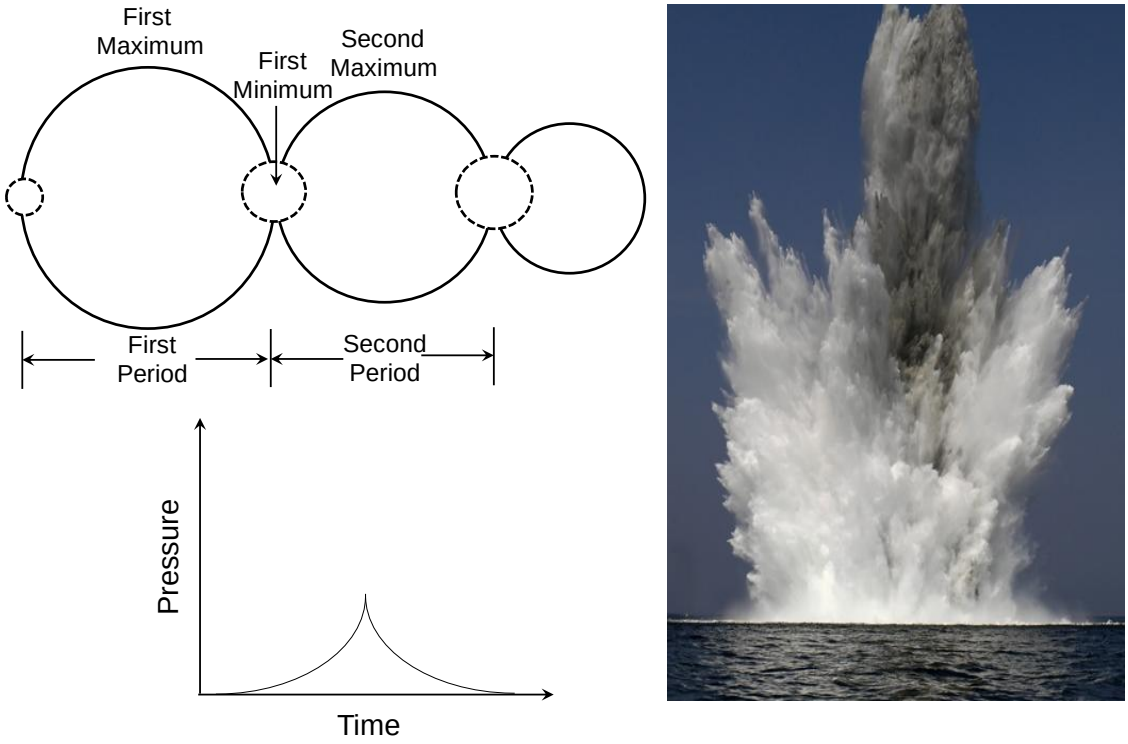

Figure 2.2 Bubble oscillations and pressure profile generated due to oscillations [1] and a "plume" created when an underwater explosion bubble reaches the water surface.

Figure 2.2 shows the oscillations experienced by a gas-bubble as it expands and contracts and a schematic of the pressure generated due to oscillations. Unlike the exponentially decaying pressure profile after detonation, pressure generated by bubble oscillations causes a gradual rise in pressure followed by a decrease in pressure on the order of milliseconds. The peak pressure generated by each successive oscillation is 20% less than the previous one.

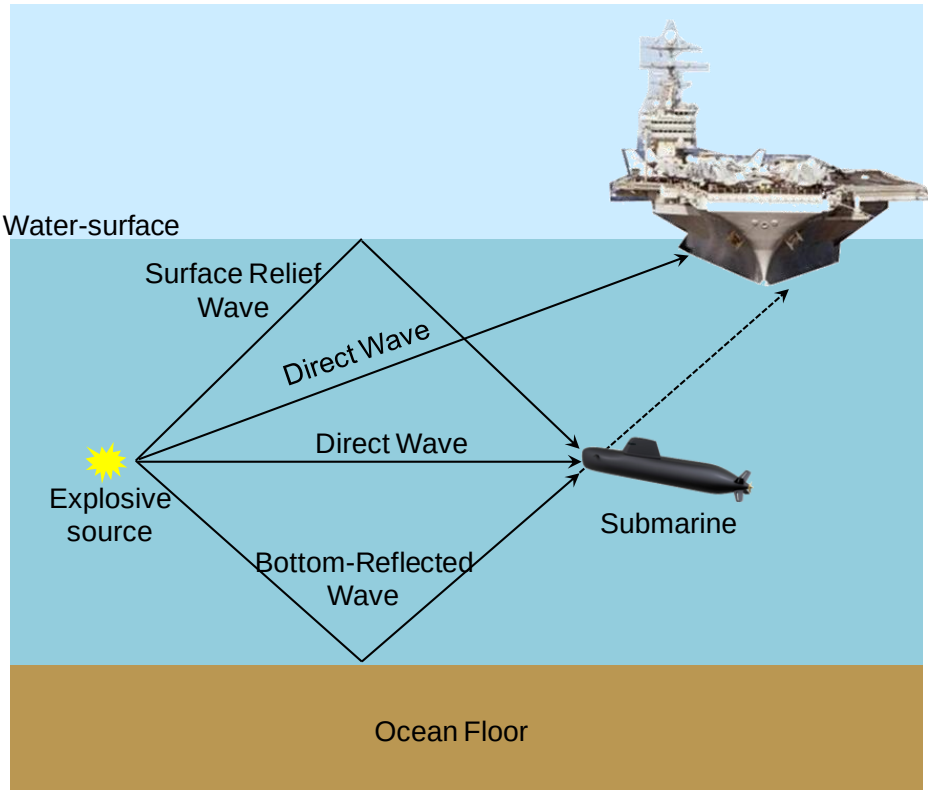

Figure 2.3 Types of waves generated by an underwater explosion [3].

Since the initial shock wave creates a high-magnitude impulse, subsequent pressure pulses due to bubble oscillations can be neglected - except in one special case. If the gas-bubble rises underneath the ship hull, it can create complex loads on the structure.

The rising gas bubble creates large pressures and pushes the ship hull outwards. When the bubble collapses, it pulls the hull inwards towards the center of the bubble. Consequently, this complex loading condition can create significant damage - sometimes exceeding the damage caused by the initial shock wave. If the frequency of the bubble oscillations matches the natural frequency of the ship structures, it can lead to large bending moments and cause whipping damage.

Close to the shore, detonation can create three types of waves - (1) direct wave from the explosion, which travels at the highest speed and reaches the ship earlier than the rest of the waves; (2) a surface wave, created when the pressure pulse reaches the water-surface and (3) bottom-reflected wave, created when the initial pressure pulse reaches the ocean-floor and is reflected back. The types of waves that are caused by an underwater explosion are illustrated in Figure 2.3. In the research work presented in this thesis, the primary focus is on direct waves - waves that emanate from the explosion source and impinge a marine structure. The other types of waves are not considered here.

Proximity to an underwater explosion plays an important role in the dynamic behavior of a marine structure. If an underwater explosion occurs close to the ship hull, the resulting pressure wave will rupture the hull and cause significant damage to surrounding equipment. On the other hand, if the explosion occurs far from the ship, the blast wave will have a planar front and the pressure loading will be non-uniform. In this case, each section of the marine structure will respond differently to an incident pressure

pulse. The defining characteristics of a pressure pulse are the peak-pressure and pressure-time history. The peak pressure resulting from an underwater blast is given by

$$p_0 = K_1 \left(\frac{M^{1/3}}{R} \right)^{\alpha_1}, \tag{1}$$

where K_1 and α_1 are material constants (with values $K_1 = 5 \times 10^7$ and $\alpha_1 = 1.15$ for TNT), M is the mass of TNT used and R is the distance from explosive source [1, 2]. The blast decay constant θ for a pressure pulse created due to an underwater explosion is given by

$$\theta = M^{1/3} K_2 \left(\frac{M^{1/3}}{R} \right)^{\alpha_2}, \tag{2}$$

where K_2 and α_2 are material constants (with values $K_1 = 92 \times 10^6$ and $\alpha_2 = -0.22$ for TNT) source [2]. The decay constant defines the decay time for the peak-pressure. Data for TNT is reproduced in Figure 2.4. For an underwater explosion resulting from detonation of TNT, peak pressures of tens of megapascals and decay constants of hundreds of microseconds are observed.

After detonation, the shock wave generated by the explosive travels in the form of a large pressure pulse followed by exponentially decaying pressure history. The pressure wave can be described by the equation

$$p(t) = p_0 \exp\left(-\frac{t}{\theta} \right), \tag{3}$$

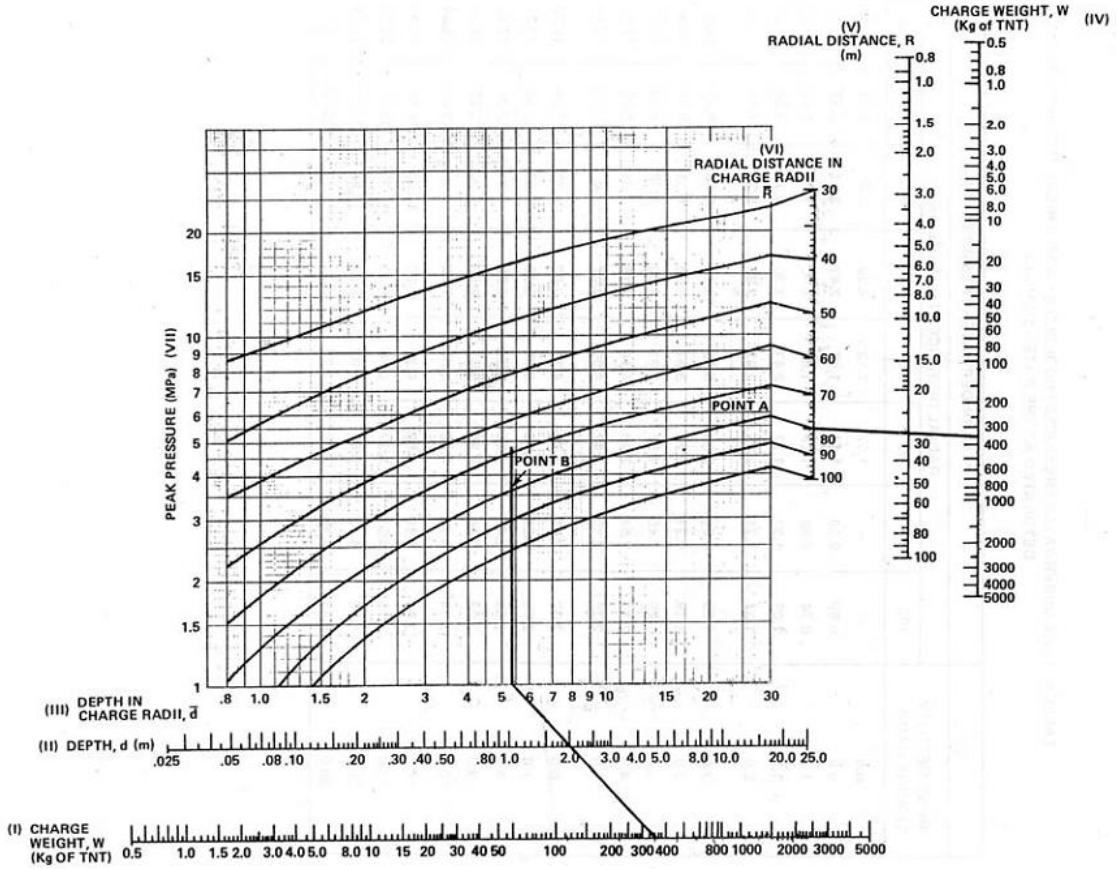

Figure 2.4 Peak pressure as a function of charge depth and charge weight. Experimental data for TNT reproduced from Swisdak [2].

where p_0 is the peak pressure, t is time at which measurement is carried out and θ is the decay constant. Figure 2.5 shows a schematic of pressure vs. time for pressure pulse created due to a typical underwater explosion. Impulse is given by

$$I = \int_0^t p(t)\,dt\,. \tag{4}$$

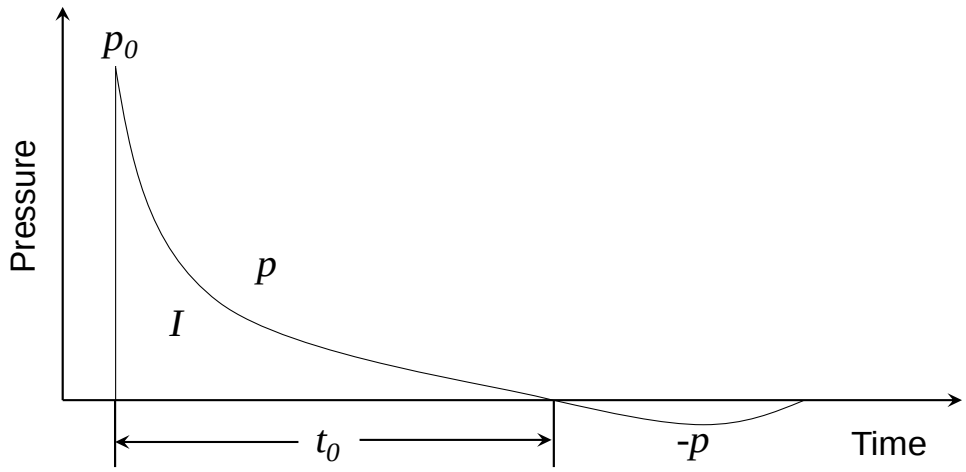

Figure 2.5 Schematic of a pressure vs. time history for a typical underwater explosion. It shows a peak pressure, followed by exponentially decaying pressure history and cavitation (negative pressure).

2.2 Fluid-Structure Interaction (FSI)

G.I. Taylor proposed the earliest solution to a fluid-structure interaction problem based on a planar wave impinging upon a free-standing, rigid plate [3, 4]. This plate has a mass per unit area m and is supported along the plate-face by a spring of stiffness k. The density of water is ρ_w and the speed of sound in water is c_w. For a plate of modeled as a half-space, the total pressure experienced by the plate, p_t, is

$$p_t = p_0 \cdot 2\exp\left(-\frac{t}{\theta}\right). \tag{5}$$

and the total impulse is

$$I_t = \int_0^t p(t)\,dt = 2p_0\theta. \tag{6}$$

Now consider a plate of finite mass. At the water-structure interface, the incident and reflected pressure waves are superimposed and the total pressure is twice that of wave pressure. The combination of incident pressure and equation-of-motion for the plate gives the total pressure acting on the plate

$$p_t = p_0\left(\exp\left(-\frac{t}{\theta}\right)+\phi(t)\right), \tag{7}$$

where the function $\phi(t)$ is dependent on other parameters such that

$$\phi(t) = f\left[t,\theta,k,m,\rho_w,c_w\right]. \tag{8}$$

The impulse per unit area is given by

$$I = \frac{mp_0}{\rho_w c_w}\left(\exp\left(-\frac{t}{\theta}\right)-\phi\right). \tag{9}$$

To scale the effects of underwater explosions due to changes in the quantity of explosive, distance from source and time, Taylor [3, 4] introduced a non-dimensional quantity, ψ, such that

$$\psi = \frac{\rho_w c_w \theta}{m}. \tag{10}$$

This is the ratio of the product of mechanical impedance of water and decay coefficient to the mass of the plate under impulsive loading. As shown in Figure 2.5 , the pressure reaches zero at the water-plate interface after time t_0 such that

$$t_0 = \theta \frac{\ln \psi}{\psi - 1}. \tag{11}$$

From (9), (10) and (11), the impulse becomes

$$I_t = I_0 \left(\psi^{\frac{\psi}{1-\psi}} \right). \tag{12}$$

I_t is directly proportional to mass per unit area m. Hence, as the mass of the structure increases, the impulse and momentum imparted to the structure also increase.

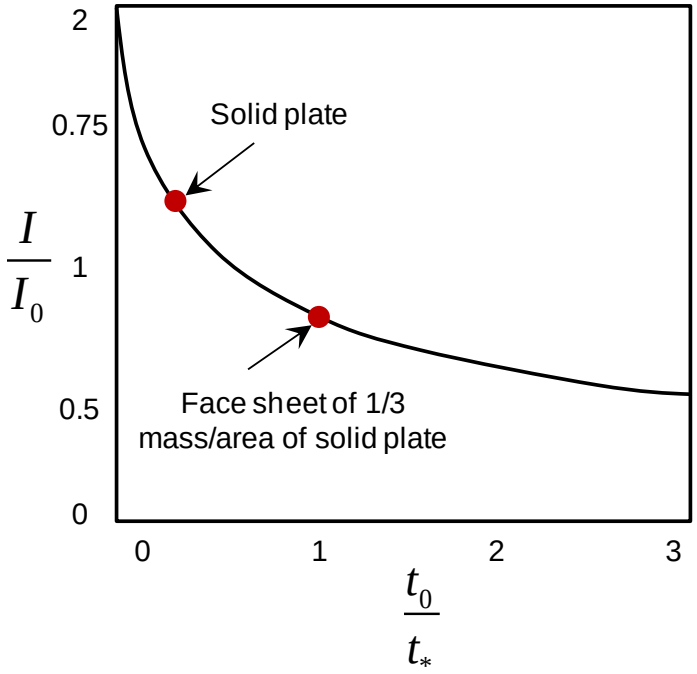

Figure 2.6 Fluid-structure interaction in water: sandwich plate vs. monolithic plate [3, 5].

Figure 2.6 shows the fluid-structure interaction for a solid plate and sandwich plate subjected to underwater blasts. The impulse magnitude is plotted as a function of

plate mass. A sandwich structure face-sheet acquires significantly lesser momentum than a monolithic plate three times the mass of the face-sheet. Clearly, lighter structures are beneficial and enable the exploitation of the FSI effect. For experiments and simulations carried out in this research, the areal mass of all structures is constant unless stated otherwise.

Since the mechanical impedance of water is much higher than air, underwater blasts travel large distances before attenuating sufficiently to be harmless. When underwater blast waves interact with marine structures, they can cause significant plastic dissipation and fracture. For large unsupported ship sections, damage is in the form of bending and tensile necking. For supported ship sections, damage is in the form of shear rupture and tearing. Figure 2.7 shows the damage in US navy ship the USS Tripoli due to an underwater mine. The oblique view shows the hull sheared off at supports. The front view shows significant petalling with characteristic tearing damage.

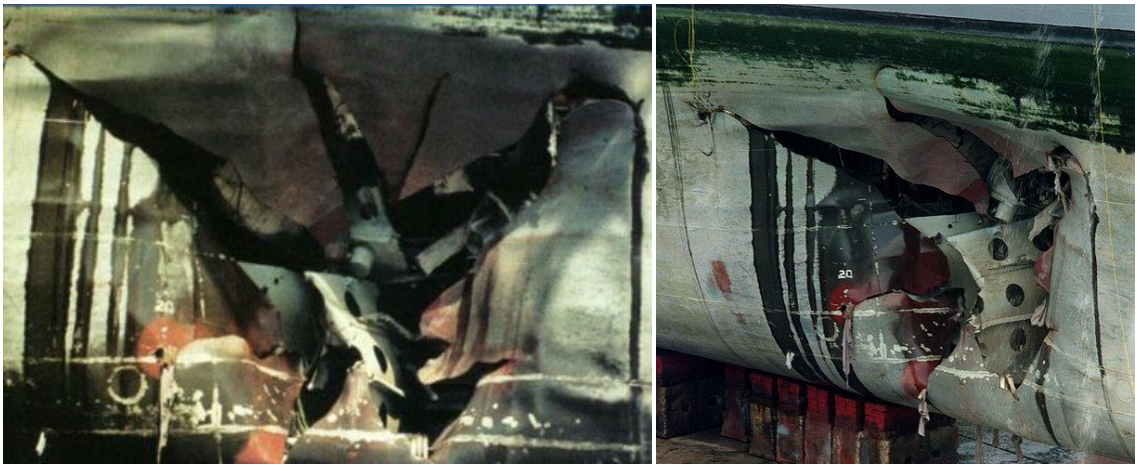

Figure 2.7 Hull damage in USS Tripoli. Photographs from US Navy archives [6].

Figure 2.8 shows the damage in USS Cole due to a combination of impact and blast wave loading.

Figure 2.8 Hull damage in USS Cole. Photographs from US Navy archives [7].

Figure 2.9 Cracked hull of USS Princeton. Photographs from US Navy archives [8].

Figure 2.9 shows the cracked hull of the USS Princeton. An underwater blast resulted in shock wave loading from beneath the ship. The gas-bubble formed due to this explosion rose underneath the ship and resulted in bending of the hull.

2.3 Review of the dynamic response of monolithic plates

Metallic structures, steels in particular, have been the lynchpin of naval ship-building for many years. Early research in the dynamic response of metallic structures was motivated by the need to improve the blast resistance of naval vessels and design better weapons during World War II. Initial work focused on dynamic plasticity in clamped circular thin-plates. Early experimental investigations were carried out by Taylor [9] who measured the center-displacement and deformed volume of an impulsively loaded thin diaphragm. Travis and Johnson [10] studied explosive forming of metallic plates while Johnson, Poynton et al. [11] developed diagnostics to measure the displacement and velocity of plates using pin-contacts. Williams [12] reported the first instance of high-speed dynamic imaging of blast-loaded plates. Finnie [13] carried out a parametric study by varying the charge mass and stand-off distance and its effect on thin plates. Bednarski [14] filmed high-speed deformation in membranes at ~6000 frames per second. Symonds and Jones [15] studied the bending behavior of thin plates while Bodner and Symonds [16] reported dynamic plasticity in clamped plates and extended this research to viscoelastic structures [17].

Taylor [9], Richardson and Kirkwood [18] and Hudson [19] carried out theoretical studies of the dynamic response of thin plates. They proposed solutions based

on bending and plastic deformation. Frederick [20] and Griffith and Vanzant [21] theorized dynamic load carrying capacities for thin plates that were significantly greater than corresponding static load carrying capacities. These studies showed that shear-strain increased with the rate-of-loading. For high-rate loads, circumferential strains were negligible. Hopkins and Prager [22] proposed an exact solution based on a thin plate subjected to transverse loads for a non-hardening plastic material and Tresca flow rule. Wang and Hopkins [23] and Florence [24] proposed a similar solution for a circular clamped plate - showing that circumferentially supported plates simplified the problem significantly. Hopkins [25] proposed a more general theory for plates subjected to non-uniform transverse loads while Shapiro [26] studied a thin plate supported at the center and loaded at the circumference.

Other studies carried out during this period focused on variations in material models, materials and loading configurations. Detailed reviews of experimental and theoretical work are provided by Jones [27] and Nurick [28, 29]. These studies revealed significant fundamental differences between the static and dynamic deformation mechanisms in clamped plates. Quasi-static loading causes stationary hinges to form in the metal plates followed by collapse. Dynamic loading leads to a hinge circle formed near the loading area. The velocity of the plates reduces linearly between the clamped edge and the center.

2.4 Review of the dynamic response of metallic sandwich structures

Sandwich structures first found application in the aerospace industry due to high strength-to-weight ratios, exceptional bending-resistance, durability and low life-cycle costs. In recent years, sandwich structures with strong facesheets and lightweight cores have become central structural components of blast resistant naval vessels. By virtue of the combination of a thick core and thin facesheets, sandwich structures achieve higher shear-stiffness-to-weight ratios and bending-stiffness-to-weight ratios than equivalent homogeneous plates made exclusively of the core material or the facesheet material. Additionally, sandwich cores can be designed to fulfill specific functionalities. Sandwich structures consist of two face sheets of high-stiffness material and a core of significantly lower stiffness and density. The spatial separation provided by the sandwich core enables these structures to sustain high shear and bending loads. The primary factors that influence the structural response of a sandwich structure are (1) facesheet thickness, (2) core thickness and (3) core density.

Zenkert [30] provided a review of the mechanics of sandwich structures, expanding on the previous work of Plantema [31] and Allen [32]. A major advantage of sandwich structures is the ability to use a variety of materials and core geometries - called topologies. In metallic structures, thin steel sheets are commonly used for faces while cores consist of honeycombs and metal foams. In composite sandwich structures, faces are often composed of stiff carbon-fiber or glass-fiber sheets and the cores are manufactured from polymeric foams. Underwater blast response of both metallic and composite sandwich structures is reported in this thesis.

The response of sandwich plates subject to underwater impulsive loading has attracted significant research interest. Experiments and computations focusing on different core topologies, specimen sizes, loading configurations and optimization have been carried out. Fleck and co-workers [33-43] have carried out analytical studies and numerical simulations of sandwich structures subjected to blast loads. Simultaneously, numerical simulations and optimization studies have been carried out by Hutchinson and co-workers [5, 44-50]. Constitutive models have been developed to smear the core into a continuum representation in order to simplify computations [51, 52]. These studies show that fluid-structure interaction needs to be considered to accurately characterize impulsive loads.

Sandwich structures subjected to exponentially decaying pressure histories outperform those subjected to instantaneous loads. Sandwich structures handily out-perform monolithic plates when deformation is dominated by bending. In the stretching regime, monolithic plates, due to their susceptibility to necking, show higher plastic dissipation than sandwich plates. Results show that core design greatly influences dynamic response of sandwich structures. Stiff cores perform poorly while light cores exhibit higher blast mitigation. A combination of buckling and stretching in the core provides the highest blast mitigation. For computational studies, continuum cores cannot accurately capture the various damage modes associated with prismatic sandwich structures. Rupture and core buckling can only be evaluated using detailed finite element simulations with explicitly modeled cores. Figure 2.10 shows experimental results for

sandwich plates subjected to air-shocks. Sandwich panels outperform monolithic panels at all loading intensities.

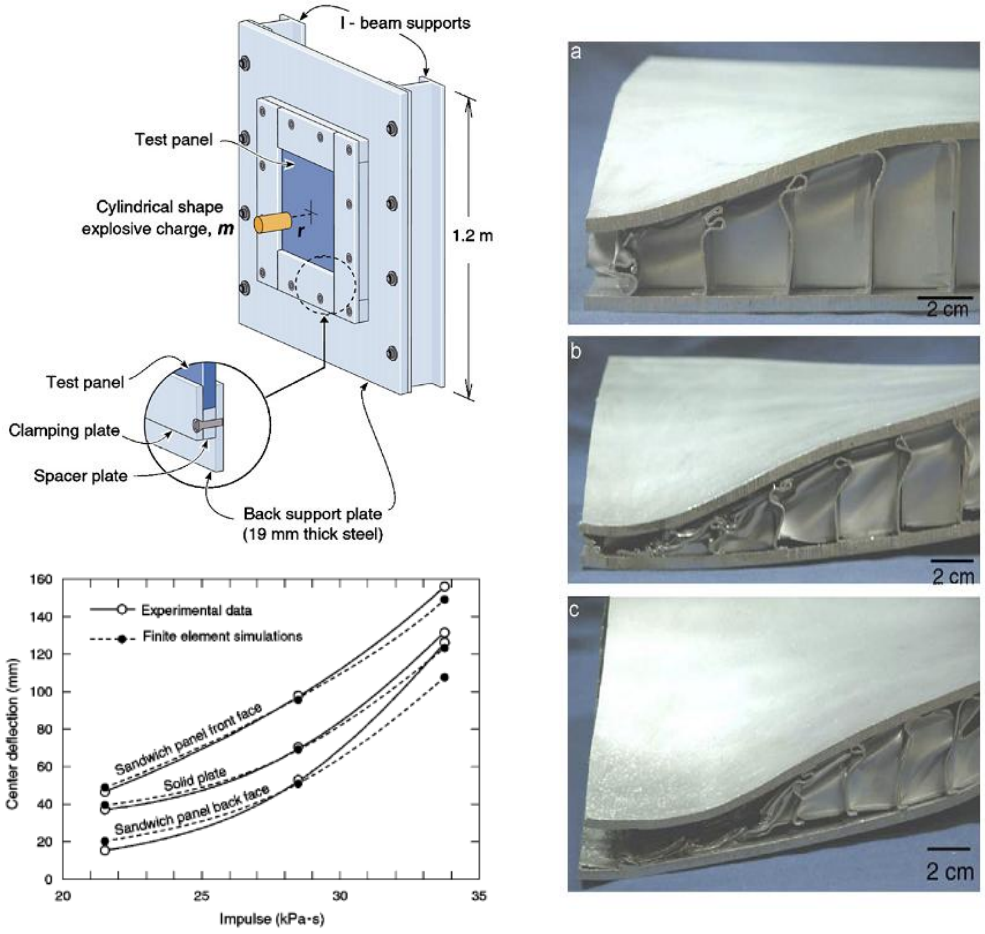

Figure 2.10 Dynamic response of sandwich plates with square honeycombs subjected to air-shocks [53]. Deflections are plotted as functions of impulse. Sandwich panels outperform monolithic panels at all loading intensities.

Advances in manufacturing techniques have led to studies focusing on complex core topologies. Studies on prismatic honeycombs [54] and I-beams [55] demonstrate that by aligning the cell-walls in the direction perpendicular to the faces, honeycomb structures can achieve high out-of-plane stiffness and by aligning them parallel to the

faces, honeycomb structures can achieve high in-plane stiffness. Recently, studies involving truss cores [56-62] and Kagome cores [63-65] have been carried out. Owing to their inclined members, these cores exhibit a much flatter stress-strain curve than honeycombs and present less resistance to buckling. While this leads to smaller out-of-plane stiffness in comparison to honeycombs, it also reduces the likelihood of front-face perforation. Another advantage of truss cores is that these structures are suitable for fluid-flow through the core.

2.5 Review of the dynamic response of composite structures

While previous research in blast mitigation has focused on metallic sandwich structures, there is a need for further research in a number of areas, especially with regard to composite sandwich structures. In particular, the use of novel materials and configurations for enhanced blast mitigation capabilities, the response of facesheets under very high pressures and the response of structures under submerged conditions are some important issues yet to be explored and fully quantified. Composite sandwich structures consist of thin, stiff fiber-reinforced composite facesheets and polymeric foam cores.

Facesheets manufactured from fiber-reinforced composites play an important role in determining the shear and bending resistances and energy dissipation. Mouritz [66, 67] reported that the primary mechanisms for energy absorption and failure in fiber-reinforced composite facesheets are cracking, delamination, fiber breakage and fragmentation. Investigators examined the effect of strain-rate on strength, failure and moduli and there is a significant increase in compressive strength at high-strain rates.

High-strain rate effects also cause high temperatures which can be traced to damage creation and evolution [66, 67]. Research on the dynamic behavior of sandwich composites has focused on low-velocity, contact-based loads such as drop weight and projectile impact [68-72]. Common failure modes that have been identified include indentation and cracking, shear band formation, buckling and delamination, core-facesheet debonding and perforation.

The core plays a very important role in determining the dynamic response of sandwich composites because it accounts for the largest fraction of the overall energy dissipated. The research work presented here involved PVC foams manufactured by DIAB Inc [73], which are primarily used in large wind-turbine blades which require high shear-and-bending resistances. Split-Hopkinson Pressure Bar apparatuses have been employed to measure the stress-strain behavior of PVC foams at high strain-rates [74-78]. Experiments reveal that PVC foams have mild strain-rate sensitivity in the strain-rate range of $\dot{\varepsilon} = 10^{-2}$ to $10^{3}\,\mathrm{s}^{-1}$ and negligible strain-rate sensitivity rate in the strain-rate range of $\dot{\varepsilon} = 10^{-4}$ to $10^{-2}\,\mathrm{s}^{-1}$. The primary mechanism for energy absorption in foam cores is local wall collapse and volumetric, stress-saturated compression.

There have been a few investigations pertaining to the dynamic response of sandwich composites subjected to impulsive loads. Shukla and co-workers [79-83] examined the dynamic response of woven E-glass composite facesheets and stitched core sandwich structures to air-based shock loading and concluded that stitched cores exhibit superior mechanical performance. They observed an increase in blast resistance when

sandwich structure cores were multi-layered with increasing relative core densities. Failure was primarily in the form core-facesheet debonding, core-shear cracking, buckling and matrix-rupture. Different deformation mechanisms and failure modes are shown in Figure 2.11. Inclined cracks propagate from the impulsively loaded region and frontface rupture is observed. Core-crushing and bending occur simultaneously.

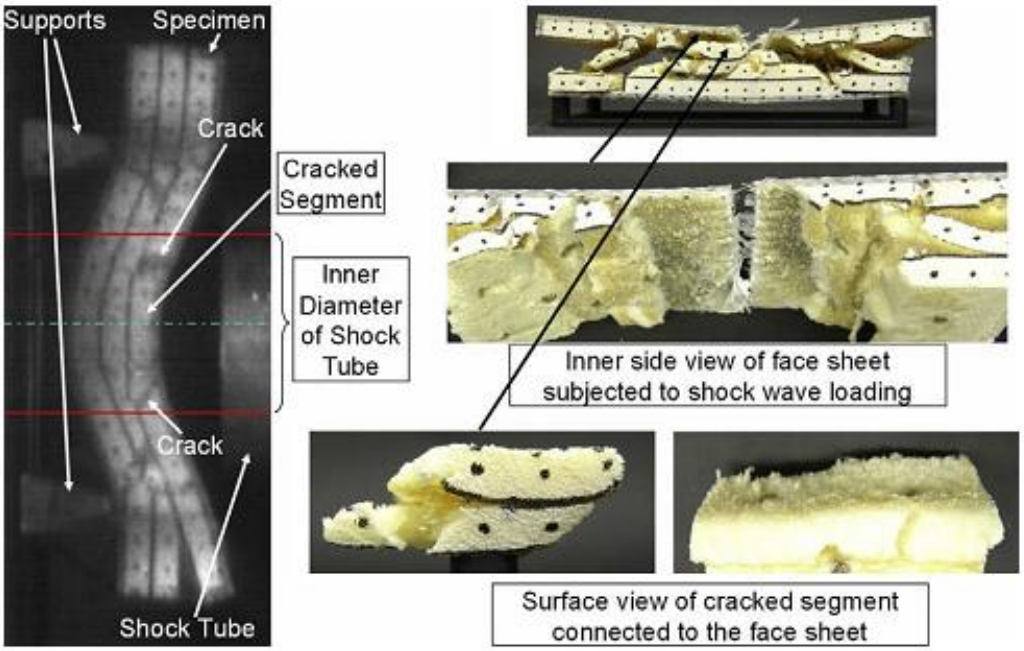

Figure 2.11 Failure modes in stepwise graded sandwich cores subjected to high intensity shock loading in air [83]. Interfacial failure is followed by rupture in backface.

Leblanc and Shukla studied the dynamic response of clamped monolithic composite plates to underwater blast loads [84] and reported that the composite layup played a significant role in dynamic behavior. Failure consisted of delamination and cracking, predominantly near the clamped boundaries. Latourte et al. [85] also reported identical damage mechanisms in sandwich structures subjected to underwater impulsive

loads. Additionally, they characterized the delamination in composite laminates using cohesive finite element modeling.

2.6 Review of experimental techniques and diagnostics

Early experiments involving impulsive loading of structures consisted of impacting sandwich structures with metal foam projectiles [35, 60, 86-89]. This strategy allowed for "patch loading" i.e. loading over an area smaller than the total clamped area. Although foam-projectile impact experiments can generate shock loads, they cannot accurately capture the effect of fluid-structure interaction, cavitation and blast loading. Consequently, in recent years there have been significant efforts to develop experimental facilities capable of generating controlled impulsive loads. Espinosa and co-workers used gas-gun based impact loading to generate underwater pressure impulses in a conical chamber [58, 90-92]. High-speed photography of Moiré-interferograms was used to measure out-of-plane displacements of sandwich structures. Wadley and co-workers [42, 53, 54, 93] developed an experimental facility called the "Dynocrusher" in which explosive sheets were used to generate planar pressure impulses in a water-tank. Diagnostics were primarily force-measurements and post-mortem characterizations. Researchers from US Navy have developed an underwater blast loading facility consisting of a clamped plate and TNT based impulsive load generation [84]. The diagnostics consisted of dynamic force transducers to evaluate the impulses transmitted by the marine structures.

2.7 Concluding remarks

Since G. I. Taylor's pioneering work on underwater explosions and the dynamic behavior of free-standing thin-plates, there have been a number of studies to quantify the effects of an underwater blasts on marine structures. Due to high shear-and-bending resistances and low masses, sandwich structures are increasingly being used in applications that require cost-effective, durable and blast-resistant structures. The dynamic response of sandwich structures to underwater impulsive loads presents a rich source of engineering problems - experimental, analytical and computational.

Recent investigations in this area have shown that sandwich-structures consistently outperform monolithic structures of identical mass. The dynamic strength of the sandwich core is an important factor in determining the response of sandwich structures. Sandwich structures with high-stiffness cores are prone to core cracking and frontface rupture, while those with low-density cores enable core-wall buckling prior to frontface shear rupture. The behavior of sandwich structures subjected to impulsive loads is governed by a number of structural and material properties.

While metallic sandwich structures have been studied exhaustively, there is a significant dearth of knowledge pertaining to composite sandwich structures. This work is aimed at providing insights into the dynamic behavior of sandwich composites subjected to underwater impulsive loads. This thesis focuses on the dynamic deformation, damage and failure in sandwich composites comprising of fiber-reinforced composite facesheets and polymeric foam cores. Experiments and finite-element simulations are

used to evaluate the blast resistance of these structures. The manufacturing techniques and constitutive models for the materials considered in experiments and simulations are discussed in the next section.

3. MATERIALS

3.1 Introduction

Chapter 1 provided a review of underwater blasts, metallic and composite marine structures and experimental techniques. This chapter provides descriptions of all the materials used in experiments and simulations. This includes manufacturing techniques for sandwich structures as well as the different constitutive and damage models that are implemented in finite element analysis.

In this research, a Vacuum Assisted Resin Transfer Molding (VARTM) technique is used to manufacture the composite laminates used in monolithic composites and sandwich faces. PVC foams of three different densities $\left(60, 100 \text{ and } 200 \text{ kg}/\text{m}^3\right)$ are obtained from Swedish manufacturer DIAB Inc [73]. The PVC foams and composite laminates are joined using an epoxy adhesive.

In finite-element simulations, the fiber-reinforced composites are described with a linear elastic constitutive model and stress based failure criteria. The PVC foams are described using a constitutive model specifically developed for cellular solids and a strain based failure criteria. Aluminum and steel, used for projectiles and water-chamber respectively, are specified using linear-elastic constitutive models. A Lagrangian implementation of the Mie-Gruneisen equation of state is used to model the shock response of water.

3.2 Composite materials

3.2.1 Introduction

Due to their high-strength to weight ratio and low corrosion, composites have found extensive use in aerospace and marine applications involving sandwich structures. Over the last decade, there have been a number of new developments in the use of fiber-reinforced composites for naval vessels leading to improvements in manufacturing, stealth technology, range, payload-carrying-capacity and durability.

Fiber-matrix composites are composed of two distinct phases: (1) reinforcements like glass-fibers or carbon-fibers and (2) matrix materials like epoxy, polyester, etc. These materials can be molded into complex shapes using relatively simple manufacturing techniques. The strength and stiffness of the finished composite is determined by the volume fraction of glass fibers and directionality of fibers with respect to external loads. E-glass fibers are the most widely used reinforcement for composite materials due to their low cost and high-strength. Matrix materials are usually thermosetting resins like polyesters and epoxies.

The matrix is primarily used as a medium to hold fibers and can be varied depending on the final application of the material. The method of fabrication depends on the curing temperature, curing time and volatilization of the resin. For high corrosion resistance and a smooth water-proof finish, epoxy is recommended. However, epoxy resins are five times as costly as polyester resins and can prove prohibitively expensive for large structures. Consequently, polyester and vinyl-ester resins are very popular in the

ship-building industry. While polyester resins offer good fire-resistance and cohesion, resulting composite structures may contain a high void-fraction caused by water-vapor emission during curing. Sufficient venting and vacuum can prevent air-voids from developing. The composite materials used in this research - E-glass/polyester - make up a large portion of marine composites manufacturing.

E-glass fibers have an ultimate tensile strength of ~2000 MPa at tensile strain of ~2.5% and have negligible temperature dependence in the range of service temperatures experienced by marine structures. The matrix alone has an ultimate tensile strength of ~100 MPa at a tensile strain of ~2%. The strength of the composite material depends on loading direction and fiber orientation. A quasi-isotropic laminate loaded in the axial direction corresponding to 0^o has a tensile strength of ~1500 MPa. A Vacuum Assisted Resin Transfer Molding (VARTM) is used to manufacture the composite plates, as described in the next section.

3.2.2 Manufacturing

All composite structures are manufactured in-house at the Georgia Institute of Technology. The manufacturing technique used here is called Vacuum Assisted Resin Transfer Molding (VARTM). Some of the major advantages of VARTM over other manufacturing techniques are the ability to fabricate complex parts with high fiber fraction. Since no hand layup is involved, the process can produce composites at a high rate with minimal losses in resin and fiber. It is relatively safe because the system is always under vacuum and the amount of resin required can be measured accurately.

Figure 3.1 shows a schematic of a VARTM process with different layers - glass fabric, core, vacuum-bag and resin-supply lines.

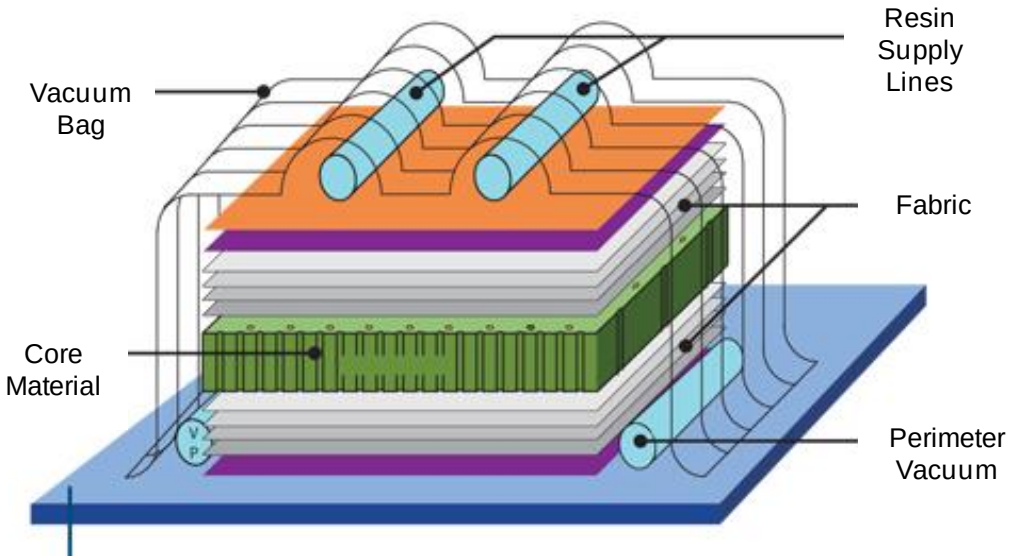

Figure 3.1 Schematic of set-up for Vacuum Assisted Resin Transfer Molding (VARTM) to fabricate flat sandwich panels. Image courtesy Northrop Grumman Shipbuilding [94].

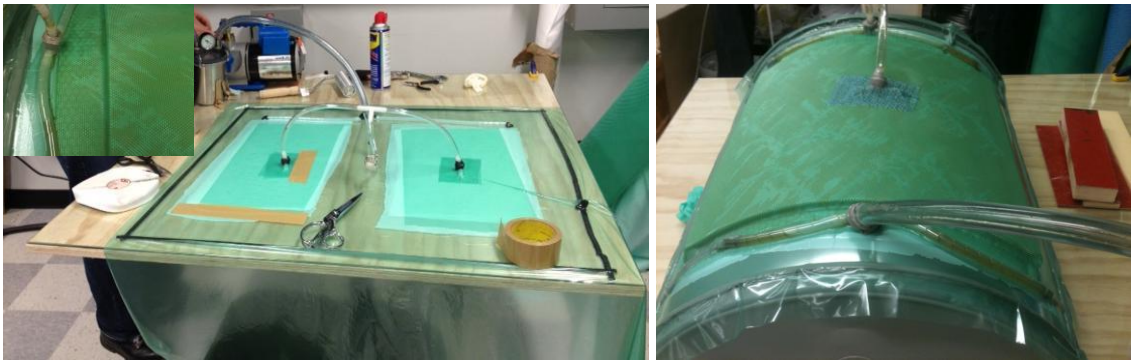

Figure 3.2 Photographs of lab-scale VARTM process for manufacturing planar and curved sandwich structures.

After ensuring that the vacuum-bag is securely taped to the mold, a vacuum-pump is used to evacuate the vacuum-bag. In the absence of leaks, the resin supply lines are submerged in a pot containing a mixture of resin and hardener. The resin is sucked through the supply tube and impregnates the previously dry fibers. The vacuum is removed only after the resin has gelled completely and there is no possibility of flowing. Then the system can be cured in an oven or at room-temperature; high-temperature (~75^{o}C) curing requires 1 hour while room-temperature curing requires 24 hours. "Co-curing" is a technique in which the facesheets and the core are cured together. Another technique is to fabricate the facesheets of required thickness and then join the core and facesheet using an adhesive. The latter method is used in this research. Figure 3.2 shows photographs of the manufacturing facility. Planar as well as curved structures can be manufactured using VARTM.

Unidirectional glass-fiber fabrics were stacked in the pattern shown in Figure 3.3 to create a "quasi-isotropic" layup - (0/45/-45/90)s. Four layers of fabric give a thickness of 0.25 mm. This process is repeated to achieve the desired thickness of 3 mm for sandwich structure facesheets and 6 mm for monolithic structures. Sandwich structures are constructed by joining the facesheets to the PVC foam cores using epoxy adhesive. The total areal mass of the structures is kept constant to facilitate comparison of blast resistance. Due to differences in the density of the core materials, each structure has a different thickness.

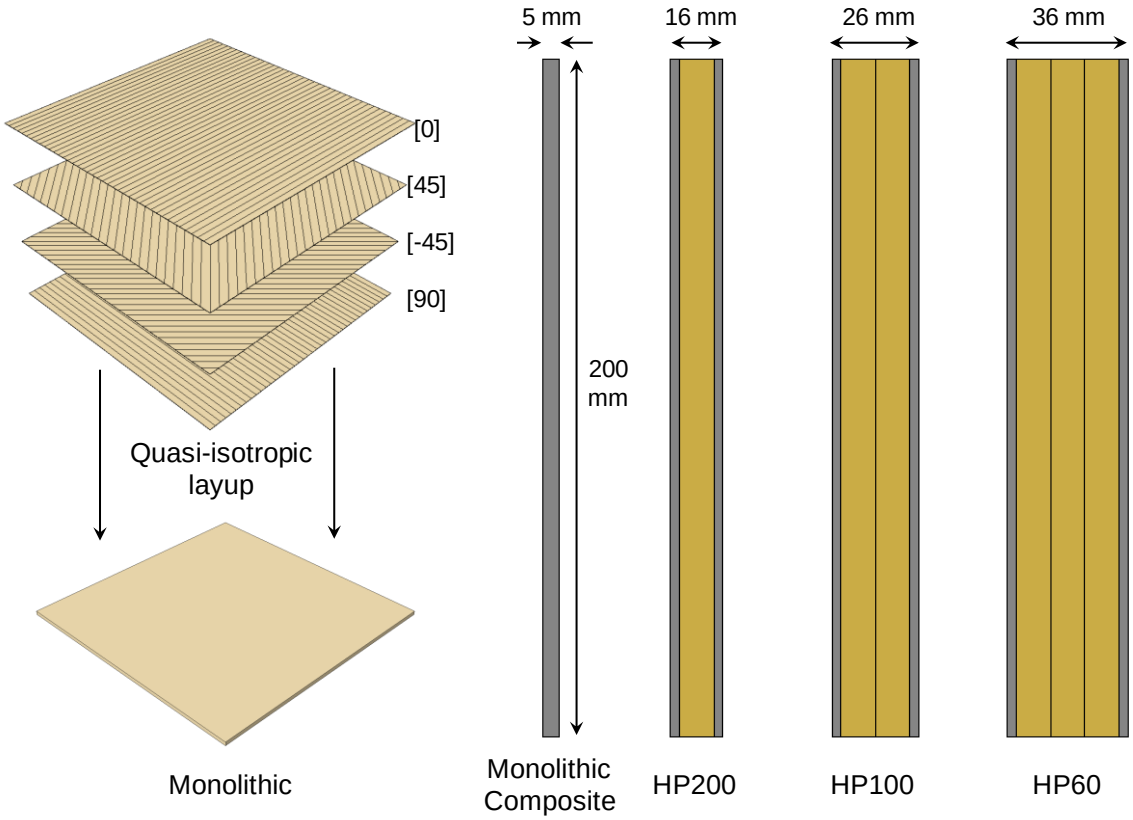

Figure 3.3 Quasi-isotropic layup in a composite sheet and sandwich structures with different core materials. For 2-D plane-strain simulations, the failure modes are largely insensitive to layup. However, 3-D simulations are significantly influenced by the layup in face-laminates.

3.2.3 Constitutive modeling of composite materials

Due to the inherently heterogeneous nature of fiber-reinforced composites, interfacial separation plays a very important role in deformation. Interfacial separation of directionally stacked layers in the composite is called delamination. Delamination requires very little energy in comparison to matrix cracking or fiber failure and hence it is the dominant damage mode in composite materials subjected to impact or impulsive loads. For delamination to initiate, matrix cracking has to occur. It has been shown that

interlaminar cracks travel large distances in relatively short times and can lead to significant deterioration in laminate strength [95]. Similarly, core-facesheet separation is an important damage mode that occurs due to interfacial separation and fracture. If the bond between facesheet and core is weak, interfacial separation occurs. If the bond between the facesheet and the core is strong, tensile fracture in the foam leads to separation.

Some commonly used metrics to evaluate the damage resistance of composites to impact loads are impact energy, displacement, delamination-area and extent of rupture. These metrics all depend on the fundamental damage mechanisms in a fiber-reinforced composite viz. matrix tensile and compressive cracking, and fiber tensile and compressive cracking.

Based on the energy required for initiation, matrix damage occurs first, followed by combined fiber-matrix damage, termed "fiber-pullout" and finally fiber fracture. Damage occurring in the facesheets is accounted for by energy-based damage evolution [96] and [97]. Both these models assume a transversely isotropic solid, such that

$$\frac{E_{11}}{E_{22}} >> 1,$$

$$\frac{T_{11}}{T_{22}} >> 1, \tag{13}$$

$$\frac{C_{11}}{C_{22}} >> 1,$$

where E, T and C are tensile-modulus, tensile-strength and compressive-strength and the subscript "11" denotes longitudinal direction while the subscript "22" denotes transverse direction. The in-plane/longitudinal shear strengths are $S_{12} = S_{31}$ while the out-of-plane/transverse shear strength is S_{23}. A transversely isotropic composite laminate with fibers oriented in the in-plane direction is shown in Figure 3.4.

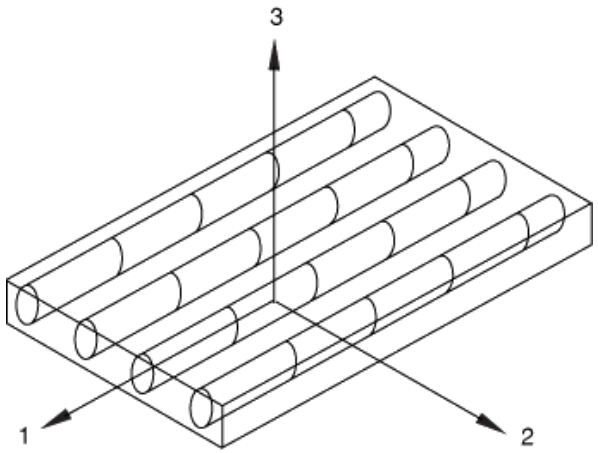

Figure 3.4 A transversely isotropic solid with fibers oriented in longitudinal direction (11).

The elastic response of a transversely isotropic material is given by

$$\begin{pmatrix} \varepsilon_{11} \\ \varepsilon_{22} \\ \gamma_{12} \end{pmatrix} = \begin{pmatrix} \frac{1}{E_{11}} & \frac{\nu_{21}}{E_{11}} & 0 \\ -\frac{\nu_{12}}{E_{22}} & \frac{1}{E_{22}} & 0 \\ 0 & 0 & \frac{1}{S_{12}} \end{pmatrix} \begin{pmatrix} \sigma_{11} \\ \sigma_{22} \\ \tau_{12} \end{pmatrix}, \tag{14}$$

where ε_{11} and ε_{22} are the strains and E_{11} and E_{22} are the moduli in directions 1 and 2 respectively. γ_{12} is the shear strain and S_{12} is the shear modulus, ν_{12} and ν_{21} are Poisson's ratios. The composite material is considered to be linear-elastic prior to damage initiation. The following damage initiation mechanisms are considered for a transversely isotropic laminate:$iddharth85

matrix tension, F_m^T, given by

$$F_m^T = \left(\frac{\sigma_{11}}{T_{11}}\right)^2 + \left(\frac{\tau_{12}}{S_{12}}\right)^2; \tag{15}$$

matrix compression F_m^C,

$$F_m^C = \left(\frac{\sigma_{22}}{2S_{23}}\right)^2 + \left(\frac{\tau_{12}}{S_{12}}\right)^2 + \left[\left(\frac{C_{22}}{2S_{23}}\right)^2 - 1\right]\frac{\sigma_{22}}{C_{22}}; \tag{16}$$

fiber tension F_f^T,

$$F_f^T = \left(\frac{\sigma_{11}}{T_{11}}\right)^2 + \left(\frac{\tau_{12}}{S_{12}}\right)^2; \tag{17}$$

and fiber compression F_f^C,

$$F_f^C = \left(\frac{\sigma_{11}}{C_{11}}\right), \tag{18}$$

where σ_{11}, σ_{22} and τ_{12} are components of effective stress tensor σ and are used to evaluate damage initiation. In finite element simulations, a material-point has an initial, undamaged value of 1 and as the material-point experiences damage, this value decreases. The lowest value is 0, after which the element is removed from the simulation. The parameters used in these calculations can be found in [98] and [99] and are shown in Table 3.1.

Table 3.1 Material parameters for facesheet (E-Glass/Epoxy).

Parameter	**Unit**	**Value**
Density	kg/m^3	2100
Tensile Modulus	MPa	44000
Transverse Modulus (E_y)	MPa	9000
Shear Modulus (G_{xy}, G_{xz}, G_{yz})	MPa	4000
Longitudinal Tensile Strength	MPa	2500
Longitudinal Compressive Strength	MPa	2000
Transverse Tensile Strength	MPa	75
Transverse Compressive Strength	MPa	150
Longitudinal Shear Strength	MPa	75
Transverse Shear Strength	MPa	75

3.3 PVC Foams

3.3.1 Mechanical behavior of PVC foams

The core is made of Divinycell H-100 PVC foam [73] . The mechanical behavior of foams is described by a volumetric hardening model in which the evolution of the yield surface is driven by the volumetric plastic strain. The stress-strain relation for the foam is shown in Figure 3.5 [76]. The response consists of three distinct regimes: (1) initial nearly elastic deformation; (2) plateau region in which deformation occurs at relatively constant stress; and (3) lock-up/densification stage beyond which the material becomes fully compacted.

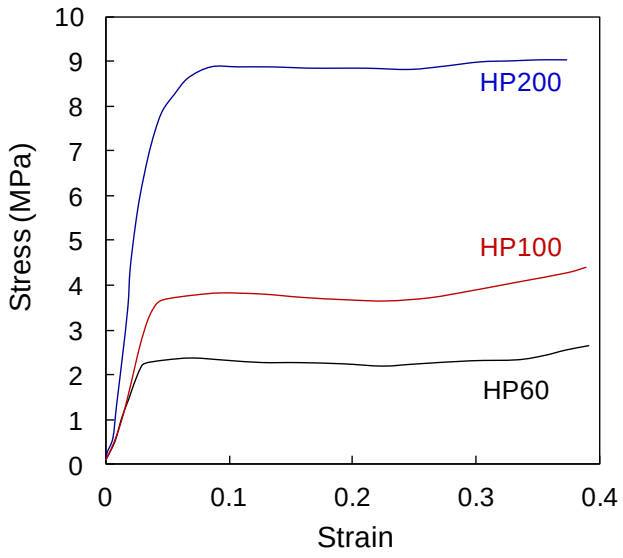

Figure 3.5 Stress-strain curve of HP60, HP100 and HP200 at a strain-rate of ~1000 s^{-1}. Note the brief elastic response followed by stress-saturated strain - the primary characteristic of foams that enable energy absorption. After complete compression, mechanical response resembles that of the parent material.

The constitutive model adopted for Dinvinycell H100 PVC foam is the one developed by Deshpande and Fleck [51, 100] and implemented in the current finite

element code Abaqus [101]. The model accounts for isotropic, dilatational plasticity. High strain-rate studies on PVC foams show a weak dependence on strain-rate [76]. Hence, the foam is assumed to be strain-rate independent in the current set of numerical simulations.

3.3.1 Constitutive modeling of PVC foams

The constitutive model implemented in this research is the one proposed by [51]. The equivalent yield stress $\hat{\sigma}$, based on uniaxial testing, is given by

$$\hat{\sigma}^2 = \frac{1}{1+\left(\frac{\alpha}{3}\right)^2}\left(\sigma_e^2 + \alpha^2\sigma_m^2\right), \tag{19}$$

where $\hat{\sigma}$ is a function of shear stress σ_e and hydrostatic stress σ_m, such that

$$\sigma_e = \sqrt{\frac{3}{2}\tau_{ij}'\tau_{ij}'} \text{ and } \sigma_m = \frac{1}{3}\sigma_{ii}, \tag{20}$$

and α is the parameter that determines the shape of the yield surface and is given by

$$\alpha = \sqrt{\frac{9}{2}\left(\frac{1-2\nu}{1+\nu}\right)}. \tag{21}$$

where $\dot{\varepsilon}_0$ is Poisson's ratio. Figure 3.6 shows experimental data for yield under complex stress states for aluminum foams of varying relative densities. Material parameters for PVC foams are given in Table 3.2.

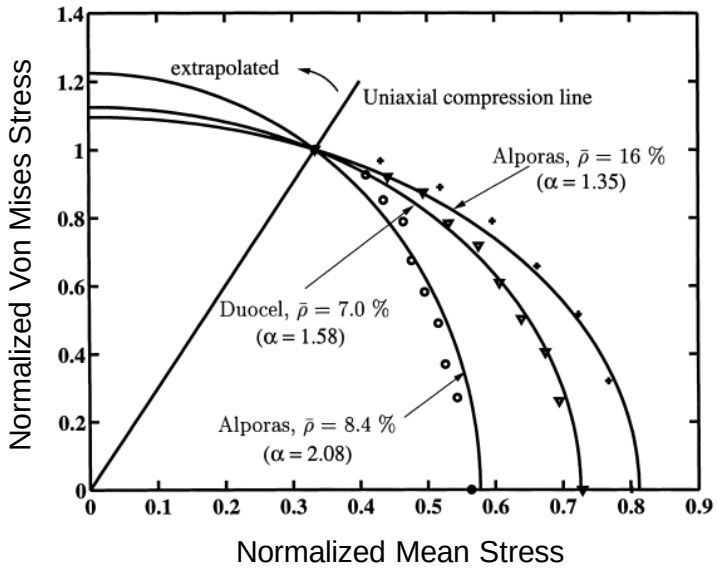

Figure 3.6 Measurements of yield under complex stress states for aluminum foams with different relative densities.

Table 3.2 Material parameters for PVC foams [73]

Parameter	**Unit**	**HP60**	**HP100**	**HP200**
Density	kg/m^3	65	100	200
Tensile Modulus	MPa	20	100	250
Tensile Strength	MPa	1.8	3.5	7.1
Compressive Modulus	MPa	74	135	310
Compressive Strength	MPa	0.95	2.0	5.4
Shear Modulus	MPa	20	35	73
Shear Strength	MPa	0.85	1.6	3.5

While previous constitutive models have not included damage or fracture, experimental results show that shear-fracture and fragmentation are significant and cannot be ignored. This issue is discussed in chapter 4. Here, a phenomenological

damage criterion proposed by Hooputra et al. [102] is implemented for predicting the onset of fracture due to shear-localization and to capture the subsequent fragmentation. The damage criterion assumes that equivalent plastic strain $\bar{\varepsilon}_D^{pl}$ at the onset of damage is dependent on stress-triaxiality and strain-rate.

$$\bar{\varepsilon}_D^{pl}\left(\eta, \dot{\bar{\varepsilon}}^{pl}\right), \tag{22}$$

where $\eta = -p/q$ is the stress triaxiality, p is the pressure stress and q is the Mises equivalent stress and $\dot{\bar{\varepsilon}}^{pl}$ is the equivalent plastic strain-rate. The fracture-properties of the parent material (in this case PVC) are used in the damage criterion. The criterion for damage initiation is

$$\omega_D = \int \frac{d\bar{\varepsilon}^{pl}}{\bar{\varepsilon}_D^{pl}\left(\eta, \dot{\bar{\varepsilon}}^{pl}\right)} = 1, \tag{23}$$

where ω_D is a state variable which increases monotonically with plastic deformation and is calculated by

$$\omega_D = \frac{\Delta\bar{\varepsilon}^{pl}}{\bar{\varepsilon}_D^{pl}\left(\eta, \dot{\bar{\varepsilon}}^{pl}\right)}. \tag{24}$$

While the ductile-damage criterion is phenomenological, it is a useful addition to the finite element model because it enables the tracking of core-cracking and fragmentation. The inclusion of a damage criterion has significant implications for energy dissipation and dynamic response.

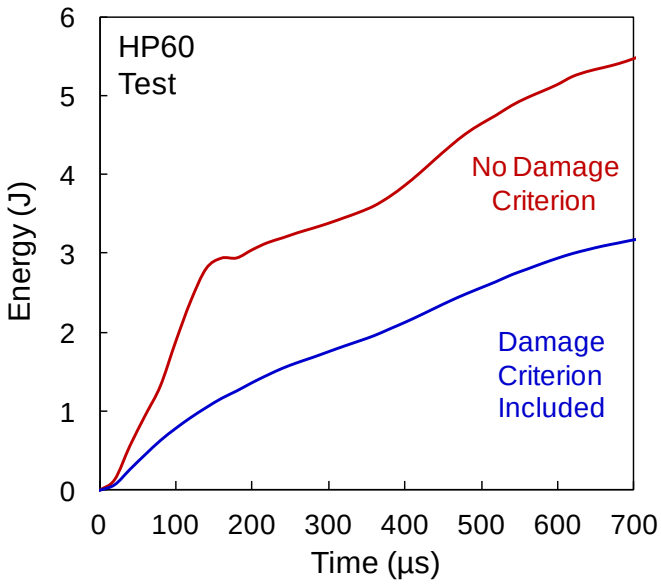

Figure 3.7 Comparison of energy-dissipation in structures with and without damage criterion. Structures in which damage criterion is included experience ~50% less energy dissipation.

Figure 3.7 shows a comparison of energy-dissipation in structures which include a damage-criterion and those which do not include a damage criterion. Foams in which a damage criterion is included absorb ~50% lesser energy as compared to foams in which a damage criterion is not included.

3.4 Water

A Lagrangian formulation is adopted to simulate wave propagation in water. The response of water is described by the Mie-Gruneisen equation of state such that

$$p = \frac{\rho_0 c_0^{\,2} \eta}{(1 - s\,\eta)^2}\left(1 - \frac{\Gamma_0 \eta}{2}\right) + \Gamma_0 \rho_0 E_m\,, \tag{25}$$

where p is the current pressure, c_0 is the speed of sound, ρ_0 is the initial density, E_m is internal energy per unit mass, Γ_0 is Grüneisen's Gamma at a reference state, $s = dU_s / dU_p$ is the Hugoniot slope coefficient, U_s is the shock wave velocity and U_p is the particle velocity which is related to U_s through a linear Hugoniot relation

$$U_S = c_0 + sU_p, \tag{26}$$

The values of the constants are listed in Table 3.3.

Table 3.3 Parameters for the Mie-Gruneisen equation of state for water

Parameter	**Unit**	**Value**
Density of water	kg/m^3	1000
Speed of sound in water	m/s	1500
Gruneisen's Gamma	-	0.1
$s = dU_S / dU_P$	-	1.75

3.5 Aluminum

The projectile and flyer plate are both made from aluminum. For the purpose of this research, the projectile and flyer-plate are both considered to be elastic. The material properties are listed in Table 3.4.

Table 3.4 Material parameters for aluminum

Parameter	Unit	Value
Density of aluminum	kg/m^3	2700
Young's modulus	GPa	70
Poisson's ratio	-	0.33

3.6 Steel

The water-chamber is fabricated with steel. In the research work presented here, the dynamic response of steel sandwich structures is not reported. Hence, a linear elastic constitutive model is implemented for steel. The material properties are listed in Table 3.5.

Table 3.5 Material parameters for steel

Parameter	Unit	Value
Density of steel	kg/m^3	8000
Young's modulus	GPa	200
Poisson's ratio	-	0.33

3.7 Concluding remarks

The manufacturing methods for sandwich composites are explained in detail in this chapter. This chapter also includes all the constitutive and damage models that are implemented i numerical calculations. The results presented in this thesis are divided into 3 chapters, all of which include computational modeling. In each of these chapters, in the

descriptions of the numerical models, the reader is referred to the corresponding section in chapter 2. The design and development of a novel experimental facility is reported in the next section.

4. UNDERWATER SHOCK LOADING SIMULATOR

4.1 Introduction

Early experiments involving impulsive loading of structures consisted of impacting sandwich structures with metal foams. On impact, the metal foams compressed rapidly and simulated the impulsive loads observed in underwater explosions. However, the loads created in this technique did not fully capture the effects of fluid structure interaction. To fully and accurately capture the effects of an underwater blast in a laboratory setting, an underwater impulsive loading facility was designed, fabricated and tested in this research. This facility is called the Underwater Shock Loading Simulator (USLS). With recent improvements in optics and lasers, there is a need for an experimental facility that can combine controlled underwater impulsive loading with state-of-the-art diagnostics to accurately characterize the dynamic response of marine structures. The main objectives of the USLS are as follows:

1. Generate controlled, uniform high-intensity underwater impulsive loads without using explosives.
2. Develop diagnostics to measure temporal and spatial evolution and failure of composite structures under a variety of impulsive loading conditions.
3. Test marine structures with water on one-side (impulse side) and water on both sides (impulse-side as well as back-side).

4. Test marine structures with different boundary conditions mimicking the various sections in a ship structure.
5. Use experimental data and supporting numerical calculations to develop material-structure-property relationships and offer solutions to improve the blast resistance of marine structures.

4.2 Design and development

The USLS has been developed as part of a research effort to study the dynamic response of composite structures to underwater blast loading. In this research work, a gas-gun based impact loading is used to create underwater pressure impulses. Figure 4.1 shows a schematic of the USLS; showing the projectile, flyer-plate, water-chamber, sandwich composite and supports. The projectile is accelerated down the length of a gas-gun barrel; the projectile then strikes a flyer plate fitted in a sealed water-chamber. The stress-wave generated inside the flyer plate is transmitted through the flyer-water interface into the water-chamber.

By varying the projectile velocity and mass, pressure waves of varying magnitudes and decay times can be generated in the water-chamber. The pressure wave generated in the water-chamber travels down the length of the chamber (~700 mm) and impinges on the target. The dynamic deformations in the target are then quantified using high-speed digital imaging. This setup generates predictable and controlled high-intensity underwater impulsive loads for testing marine structures. To validate this technique prior

to fabrication, an analytical and numerical study was carried out to determine the peak-pressures, projectile-velocities, dimensions and materials for each component.

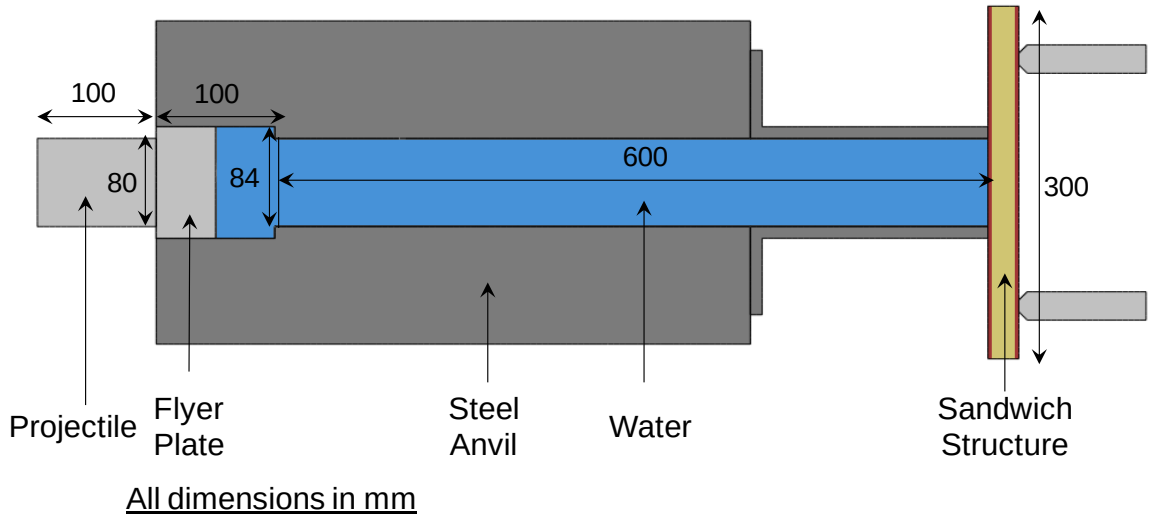

Figure 4.1 Schematic of Underwater Shock Loading Simulator (USLS). A high-velocity projectile hits the flyer-plate and creates a stress-wave which travels through the flyer-plate and into the water, generating an impulse identical to one produced by an underwater explosion.

4.3 Analytical solution to gas-gun based impulsive loading

Here, a one-dimensional analytical solution for the impulsive loads generated by the USLS is presented. An analytical solution can be divided into two distinct but connected problems:

1. projectile-flyer impact; and
2. stress-wave transmission/reflection at an interface.

Figure 4.2 shows a schematic of projectile-flyer impact with the flyer in contact with water. The water section is treated as semi-infinite for the purpose of this solution.

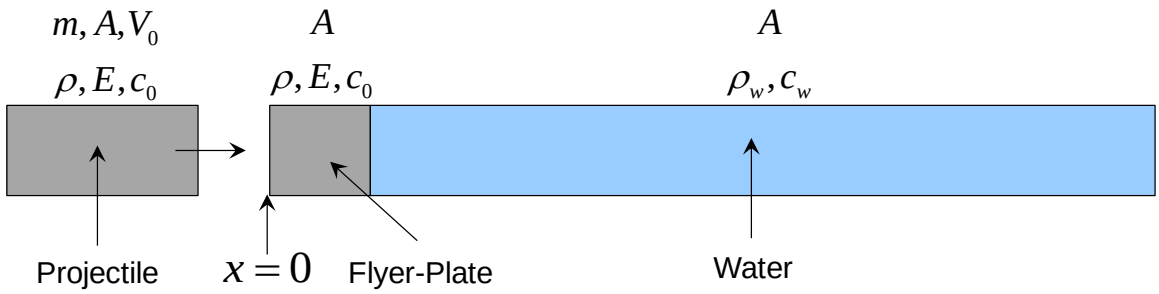

Figure 4.2 Schematic of the plate-impact and transmission-reflection problem at 2 interfaces - (1) projectile-flyer plate and (2) flyer-plate-water.

When the projectile impacts the flyer plate, it generates a stress-wave in the flyer plate. For the purpose of this analysis, consider the projectile and flyer plate to be perfectly elastic. For the projectile, the velocity is V_0, mass is m, the speed of sound in the projectile is c_0, the elastic modulus is E_0 and the cross-sectional area is A_0. The equation of motion is given by

$$E_p \frac{\partial^2 u}{\partial^2 x} = \rho_p \frac{\partial^2 u}{\partial^2 t}$$
$$\text{or} \qquad (27)$$
$$\frac{\partial^2 u}{\partial^2 x} = \frac{1}{c_p^2} \frac{\partial^2 u}{\partial^2 t}, c_p = \sqrt{\frac{E}{\rho}},$$

where u is the displacement, x is the position and t is the time. Using the general solution for the wave-equation given by D'Alembert [103] and Graff [104] and modifying it for the USLS (for the projectile and flyer-plate) gives the displacement

$$u(x,t) = \boldsymbol{I}(c_0 t - x), \qquad (28)$$

where "$\boldsymbol{I}$" denotes the incident wave. From Newton's law and conservation of momentum

$$mV_0 - \int_0^t F(t)\,dt = mV_I(t). \tag{29}$$

The initial conditions are as follows: (1) the projectile has a velocity V_0; (2) the interface between the projectile and flyer-plate is traction-free; (3) there exists stress and velocity continuity across the interface and (4) projectile and flyer-plate can both be considered elastic in the time it takes for the stress-wave to travel into the water-chamber. Using the wave-solution, the velocity at the projectile-flyer interface is given by

$$V_I(t) = \frac{d}{dt}\left[\boldsymbol{I}(c_0 t - x)\right] = c_0 \boldsymbol{I}'(c_0 t), \tag{30}$$

and the force at the projectile-flyer interface is

$$F(t) = -EA\frac{d}{dx}\left[\boldsymbol{I}(c_0 t - x)\right] = -EA\boldsymbol{I}'(c_0 t). \tag{31}$$

After substituting eqns. (31) and (30) into eqn (29), we get

$$-EA\int_0^t \boldsymbol{I}'(c_0 t)\,dt = m\left[c_0 \boldsymbol{I}'(c_0 t) - V_0\right]. \tag{32}$$

simplifying eqn. (32) gives

$$\boldsymbol{I}'(c_0 t) + \frac{EA}{mc_0^{\,2}}\boldsymbol{I}(c_0 t) = \frac{EA}{mc_0^{\,2}}\boldsymbol{I}(0)\frac{V_0}{c_0}. \tag{33}$$

The first order differential in eqn. (33) can be solved by

$$\boldsymbol{I}\left(c_0 t\right) = D\ \exp\left(-\frac{EA}{mc_0}t\right) + \boldsymbol{I}\left(0\right) + \frac{mc_0}{EA}V_0, \tag{34}$$

where D depends on initial condition such that $\boldsymbol{I}\left(0\right) = 0$. Substituting this in eqn. (34) gives

$$D = \frac{mc_0 V_0}{EA}. \tag{35}$$

Substituting eqn. (34) into eqn. (28) gives the displacement

$$u\left(0,t\right) = u\left(c_0 t\right) = \frac{mc_0 V_0}{EA}\left[1 - \exp\left(-\frac{EA}{mc_0}t\right)\right]. \tag{36}$$

The general solutions for displacement, velocity, strain and force are

$$\begin{aligned}
u\left(x,t\right) &= \frac{mc_0 V_0}{EA}\left[H\left\langle c_0 t - x\right\rangle\right]\left[1 - \exp\left(-\left(c_0 t - x\right)\frac{EA}{mc_0{}^2}\right)\right], \\
v\left(x,t\right) &= \frac{d}{dt}u\left(x,t\right) = V_0\left[H\left\langle c_0 t - x\right\rangle\right]\left[\exp\left(-\left(c_0 t - x\right)\frac{EA}{mc_0{}^2}\right)\right], \\
\varepsilon\left(x,t\right) &= \frac{d}{dx}u\left(x,t\right) = -\frac{V_0}{c_0}\left[H\left\langle c_0 t - x\right\rangle\right]\left[\exp\left(-\left(c_0 t - x\right)\frac{EA}{mc_0{}^2}\right)\right], \\
F\left(x,t\right) &= \frac{d}{dt}EAu\left(x,t\right) = \frac{EAV_0}{c_0}\left[H\left\langle c_0 t - x\right\rangle\right]\left[\exp\left(-\left(c_0 t - x\right)\frac{EA}{mc_0{}^2}\right)\right].
\end{aligned} \tag{37}$$

At the interface where the projectile and flyer-plate make contact, since $x = 0$, the generalized relations can be given by

$$u(0,t) = \frac{mc_0}{EA} V_0 \left[1 - \exp\left(-\frac{EA}{mc_0} t \right) \right],$$

$$v(0,t) = \frac{d}{dt} u(x,t) = V_0 \left[\exp\left(-\frac{EA}{mc_0} t \right) \right],$$

$$\varepsilon(0,t) = \frac{d}{dx} u(x,t) = -\frac{1}{c_0} V_0 \left[\exp\left(-\frac{EA}{mc_0} t \right) \right], \tag{38}$$

$$F(0,t) = \frac{d}{dt} EAu(x,t) = \frac{EA}{c_0} V_0 \left[\exp\left(-\frac{EA}{mc_0} t \right) \right].$$

The stress at $x = 0$ is given by

$$\sigma(0,t) = \frac{1}{A} F(0,t) = \frac{E}{c_0} V_0 \left[\exp\left(-\frac{EA}{mc_0} t \right) \right]. \tag{39}$$

Figure 4.3 shows the pressure wave generated by a projectile weighing 3.8 kg strikes the flyer-plate at a velocity of 100 m/s. The peak pressure and decay time depend on the projectile mass, velocity and the thickness of the flyer-plate.

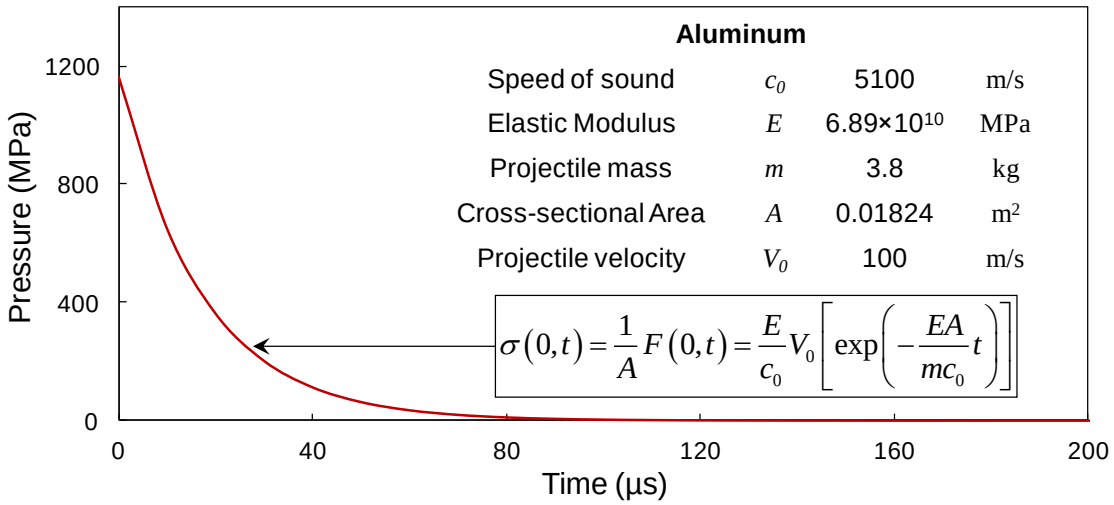

Figure 4.3 Profile of stress-wave generated in the flyer-plate after projectile impact at $x=0$.

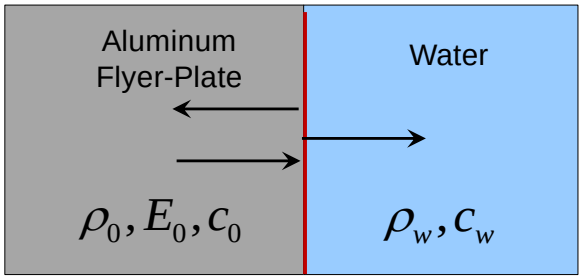

Figure 4.4 Reflection and transmission of a stress-wave at the aluminum-water interface. Aluminum transmits ~16 % of the impulse into water, a larger fraction than steel which transmits ~6%.

The stress-wave generated at the projectile-flyer interface travels through the flyer-plate and reaches the flyer-water interface in ~10 μs. Figure 4.4 shows a magnified view of the flyer-water interface. The displacement fields of particles, assuming an exponential harmonic wave solution, can be given by

$$u_{\boldsymbol{I}} = \boldsymbol{I}\left(x - c_0 t\right) = \boldsymbol{M}_{\boldsymbol{I}} \sin\left(k_0 x - \omega t\right),$$

$$u_{\boldsymbol{R}} = \boldsymbol{R}\left(x + c_0 t\right) = -\boldsymbol{M}_{\boldsymbol{R}} \sin\left[-\left(k_0 x + \omega t\right)\right], \tag{40}$$

$$u_{\boldsymbol{T}} = \boldsymbol{T}\left(x - c_w t\right) = \boldsymbol{M}_{\boldsymbol{T}} \sin\left(k_w x - \omega t\right),$$

where "$\boldsymbol{I}$","$\boldsymbol{R}$" and "$\boldsymbol{T}$" denotes the incident, reflected and transmitted waves and $\boldsymbol{M}$ is the wave amplitude. k is the wavenumber and is given by

$$k = \frac{\omega}{v} \tag{41}$$

Displacement continuity at the interface leads to

$$v\left(x,t\right) = \frac{d}{dt} u\left(x,t\right) \equiv v_{\boldsymbol{I}} + v_{\boldsymbol{R}} = v_{\boldsymbol{T}}. \tag{42}$$

Force continuity at the flyer-water interface gives

$$\sigma\left(x,t\right) = E \frac{d}{dx} u\left(x,t\right) \equiv \sigma_{\boldsymbol{I}} + \sigma_{\boldsymbol{R}} = \sigma_{\boldsymbol{T}}. \tag{43}$$

The displacement fields in reflected wave are given by

$$\boldsymbol{M}_{\boldsymbol{R}} = \frac{\rho_w c_w - \rho_0 c_0}{\rho_0 c_0 + \rho_w c_w} \boldsymbol{M}_{\boldsymbol{I}}, \tag{44}$$

and in the transmitted wave by

$$\boldsymbol{M}_{\boldsymbol{T}} = \frac{2\rho_0 c_0}{\rho_0 c_0 + \rho_w c_w} \boldsymbol{M}_{\boldsymbol{I}}. \tag{45}$$

The stress fields in reflected wave are given by

$$\sigma_R = \frac{\rho_w c_w - \rho_0 c_0}{\rho_0 c_0 + \rho_w c_w}\sigma_I, \tag{46}$$

and in the transmitted wave by

$$\sigma_T = \frac{2\rho_w c_w}{\rho_0 c_0 + \rho_w c_w}\sigma_I. \tag{47}$$

Based on the pressure vs. time plot in Figure 4.3, theoretical pressure-profiles in the flyer-plate and water-chamber are plotted in Figure 4.5. Based on eqn. (47), a steel flyer-plate would transmit 6% of the incident pressure into the water-chamber while an aluminum flyer-plate will transmit 16% of the incident pressure into the water-chamber. In the research work presented here, aluminum projectiles and flyer-plates are used.

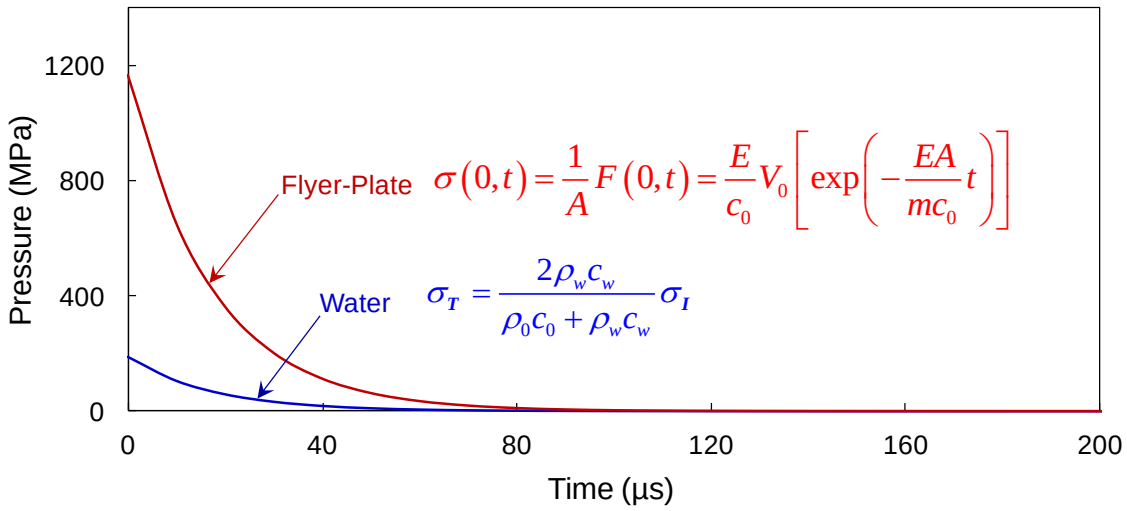

Figure 4.5 Theoretical stress-profile in the flyer-plate and pressure-profile in the water-chamber for a projectile velocity of 100m/s.

Based on theoretical calculations, it was determined that projectile velocities ranging from 25 m/s up to 200 m/s would be sufficient to generate impulsive loads of required intensities. Accordingly, the gas-reservoir capacity was finalized at 5 MPa which gives a maximum projectile velocity in excess of 500 m/s and a maximum peak pressure exceeding 500 MPa. These load intensities are representative of different amounts of explosive material and stand-off distances from the explosive source. In addition to the theoretical calculations, numerical calculations were also carried out prior to fabrication. In numerical calculations, different material properties and water-chamber dimensions were considered. Both theoretical and numerical results were used to fabricate the USLS.

4.4 Computational modeling of USLS

The theoretical calculations revealed that a gas-reservoir capacity of 5 MPa and projectile velocities up to 500 m/s are sufficient to generate underwater impulsive loads identical to those observed in underwater blasts. These theoretical calculations are supported by numerical calculations accounting for the fluid-structure interaction effect. Using the results obtained from numerical calculations, it is ensured that the stresses generated in the flyer-plate and the walls of the chamber are within acceptable limits. Figure 4.6 shows the finite element mesh for a two-dimensional computational model of the USLS. The mesh is refined near the flyer-plate and target. The water-chamber is fixed at the edges and the target is clamped. The projectile is prescribed an initial velocity and non-penetrating, frictionless contact is prescribed at all interfaces.

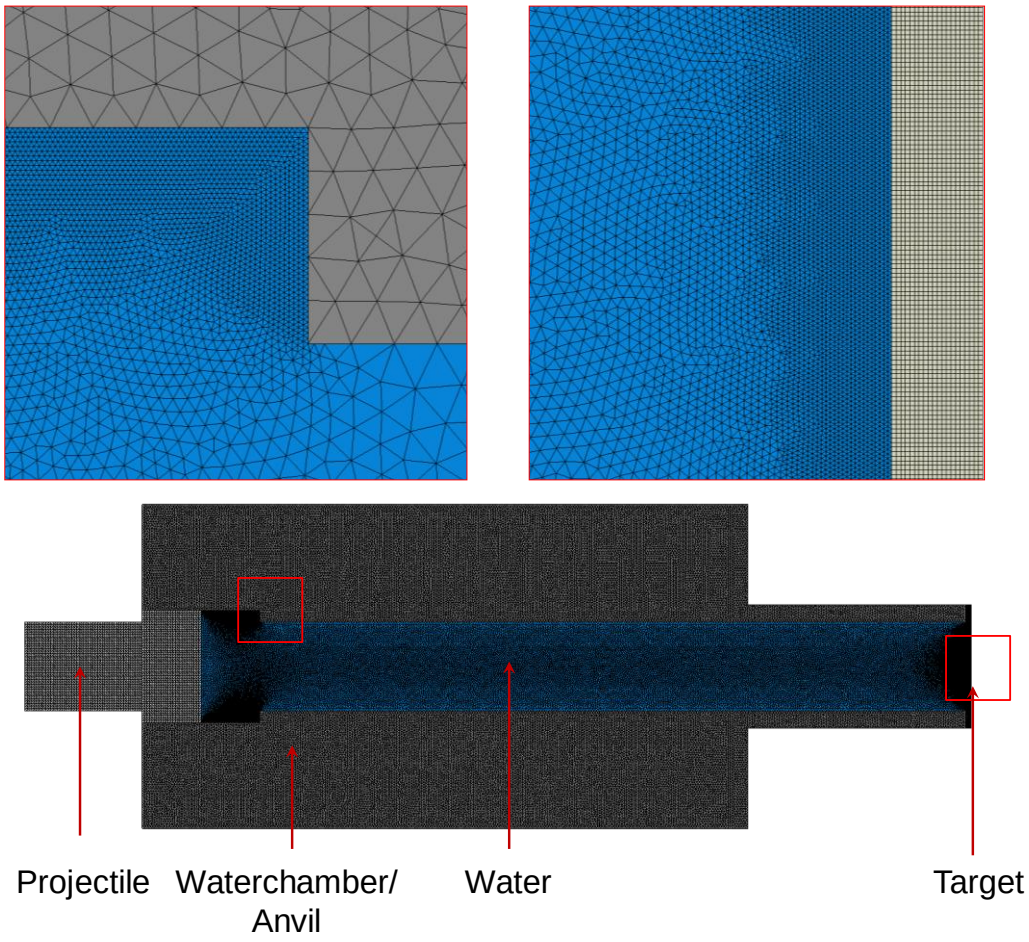

Figure 4.6 Side-view of finite element mesh for the USLS. The target is fully clamped.

The projectile strikes the flyer-plate and generates a pressure-wave in the flyer-plate which is transmitted into the water. A pressure wave generated in the water-chamber by a projectile of mass 3.8 kg travelling at 100 m/s is illustrated in Figure 4.7. The peak pressure of the impulsive wave is ~150 MPa and the wave velocity is 1300 m/s, slightly lesser than the speed of sound in water. Also shown is the effect of negative pressure at the fluid-structure interface which causes cavitation and creates complex loading conditions. The final design, fabrication and testing of the USLS are discussed in the next section.

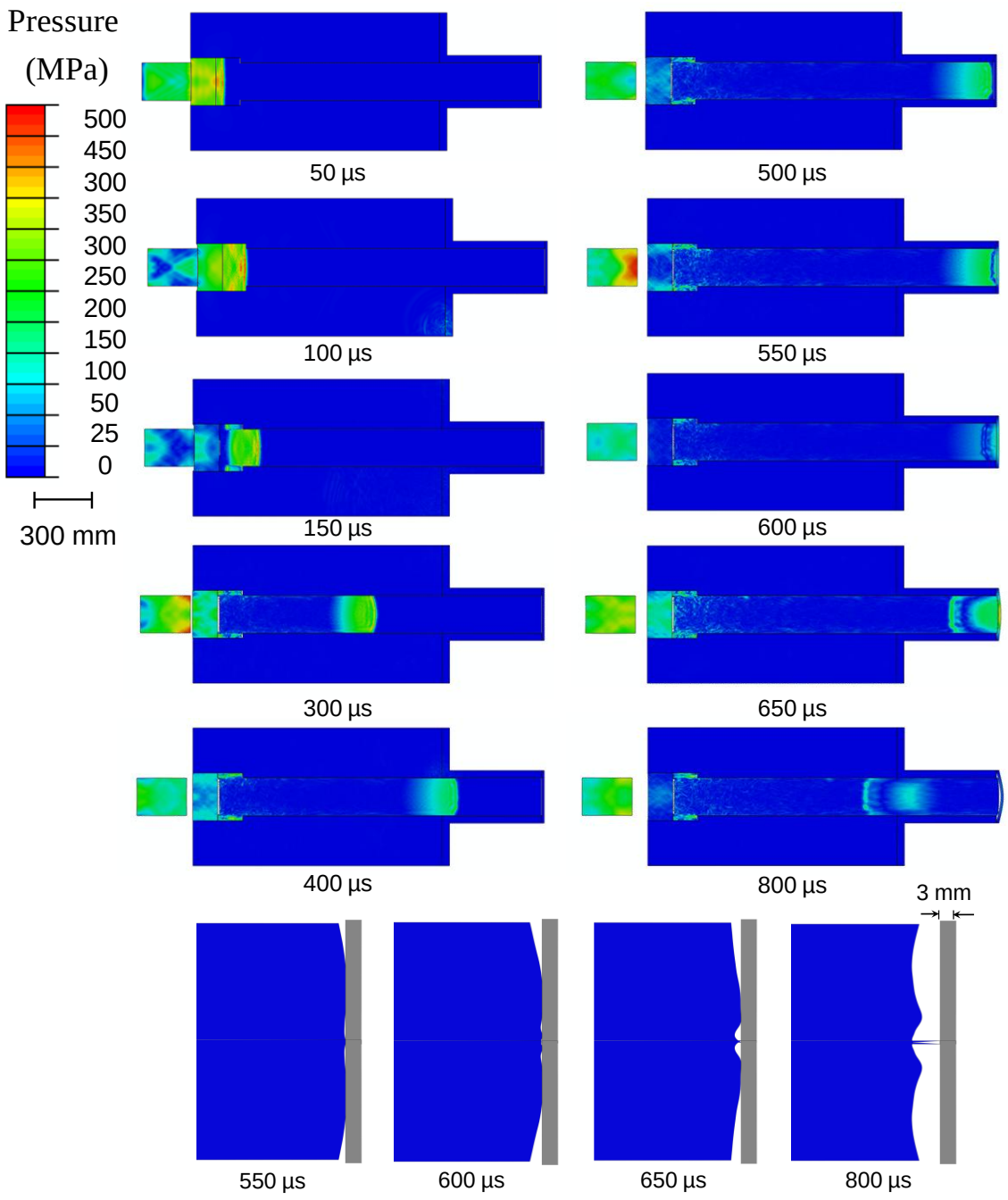

Figure 4.7 Contour plots of pressure for an impulsive wave generated in the water-chamber due to projectile impact. Cavitation at the water-structure interface is shown. Projectile velocity is 100 m/s.

4.5 Underwater Shock Loading Simulator (USLS)

The USLS is designed to enable the generation of underwater impulsive loads identical to those created by an underwater explosion. The central cavity is designed so that the pressure-waves are in the form of planar pulses which are easier to analyze than spherical pulses. Pressure histories are measured using ballistic pressure-transducers from PCB Inc. with a maximum pressure of 550 MPa, rise time of 2 μs and sampling frequency of 400 kHz. Two pressure transducers are affixed in the water-chamber to measure wave pressure, wave velocity and attenuation.

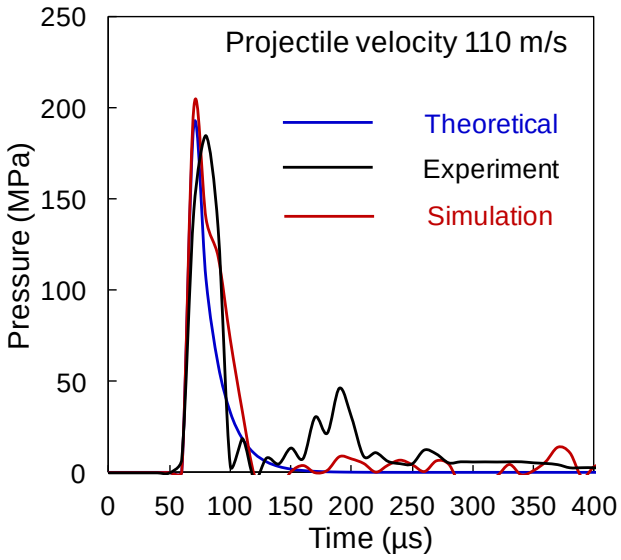

Figure 4.8 Comparison of theoretical, computational and experimental pressures in the water-chamber. Peak pressures and decay times show good agreement.

Pressure histories for all three cases are shown in Figure 4.8. Overall, the peak pressures calculated by analytical and numerical calculations and measured in the experiment are in good agreement. It is observed that the experimentally measured

impulse is slightly lesser than the theoretical impulse; conversely, the numerically calculated impulse is slightly higher than the theoretical impulse.

Figure 4.9 shows the photograph of the USLS with different components. The gas-gun, water-chamber and support-structure were fabricated by Applied Physics Inc. in Dayton, OH. The gas-reservoir maximum pressure is 5 MPa and the gas is released using a quick-acting ball-valve between the reservoir and projectile. The gun-barrel has an inner diameter of 75 mm and a total length of 3 m. When the valve is engaged, the gas escapes the reservoir and accelerates a projectile down the length of the barrel. The projectile exits the gun-barrel and strikes the flyer-plate. This flyer-plate is sealed in the water-chamber using rubber o-rings and is in contact with water.

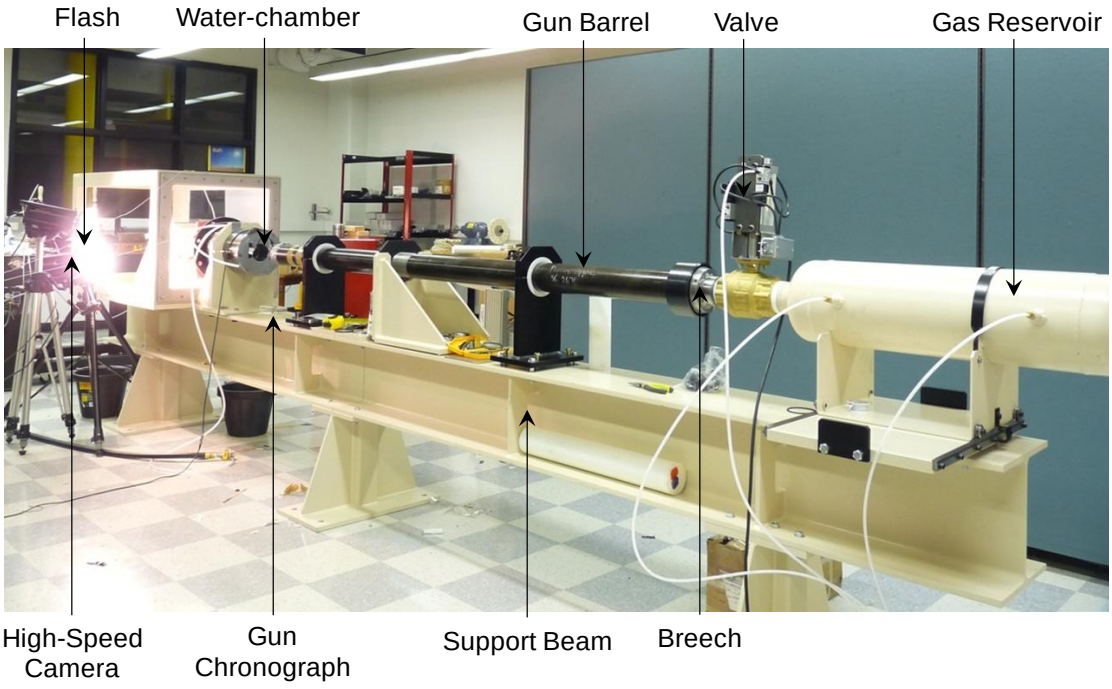

Figure 4.9 Photograph of the Underwater Shock Loading Simulator (USLS). Pictured are the gas-reservoir, gun-barrel, water-chamber and the Imacon 200D high-speed camera.

Diagnostics for the USLS consist of a high-speed camera - Imacon 200D capable of capturing 200 million frames per second and a resolution of 1368 × 1368. Figure 4.10 shows the white-light photography setup with a high-speed camera and flash. The enclosure is fitted with transparent PMMA sheets to enable in-situ high-speed digital imaging of sandwich structures subjected to impulsive loads. Previous research investigations [42] have shown that boundary conditions play an important role in dynamic behavior of marine structures. The USLS enables the testing of three types of boundary condition- free-standing, simply-supported and clamped with each boundary condition simulating different components of a naval structure. Figure 4.11 shows the two different types of boundary conditions for a composite structure.

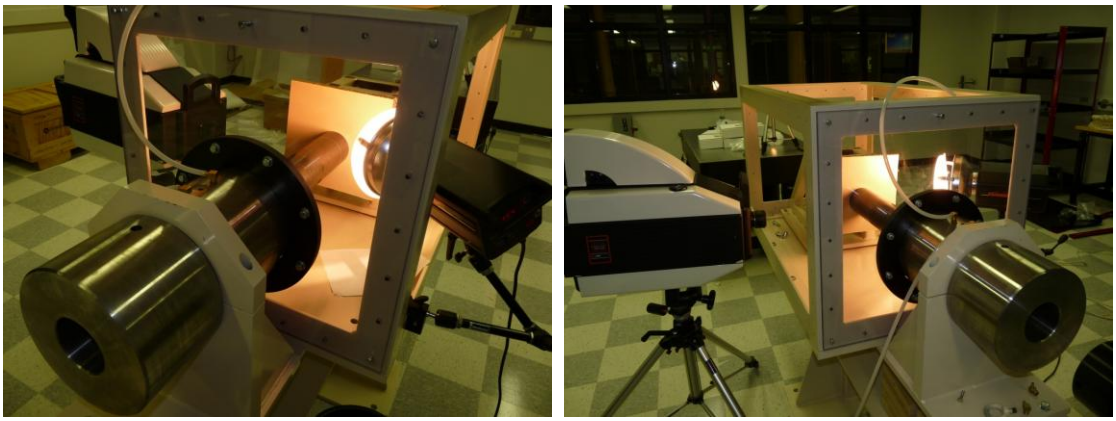

Close up of water-chamber

Figure 4.10 Close-up of water-chamber and white-light photography setup. Pictured are the high-speed camera, water-chamber and the enclosure.

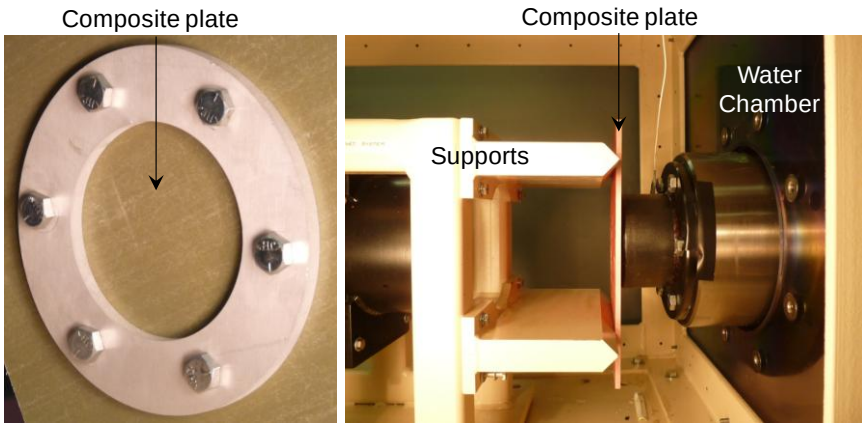

Figure 4.11 Clamped and simply-supported boundary conditions for a monolithic composite plate.

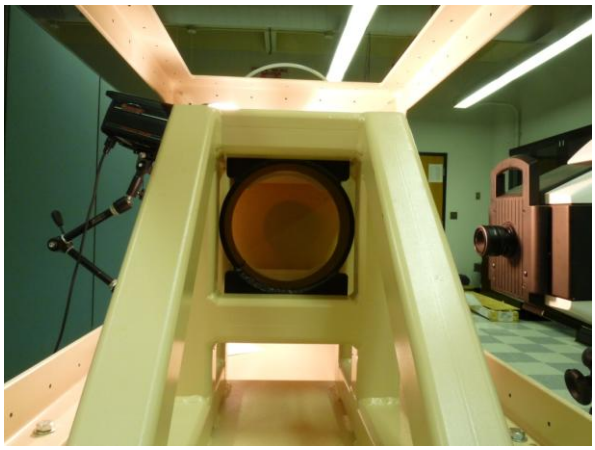

Figure 4.12 Back-view of composite plate; this enables laser interferometry on to measure in-plane and out-of-plane displacements.

Figure 4.12 shows the loading configuration as viewed from the back-side. Laser interferometric techniques like Electronic Speckle Pattern Interferometry(ESPI), speckle photography and laser vibrometry coupled with high-speed digital imaging can be used to measure in-plane and out-of-plane displacements and surface velocities. Back-face

displacements, reaction-forces and velocities are useful metrics for measuring blast-resistance.

4.6 Concluding remarks

An underwater impulsive loading facility, the Underwater Shock Loading Simulator (USLS), has been designed and fabricated. The facility employs a gas-gun based projectile-impact mechanism to generate controlled, planar underwater impulsive loads which impinge on the target structure. Impulsive loads with peak pressures exceeding 500 MPa and wave-velocities exceeding the speed of sound in water $MPa \cdot s$ can be achieved using this technique. The USLS enables the generation of controlled, planar, uniform and repeatable underwater impulsive loads. A modular support system allows in-situ high-speed digital imaging of the dynamic deformations in marine structures. An Imacon 200D high-speed camera is used to take photographs and dynamic pressure-transducers are used to measure the impulse intensity. The facility can be modified to test oblique and curved structures. A series of experiments are carried out using the USLS to evaluate the dynamic deformations and failure mechanisms in monolithic and sandwich composites. These experiments are supported by fully dynamic finite element simulations. The results from these studies are reported in the next section.

5. DYNAMIC RESPONSE OF COMPOSITE SANDWICH STRUCTURES

5.1 Introduction

In the preceding chapters, a literature review was presented followed by the different materials and manufacturing techniques. The design and development of a novel technique for generating under-water blast loads is explained. The objective of this study is to investigate the dynamic response of simply-supported composite sandwich beams to underwater impulsive loads. Composite sandwich structures are manufactured from PVC foam cores and E-glass/polyester facesheets. The areal masses of the structures are kept constant by varying core and facesheet dimensions. In experiments, white-light photography is carried out and deflection is measured with high-speed digital images. Finite element simulations are carried out accounting for facesheet damage, core crushing and core-facesheet debonding. The Hashin damage model is used to quantify damage in facesheets while a ductile-damage criterion is used to evaluate damage in the core. The dynamic response of the structures is quantified using facesheet deflections and energy absorbed in individual components. Experimental results and finite element simulations are in good agreement for air-backed structures.

5.2 Experimental procedures

Composite sandwich structures are subjected to underwater impulsive loads of varying magnitudes. Sandwich structures analyzed here are in the form of beam

specimens of length 300 mm and width 80 mm. The facesheet thickness is 3 mm and the core-thicknesses are adjusted to keep total mass constant. Facesheets are made of quasi-isotropic $(0/-45/45/90)_s$ E-glass/Polyester composites and the core is PVC foam manufactured by DIAB Inc as shown in Figure 3.3. A high-strength epoxy adhesive is used to bond the facesheet to the core. Water-jet machining is used to cut the samples into beam specimens. A simply-supported loading configuration emulates the behavior of a hull with stiffeners along the side. Table 5.1 shows the specific dimensions and areal masses of composite structures considered in this investigation.

Table 5.1 Schedule of experimental testing. The thickness of the facesheets is varied to maintain identical areal mass.

Beam Designation	**Core Density (kg/m^2)**	**Core Thickness (mm)**	**Facesheet Thickness (mm)**	**Areal Mass (kg/m^2)**
M – 1,2,3,4	-	-	6	10
HP60-1,2,3,4	60	30	2	9.04
HP100-1,2,3,4	100	20	1.6	9.2
HP200-1,2,3,4	200	10	1.5	9.12

Figure 5.1 shows the sectional view of the experimental setup and the placement of high-speed camera and illumination. Projectiles and flyer-plates are machined from aluminum alloy and are of length 80 mm and 50 mm respectively. Projectiles weigh approximately 0.8 kg. A trip-wire is held across the opening of the gun-barrel. When the projectile exits the barrel, it breaks the trip-wire and triggers the high-speed camera and flash-lights. The delay between the trigger and high-speed camera recording is ~ 1

millisecond - enough time for the planar pressure wave to travel through the water-chamber and impinge upon the target. The trip-wire also triggers the pressure-sensors which are connected to a National Instruments DAQ system. Images are obtained using a high-speed camera (Imacon 200D) and are used for the following purposes:

1. To analyze the failure modes in the sandwich structure in the form of facesheet-rupture, core-facesheet debonding, core-crushing, core shear cracking and fragmentation.
2. To determine the order-of-precedence of each failure-mode based on the time required to cause failure.
3. To compare the maximum deflections experienced by the back-face of different structures to determine blast-resistance.
4. To determine the effect of boundary-conditions on dynamic response.

Depending on the projectile velocity and mass, peak-pressures ranging from 10 to 300 MPa can be generated in the shock tube. Apart from the projectile velocity, other factors that influence the pressure pulse are projectile mass, piston plate thickness, and the shape of the water-chamber. The pressure wave can be described by the equation

$$p(t) = p_0 \exp\left(-\frac{t}{t_0}\right) \tag{48}$$

where p_0 is the peak pressure, t is time at which measurement is carried out and t_0 is the decay time. Impulse I is given by

$$I = \int_0^t p(t)\,dt \tag{49}$$

A non-dimensional impulse is

$$\bar{I} = \frac{I}{\rho_w c_w \sqrt{A}}, \tag{50}$$

where ρ_w is the density of water, c_w is the speed of sound water and A is the area under impulsive loading.

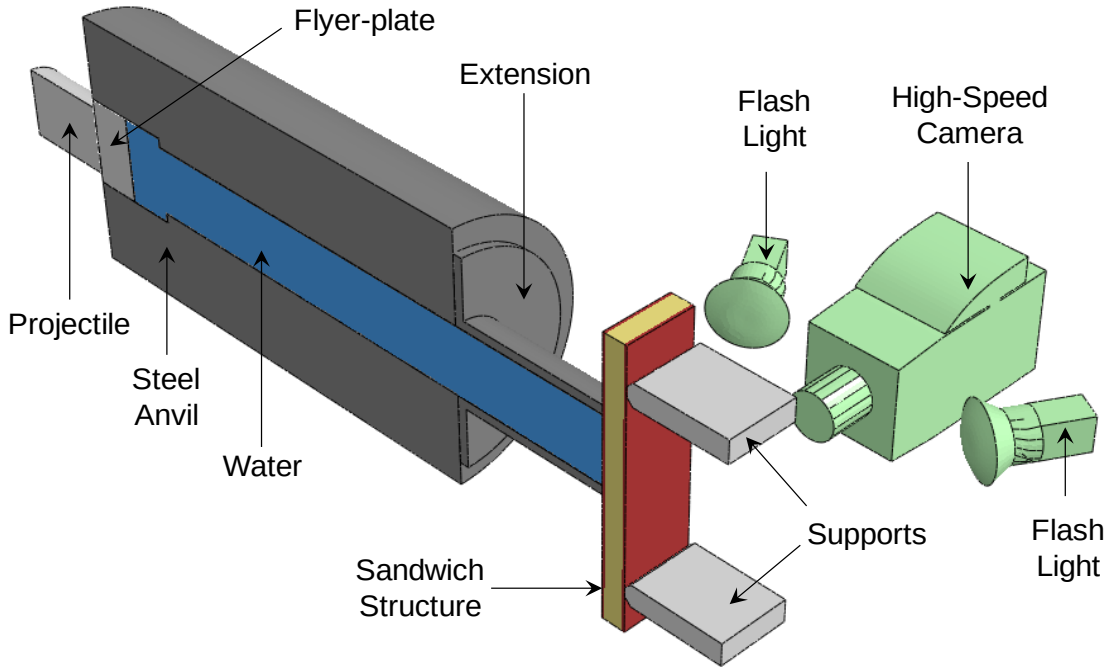

Figure 5.1 Sectional view of USLS and simply-supported sandwich structure showing the placement of high-speed camera and flash-lights.

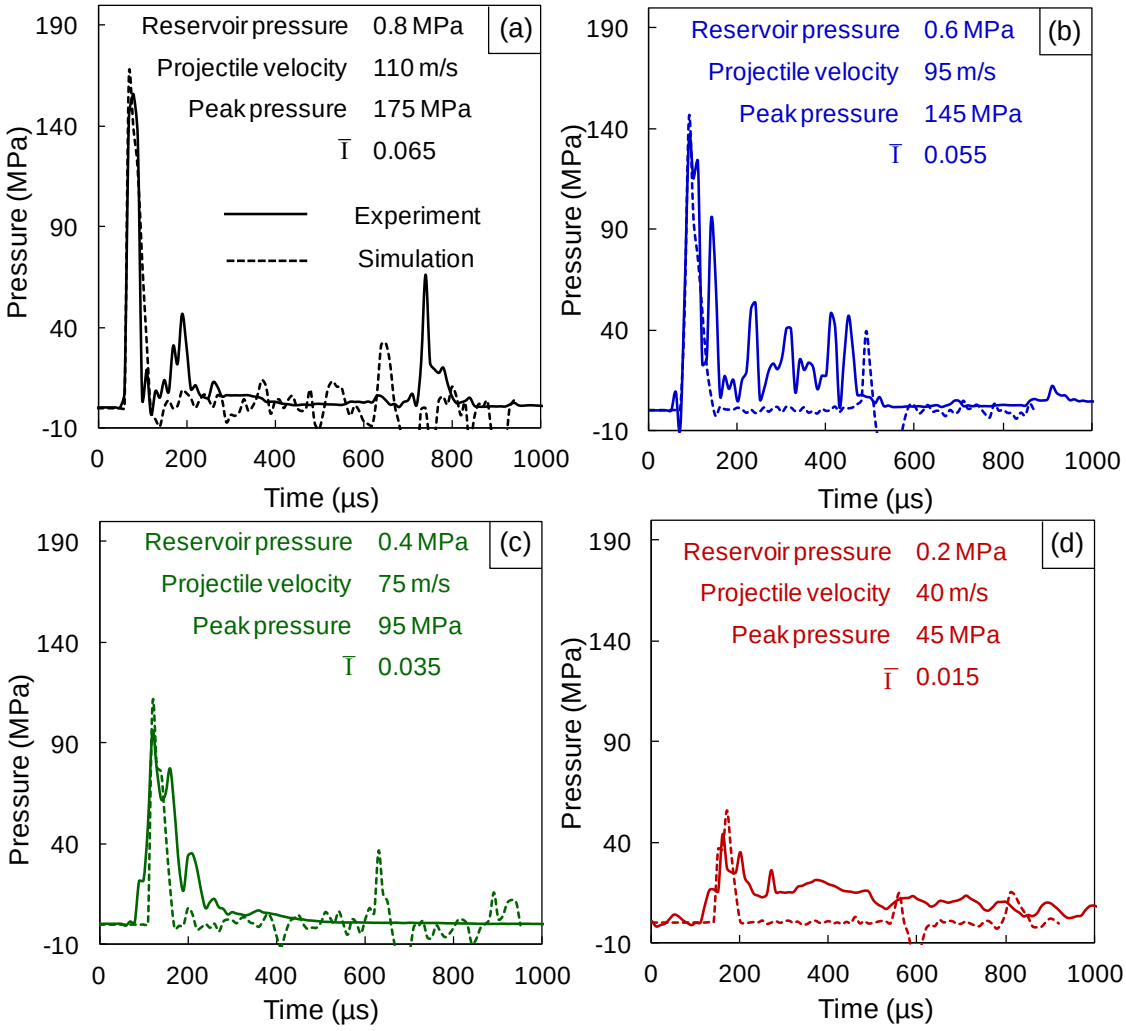

Figure 5.2 Comparison of numerical and experimental pressure histories in the water-chamber for four different projectile velocities and impulse magnitudes $\bar{I} = 0.015, 0.035, 0.055, 0.065$.

Figure 5.2 shows the pressure histories corresponding to four different projectile velocities. Pressures are measured using dynamic pressure transducers capable of maximum pressure measurement up to 500 MPa. The rise time of the pressure-pulses is on the order of 25 μs and the decay time is on the order of 800 μs. The solid lines show experimentally measured pressure histories while the dotted lines show the numerically

calculated pressure histories. The cylindrical shape of the shock tube allows a uniform pressure to be applied to the target over the area of contact. The impulse magnitudes are $\bar{I} = 0.015, 0.035, 0.055, 0.065$.

5.3 High-speed digital imaging

Monolithic E-glass/polyester beams are subjected to underwater impulsive loads. Figure 5.3 shows a montage of sequential high-speed photographs for a monolithic composite plate subjected to underwater impulsive loads. The projectile velocity is 75 m/s and the peak-pressure is 95 MPa - the impulse corresponds to $\bar{I} = 0.035$ shown in Figure 5.2 (c). A thin film used for sealing the water-chamber can be seen in addition to the water spurting out of the water-chamber. The deformation can be divided into two regimes - (1) flexural wave propagation and (2) overall deflection. Typically, flexural waves originating at the fluid-structure interface travel towards the supports within ~50 μs. Overall structural deflection initiates when the back-face (in this case the entire structure) starts moving. The displacement of the back-face is tracked at the mid-plane and compared with that of other structures.

While the deformation and damage in sandwich structures can be tracked using high-speed digital imaging, the monolithic composite plate is quite thin and damage mechanisms are hard to discern. These damage mechanisms are revealed in post-mortem photographs of the monolithic composite plate - shown in Figure 5.4 (a), (b) and (c). Figure 5.4 (a) shows the deformed monolithic plate with easily discernible "hinges"

formed near the loading area; Figure 5.4 (b) and (c) show delamination between successive layers in the laminate, matrix-cracking, fiber-pullout and rupture. While the deflection is relatively uniform over the length of the composite plate, damage mechanisms are predominantly observed near the circumference of the shock-tube and near the supports. This indicates high shear dependence in damage creation. sandwich structures.

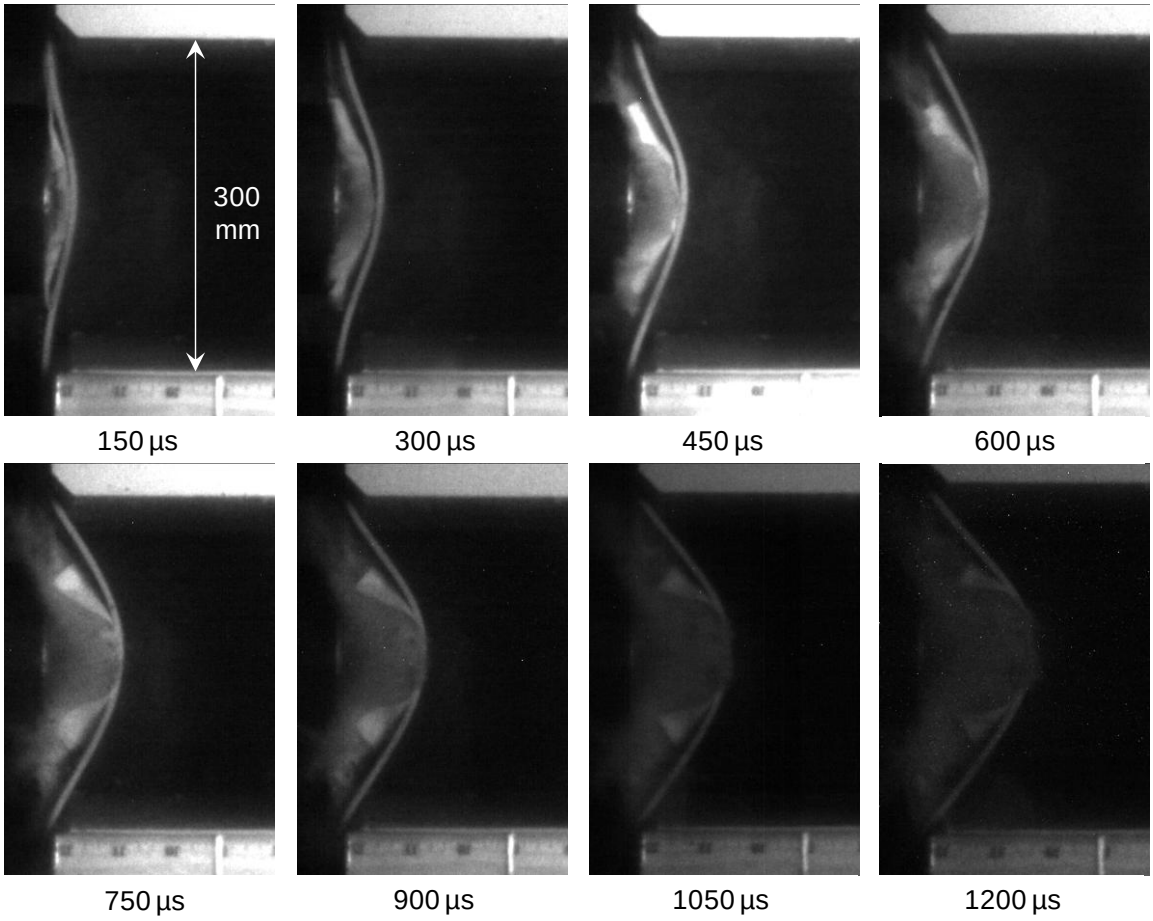

Figure 5.3 Sequence of high-speed photographs showing the deformation in a monolithic composite plate subjected to underwater impulsive loading with $\bar{I} = 0.035$.

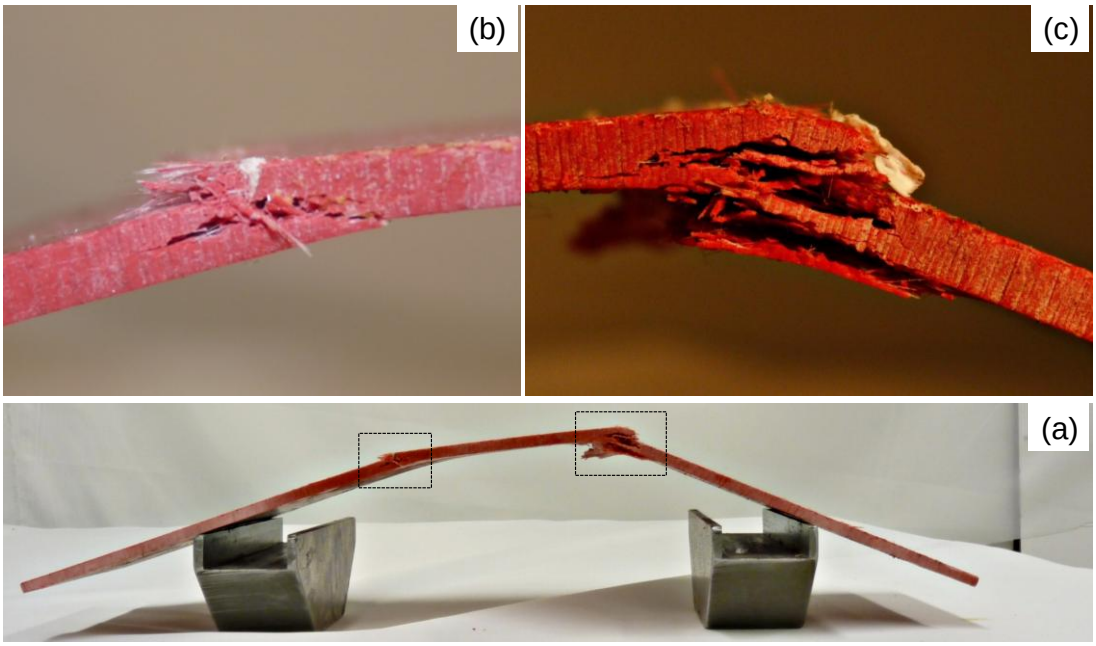

Figure 5.4 Post-mortem photographs of impulsively loaded composite plates with cross-sections showing inter-laminar delamination, matrix-cracking, fiber-matrix debonding, fiber-pullout and intra-laminar cracking.

Figure 5.5 shows a sequence of high-speed photographs of a composite sandwich structure with a Divinycell HP200 core subjected to underwater impulsive loading. Immediately after the onset of deformation, flexural waves travel through the front-face, severing the core-facesheet bond. In cases where the core-facesheet bond is very strong, a layer of core material is torn away by the facesheet due to the low tensile strength of PVC core material. Core-face debonding and core-failure, due to cracking and fragmentation, is observed at $t = 50\,\mu s$. Core-crushing, a mechanical property that makes composite sandwich structures very attractive for marine applications commences at $t = 150\,\mu s$ and is restricted to the region close to the loading area. The back-face ruptures at $t = 1550\,\mu s$.

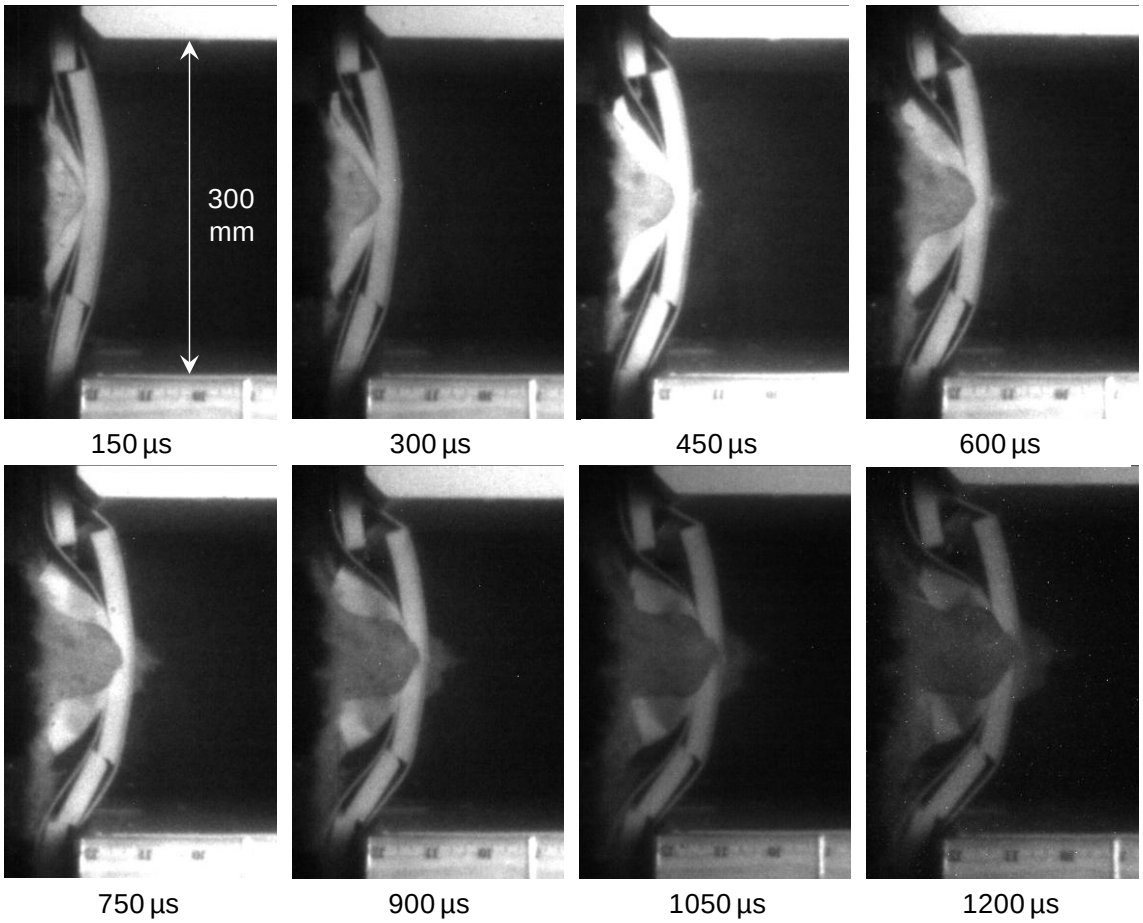

Figure 5.5 Sequence of high-speed photographs showing the deformation in a sandwich structure with HP200 core subjected to underwater impulsive loading with $\bar{I} = 0.035$. Large-scale core-front-face debonding and core-fragmentation can be observed. The core fractures prior to core-compression and rupture occurs at $t = 900\,\mu s$.

Figure 5.6 shows a sequence of high-speed photographs of a composite sandwich structure with a Divinycell HP100 core subjected to underwater impulsive loading. Core-facesheet debonding and composite face wrinkling failure and core-indentation can be seen at $t = 150\,\mu s$. In this type of failure mechanism, the core-material fails in a highly localized region and causes compressive loading and buckling in the front-face. Shear-

dominated cracks originate near the supports at $t = 300\,\mu s$ and lead to core fracture. Back-face ruptures at $t = 900\,\mu s$.

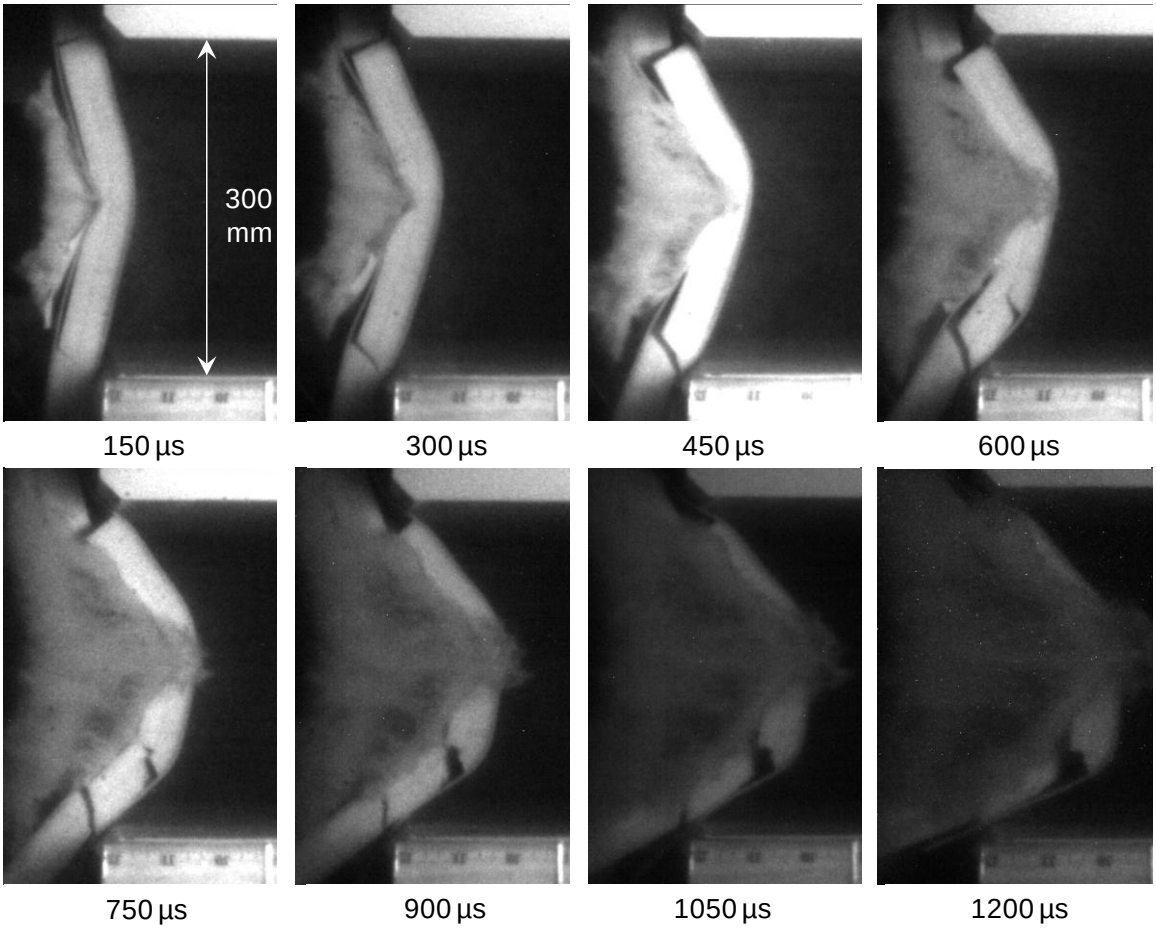

Figure 5.6 Sequence of high-speed photographs showing the deformation in a sandwich composite with HP100 core subjected to underwater impulsive loading with $\bar{I} = 0.035$. Front-face wrinkling and core-indentation occurs at $t = 300\,\mu s$. Inclined cracks initiated at $t = 600\,\mu s$ followed by rupture at $t = 900\,\mu s$.

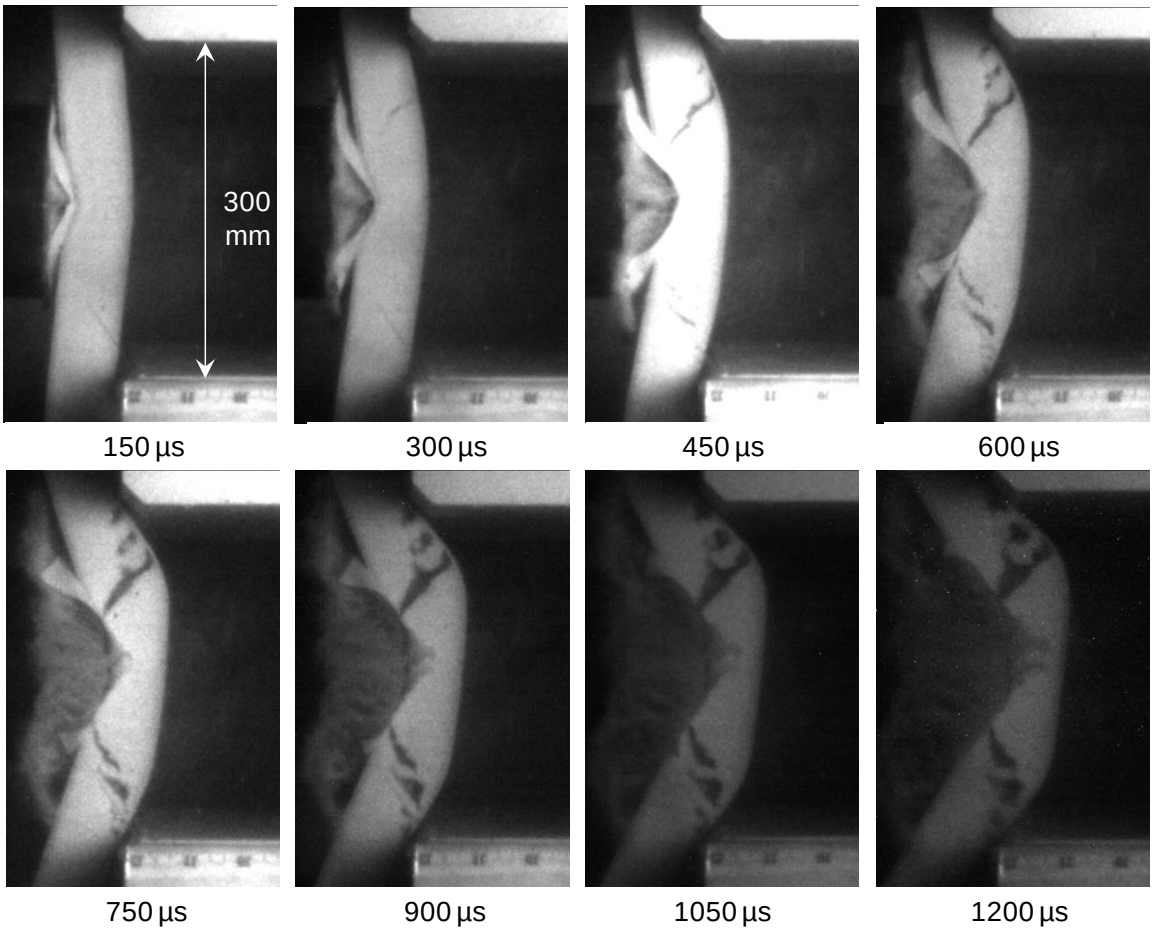

Figure 5.7 Sequence of high-speed photographs showing the deformation in a sandwich composite with HP60 core subjected to underwater impulsive loading with $\bar{I} = 0.035$. Deformation in the core is quite uniform and bending deformation occurs prior to core-cracking. Core-face debonding is relatively less widespread and facesheet wrinkling does not occur. Core-crushing occurs simultaneously with core-tensile cracking.

Figure 5.7 shows a sequence of high-speed photographs of a composite sandwich structure with a Divinycell HP60 core subjected to underwater impulsive loading. The dynamic response of the sandwich structure with a HP60 core is quite different than those with HP100 or HP200 cores - in that there is no core-shear cracking, front-face-wrinkling and core-face debonding. Core-compression commences immediately after the onset of

loading at $t = 150\,\mu s$ and inclined cracks originate near the loading circumference area. These cracks propagate from the front-face to the back-face and branch into three cracks (at $t = 450\,\mu s$) near the back-face - causing core-back-face debonding. Core-compression and core-cracking occur simultaneously with crack propagation through the core. This structure does *not* experience large-scale core-face debonding or rupture of the back-face.

The midpoint deflections for each composite structure (obtained using high-speed photographs of the side-view) are shown in Figure 5.8. The monolithic composite structure is used as a benchmark for comparison with other structures. The lesser the deflection is compared to the monolithic composite plate, the better is the blast-resistance. Figure 5.8 (a) shows the normalized deflection, Δ/L (where Δ is deflection and L is the span of the sandwich beam), of composite structures to an underwater impulsive load corresponding to $\bar{I} = 0.035$ shown in Figure 5.2 (c). Monolithic composite experiences the greatest deflection at the highest rate in comparison to the sandwich structures.

The sandwich structure with HP100 core initially exhibits a rate of deformation that is identical to the sandwich structure with HP200 core but the dynamic response of HP100 core diverges at $t = 400\,\mu s$ and the rate of deflection reduces. For the sandwich structure with HP60 core, the rate of deflection is the lowest of all three sandwich structures. In terms of overall deflection at $t = 1000\,\mu s$, the sandwich structure with HP200 core deflects ~20% less than the monolithic composite, sandwich structure with

HP100 core deflects ~60% less than the monolithic composite and the sandwich structure with HP60 core deflects ~70% less than the monolithic composite.

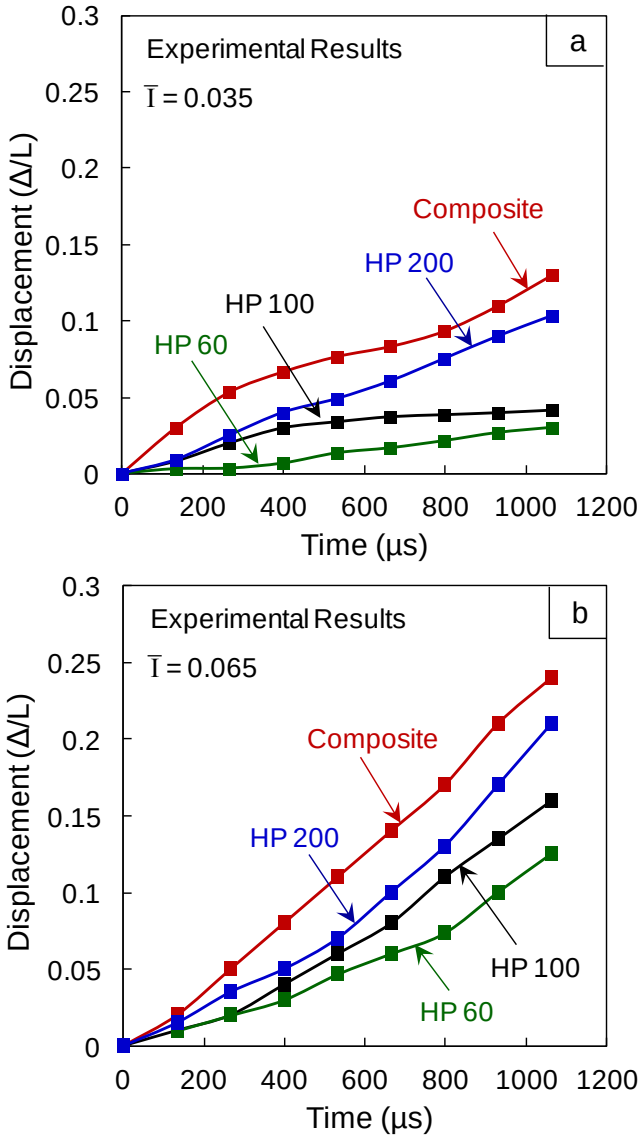

Figure 5.8 Experimentally measured mid-point displacements as a function of time for different structural configurations for (a) $\bar{I} = 0.035$ and (b) $\bar{I} = 0.065$.

Figure 5.8 (b) shows the time histories of midpoint displacements of composite structures subjected to an underwater impulsive load corresponding to $\bar{I} = 0.065$ shown

in Figure 5.2 (a). The deflections follow a similar trend as described for Figure 5.8 (a). Due the higher load intensity, the sandwich structure with HP200 core deflects ~10% less than the monolithic composite, sandwich structure with HP100 core deflects ~30% less than the monolithic composite and the sandwich structure with HP60 core deflects ~45% less than the monolithic composite.

Figure 5.9 shows the normalized deflection, Δ/L (where Δ is deflection and L is the span of the sandwich beam) at $t = 1000\,\mu s$ as a function of impulse for all the composite structures tested here. The monolithic composite shows highest deflection for all load intensities followed by the sandwich structure with HP200 core. Compared to the monolithic sandwich structure (if the Δ/L for monolithic composite is 100%), the deflection in the sandwich structure with HP200 core is ~20% smaller, that with HP100 core is ~60% smaller and that with HP60 core is ~66% smaller. The deflections experienced by sandwich structures with HP60 and HP100 cores are quite similar, with the HP60 core outperforming the HP100 core by a small margin – particularly at higher load intensities. Finite element simulations are carried out to enable energy evaluation in sandwich structures and to enable the testing of other loading configurations including water-backed structures, clamped boundary conditions, oblique loads and curved structures.

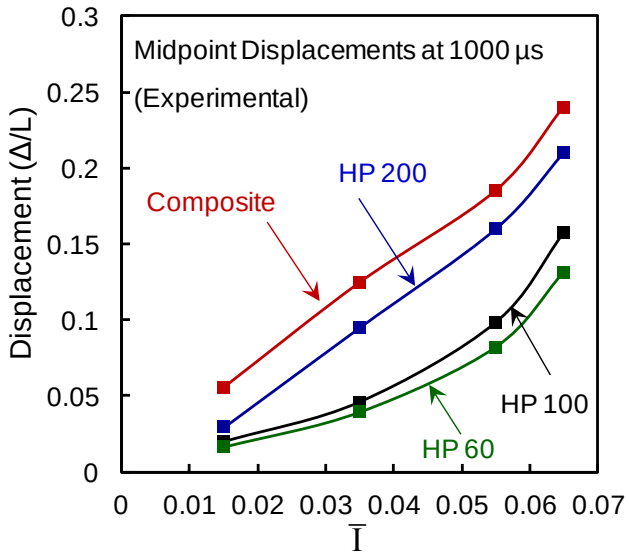

Figure 5.9 Displacement as a function of impulse for composite structures with different cores. On a per-weight basis, low-density cores consistently outperform high-density cores. Sandwich structures are superior to monolithic composite plates.

5.4 Finite element simulations

The commercial code, Abaqus/Explicit, is used to carry out detailed, fully-dynamic finite element simulations accounting for deformation and damage in sandwich structures and fluid-structure interaction at the water-structure interface. Cohesive element based contact is implemented at the interfaces between the faces and core. The cohesive elements follow the bilinear traction-separation law. Non-penetrating, frictionless contacts are implemented at the water-structure interface, flyer-water interface, projectile-flyer interface and structure-supports interfaces. Components consisting of composites and PVC foams are meshed with 2-D 8-node brick elements with 5 integration points through the thickness. The constitutive and damage models for these materials – glass fiber composite, PVC foam, water and aluminum - are explained

in detail in chapter 2. A comparison of finite-element simulations and experiments is presented in the following section. Finite-element simulations are then extended to other loading configurations.

Figure 5.10 shows a comparison of high-speed photographs from experiments and damage contour plots from simulations. The contour plots at four successive time steps after the onset of loading are shown in addition to a magnified view of damage in the core. The high-speed photographs captured in-situ during experiments have been explained in the previous section. In the finite-element simulations, at $t = 150\,\mu s$, the impulsive loads are transmitted through the facesheet and core experiences strains at and inclined angle in two directions - away from the loading area, towards the supports and from loading area towards the central region. Initially, strains in the core are a result of elastic deformation which is completely recoverable.

At $t = 400\,\mu s,$ core-crushing (permanent, plastic deformation) is observed in the central region and cracks propagate towards the supports. At $t = 700\,\mu s,$ crack-branching and core-fragmentation are observed at the loading circumference. The frontface wrinkles under compressive loading and causes to core-face debonding. The entire structure achieves a common velocity at $t = 1000\,\mu s.$ While damage in the front-face is widespread, the back-face is relatively undamaged. Figure 5.11 shows the dynamic deformation in monolithic composite plate and sandwich structures with HP200, HP100 and HP60 cores at $t = 1000\,\mu s.$

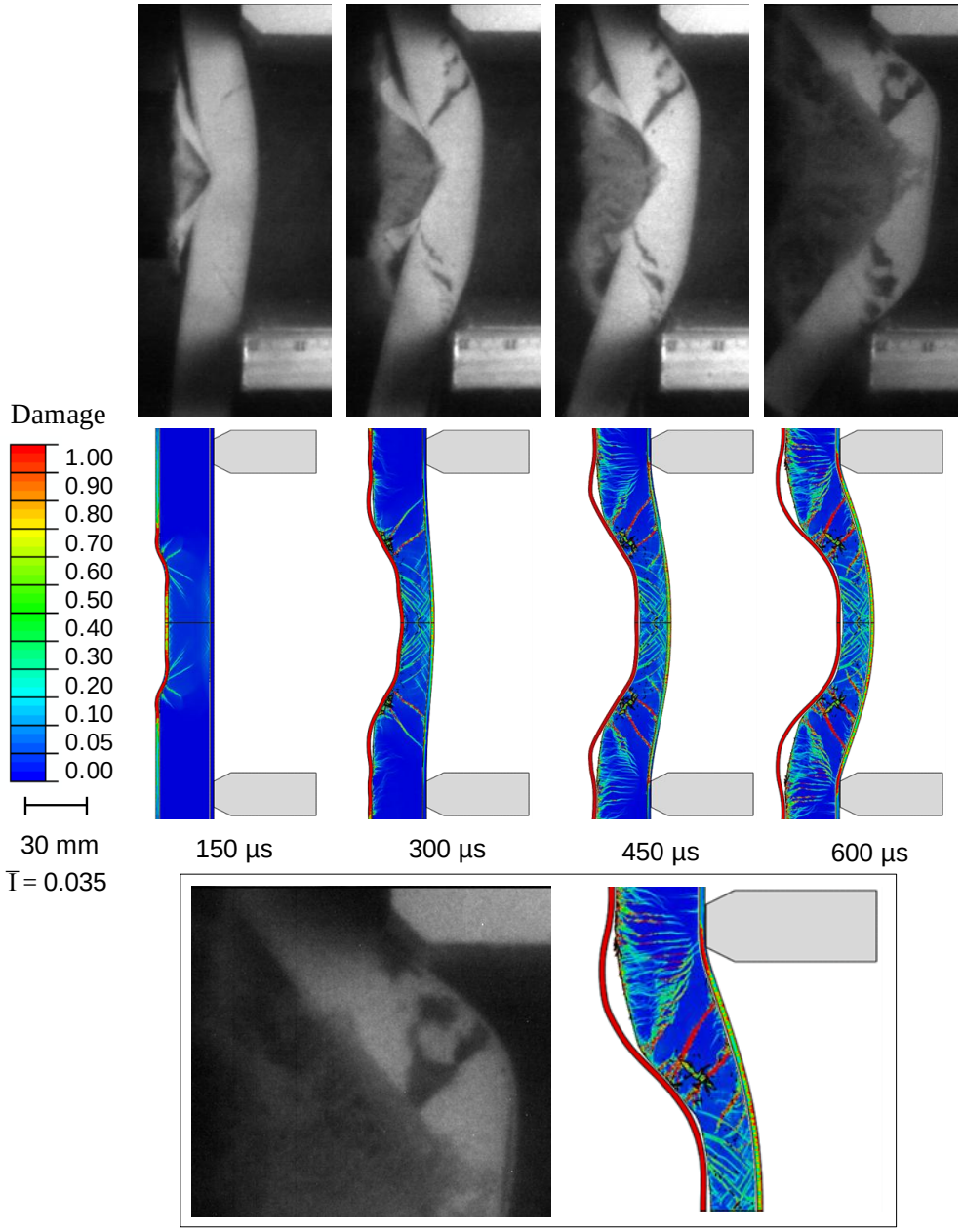

Figure 5.10 Comparison of experimental and computational deformation sequences for a sandwich structure with HP60 core. The deformation modes - core-cracking, core-frontface debonding and core-crushing - are accurately captured in the finite-element simulations. The magnified view show core-branching and fragmentation.

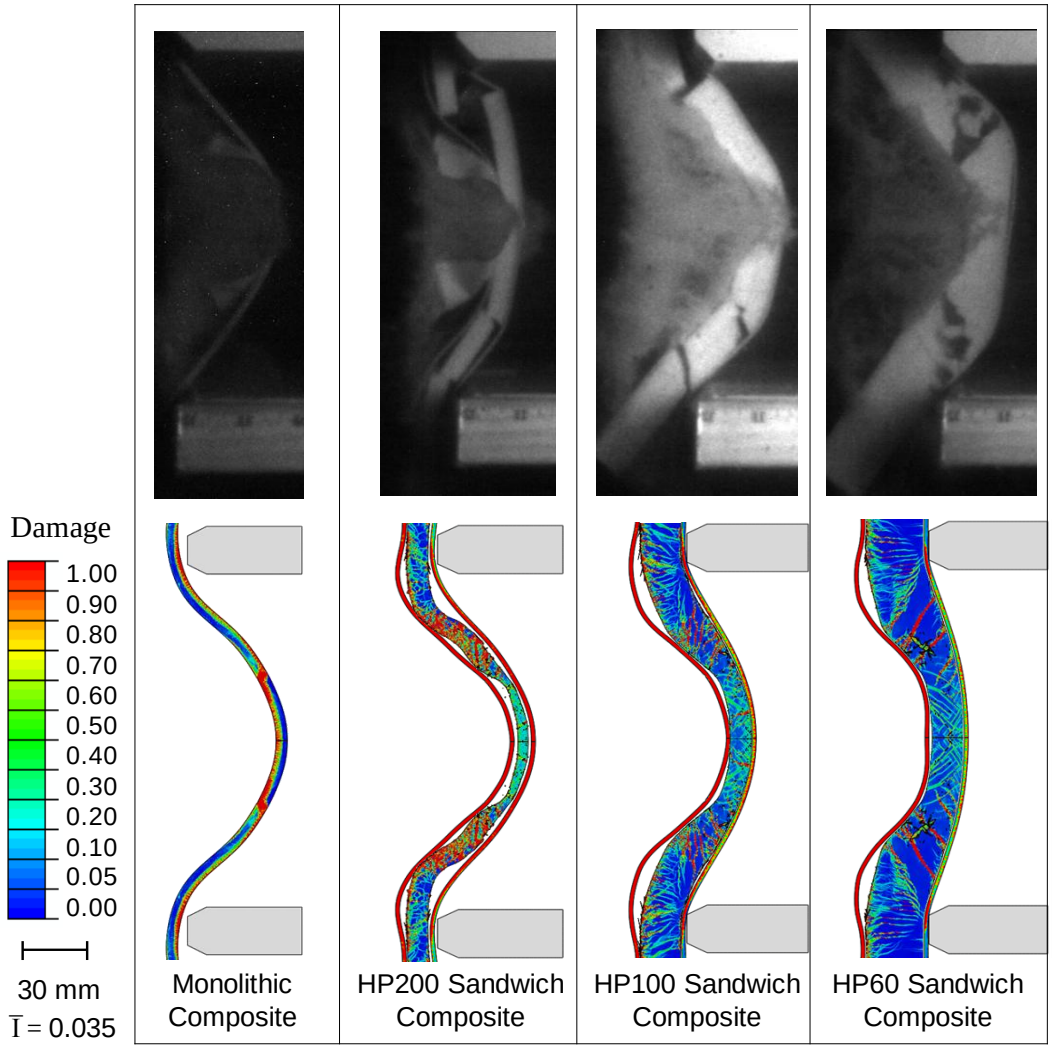

Figure 5.11 Comparison of experimental and computational deformation sequences for different composite structures at 1000 μs. The dynamic deformations and failure modes are accurately captured in the finite element simulations including matrix-cracking, core-cracking, core-face debonding and core-crushing. Note that rate-effects are *not* implemented in the simulations.

Although the finite-simulations accurately capture various deformation and damage mechanisms in the composite plate, the sandwich-structure cores exhibit an unexpectedly high rate-dependence. Recall that uniaxial compressive tests carried out on core materials [76] have shown remarkably weak rate-dependence for HP100 and HP200

core materials ranging from strain-rates of 10^{-1} to 10^{-4}. Conversely, the experiments performed in this research show a relatively stronger rate dependence when sandwich structures are subjected to multi-axial, complex loading conditions. HP200 cores fracture immediately after the onset of loading and core-compression/crushing occur *after* complete core collapse. HP100 cores experience core-crushing and core-face debonding followed by cracking and complete core collapse. HP60 cores undergo cracking and crack-branching after core-compression and crushing and exhibit the lowest rate dependence of all core materials studied here. This indicates that rate-effects are exacerbated as core-density increases.

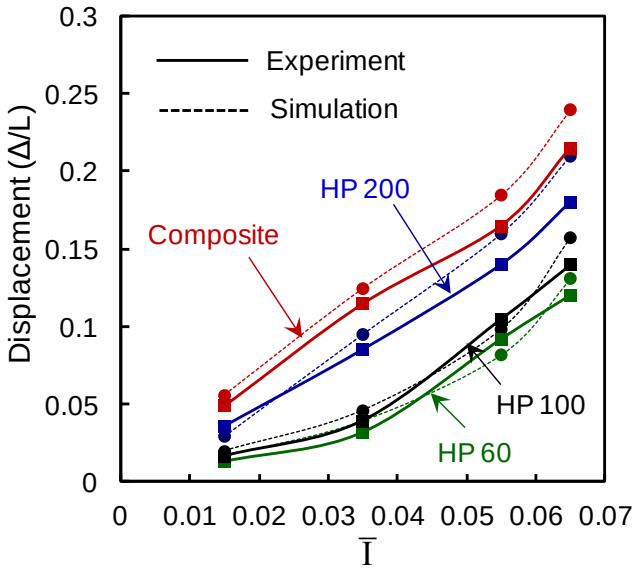

Figure 5.12 Comparison of experimental and computational results for back-face deflection as a function of impulse for composite structures with different cores.

Figure 5.12 shows a comparison of experimental and numerically obtained normalized displacements as a function of load intensity for different composite

structures at $t = 1000\,\mu s$. Finite-element simulations are within ~10% of experimental values and follow a similar trend – low-density, thick cores outperform high-density, thin cores on a *per-weight* basis. The dynamic deformations in sandwich structures are influenced by the geometric factors like thickness, length and width. However, geometric dependence is *not* considered in this set of experiments and simulations.

In a marine structure, stiffeners and other structural components are added for improved impulsive load resistance. In most naval designs, there exists a span of the hull between successive stiffeners. When an impulse impinges on a naval structure, it generates flexural waves that travel perpendicular to the direction of the stiffeners. Therefore, a useful metric to determine blast resistance is the reaction force experienced by the supports and the impulse transmitted by the structure. In finite element simulations, the reaction force is measured at the supports and the transmitted impulse is calculated by dividing the reaction force with area of the front-face and integrating over time. Figure 5.13 (a) and (b) shows the *averaged* reaction force and transmitted impulse respectively as functions of time for an impulse corresponding to $\bar{I} = 0.035$ shown in Figure 5.2 (c). The composite plate transmits the highest impulse.

In comparison to the composite plate, the sandwich structure with HP200 core transmits ~40% less impulse, the one with HP100 cores transmit ~60% less impulse and the one with HP60 core transmits ~66% less impulse. Note that the monolithic composite structure loses contact with the supports after 600 μs.

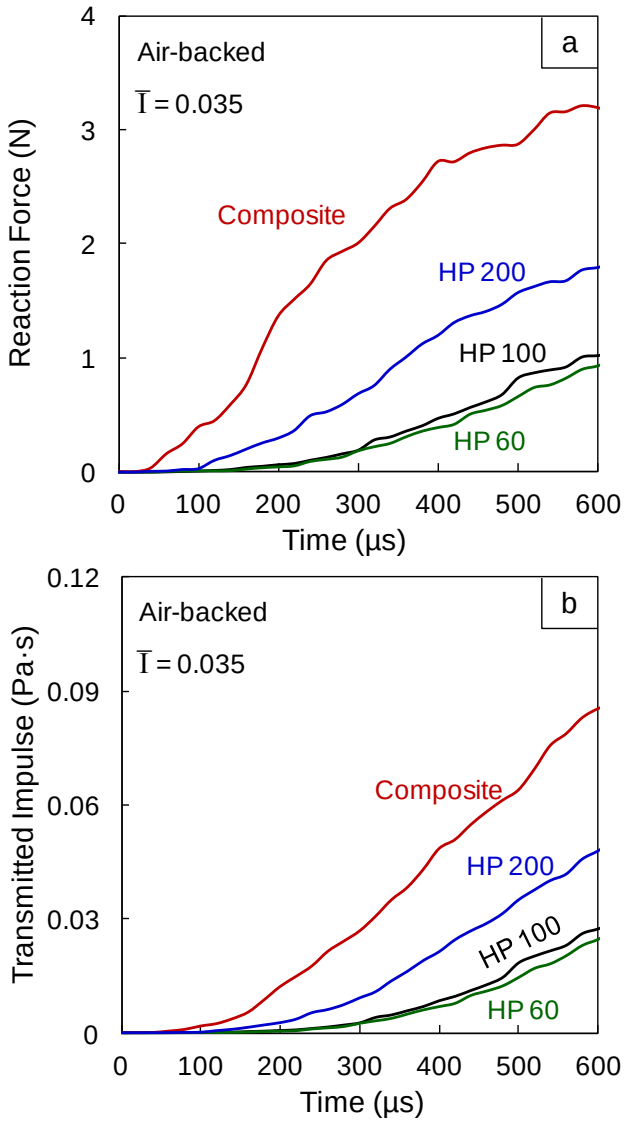

Figure 5.13 Computational results for (a) reaction forces (averaged over the end-nodes of the supports) and (b) transmitted impulses as functions of time for different composite structures.

Figure 5.14 shows the transmitted impulses as a function of impulse for different structures. In comparison to the monolithic composite plate, the sandwich structure with HP200 core transmits ~20% less impulse, that with HP100 core transmits ~50% less impulse and that with HP60 core transmits ~60% less impulse. HP60 and HP100 cores

exhibit identical characteristics while HP200 and monolithic composite beams transmit much higher impulses, echoing the trends observed for deflections. Weak-cores consistently outperform strong-cores for all load intensities.

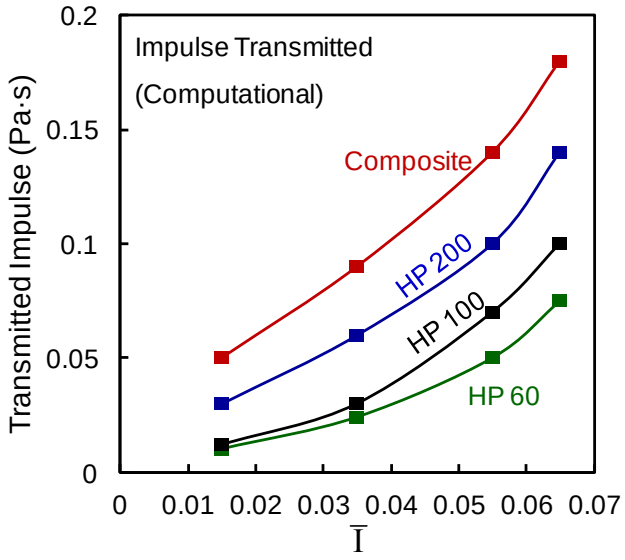

Figure 5.14 Computational results for transmitted impulses as a function of peak-pressure for different composite structures.

5.5 Very high-strain-rate response of composite sandwich structures

A separate study was carried out to test the sandwich structures under very intense pressure loads. This study is included in a separate section because the rate-effects for this impulse magnitude are significantly higher. The projectile was accelerated to a velocity of 210 m/s and generated a peak pressure of 245 MPa, shown in Figure 5.15.

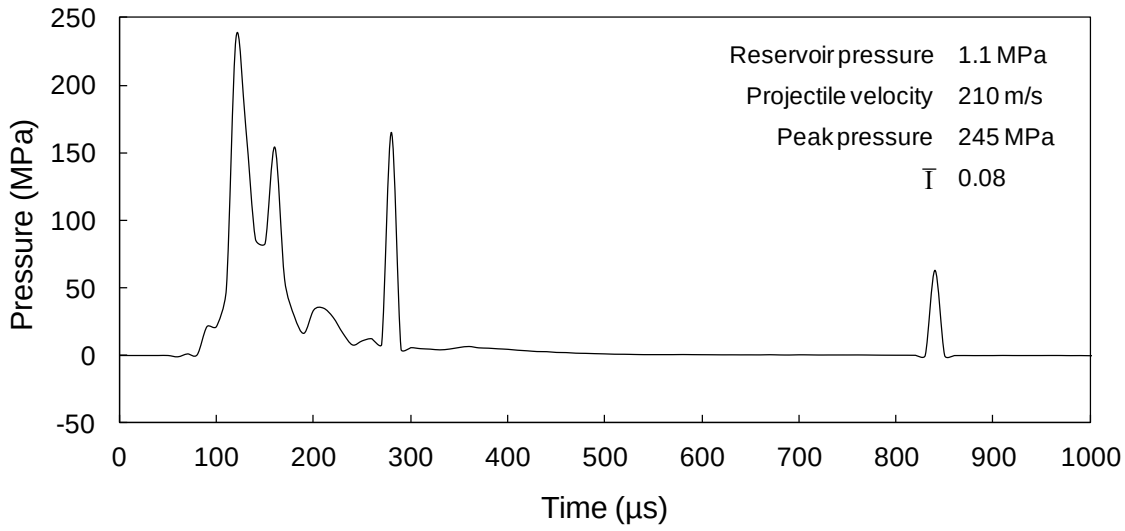

Figure 5.15 Pressure history for an impulse produced by a projectile of velocity 210 m/s and $\bar{I} = 0.08$.

Figure 5.16 shows a sequence of high-speed photographs showing the deformation in different composite structures. Figure 5.16 (a) shows the dynamic response of monolithic composite plate - which is quite identical to previously discussed high-speed photographs of a monolithic composite beam.

Figure 5.16 (b) shows the dynamic response of a sandwich structure with HP200 core. The core fractures in a direction perpendicular to the planar wave and causes considerable core-face debonding in both the front and the back-faces. Core-compression is negligible and fragmentation is observed near the supports.

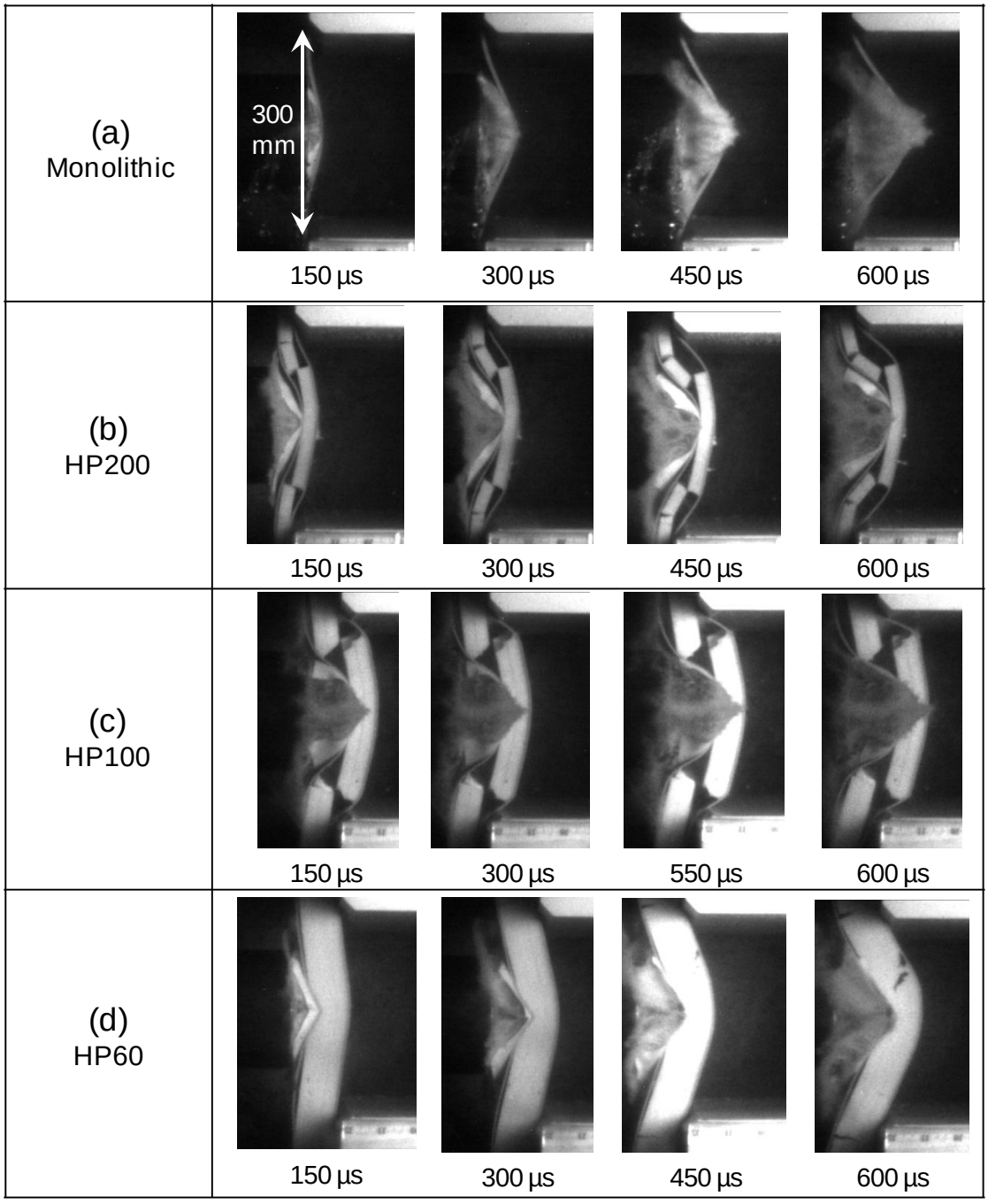

Figure 5.16 Sequence of high-speed photographs showing the deformation in composite structures : (a) monolithic plate; (b) HP200; (c) HP100 and (d) HP60.

Figure 5.16 (c) shows the dynamic response of a sandwich structure with HP100 core. The HP100 core fractures at an inclined angle from the loading area and simultaneously undergoes core-compression and crushing. The dynamic response of a sandwich structure with an HP60 core is shown in Figure 5.16 (d). Core-compression and frontface-wrinkling failure is observed at $t = 150\,\mu s.$ Core indentation occurs at $t = 300\,\mu s$ and the core starts cracking at $t = 450\,\mu s.$ Damage and deformation in the sandwich structure with a HP60 core is significantly lesser than in other composite structures. Sandwich structures with HP60 cores undergo higher bending.

Figure 5.17 shows the midpoint displacements as functions of time for the four different composite structures subjected to underwater impulsive load corresponding to Figure 5.15. The sandwich structures with HP 200 and HP100 cores and the monolithic structures show identical deformation histories reaching a Δ/L value of 0.25 at approximately the same rate. The sandwich structure with HP60 cores shows superior blast mitigation, deflecting at a lower rate and reaching a Δ/L value of 0.17, ~30% lesser than the other sandwich structures. The rate of deflection in the HP60 sandwich structure is close to the other structures till $t = 600\,\mu s$ and then reduces over the remaining time. This study clearly shows that thick, low-density cores consistently outperform high-density cores. The primary damage modes in low-density cores are core-indentation and tensile-fracture.

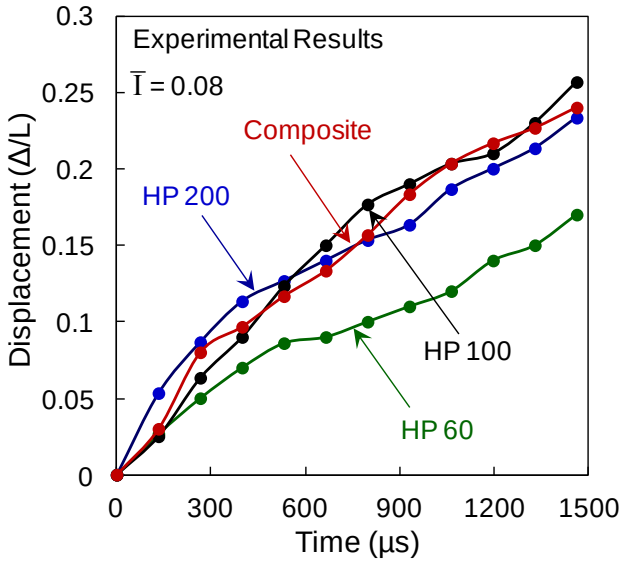

Figure 5.17 Midpoint displacements as a function of time for high-intensity loading. The sandwich structure with low-density core outperforms the sandwich structures with stiffer cores.

5.6 Structural Design

Figure 5.18 shows the normalized deflections (Δ/L) for all 16 configurations as functions of impulse $\bar{I}$ and relative density $\bar{\rho}$. The vertical axis shows the normalized deflection. At all impulse magnitudes, structures with the lowest relative density experience the least deflections. The deflections increase with increasing relative density as well as impulse magnitudes. HP200 cores perform only marginally better than monolithic structures. HP100 and HP60 cores exhibit significantly higher blast resistances in comparison to HP200 core and the monolithic composite. The relationship between deflection in air-backed structures (Δ/L_{AB}), and incident impulse $(\bar{I})$ and relative density $(\bar{\rho})$ can be given by

$$\Delta / L_{AB} = 16.54 \cdot \bar{\rho}^{(0.45)} \cdot \bar{I}^{(1.28)}. \tag{51}$$

The energy dissipation for all 16 configurations as a function of impulse $(\bar{I})$ and relative density $(\bar{\rho})$ is shown in Figure 5.19. The energy dissipation in sandwich structures is strongly influenced by both core relative density and impulse magnitude. Monolithic composite laminates consistently dissipate higher amounts of energy in comparison to the sandwich structures. The variation of energy dissipation in air-backed structures (E_{AB}) can be quantified using the non-dimensional terms $\bar{I}$ and $\bar{\rho}$ as,

$$E_{AB} = 657 \cdot \bar{\rho}^{(0.38)} \cdot \bar{I}^{(1.01)}. \tag{52}$$

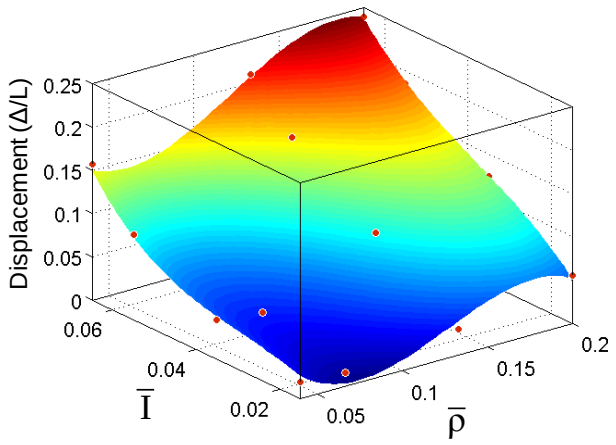

Figure 5.18 Normalized displacement in air-backed structures as function of incident impulse $\bar{I}$ and core relative density $\bar{\rho}$.

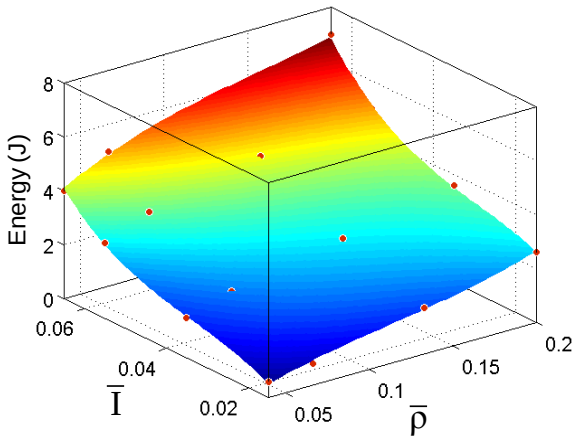

Figure 5.19 Energy dissipated due to inelastic deformation in air-backed structures as a function of incident impulse $\bar{I}$ and core relative density $\bar{\rho}$.

While structures with low relative densities exhibit low deflections, these structures also exhibit lower energy absorbency compared to those with high relative densities. The fact that structures which dissipate more energies also exhibit higher deflections indicates that the internal failure modes in the sandwich structures have a considerable effect on dynamic response. Alleviating the effects of damage mechanisms in the sandwich structure can significantly improve overall blast resistance.

The preceding discussions have focused on the deformation, deflection and of energy dissipation in composite structures subjected to underwater impulsive loads. In particular, the results of parametric studies have been presented in a format wherein the response variables are functions of the loading (impulse magnitude) and structural attributes (relative density). In structural design, the necessary performance objectives are specified and the structural attributes that fulfill these objectives are identified. Figures

5.18 and 5.19 show the effect of loading and structural attributes on dynamic response and give material-structure-performance relationships. It should be noted that deflection and energy dissipation constitute competing performance requirements. An optimal composite structure design needs to balance low deflection and high energy dissipation. This balance is application-specific and may not be universal. The relations developed in this study allow the identification of optimal structural designs for given combination of deflection, energy dissipation and impulse transmission requirements. For a fixed value of deflection or energy dissipation, the optimum value of relative density for a specific impulsive load can be achieved by varying the material properties of the monolithic plate or sandwich core.

The material-structure-performance relations can be used to inform naval structural design with the precaution that they should only be used for the material, structural parameter ranges and loading conditions considered. Additionally, this study is concerned with the dynamic response of composite structures of equivalent mass. This necessitates significant variations in structural thickness to account for changes in relative densities, which is an important geometric consideration in naval structural design. As the relative density of the structure increases, structural thickness decreases significantly. Structures with high relative densities exhibit higher energy dissipation per unit volume. This aspect is not investigated in the current analysis.

5.7 Concluding remarks

A novel experimental technique to generate underwater impulsive loads is designed and tested. Simply-supported sandwich composites with E-glass/polyester facesheets and PVC foam cores [73] are subjected to a range of underwater impulsive loads. The backface deflections are tracked using in-situ high-speed digital imaging with an Imacon 200D high-speed camera at a frame rate of ~20000 frames per second.

Finite element simulations are carried out, accounting for FSI effects, damage in the form of core-cracking and fragmentation, matrix-cracking and core-face debonding. The dynamic response of panels is investigated using this computational model and shows that the experiments and simulations are in good agreement. The model is then extended to different loading configurations that include a water-backed/submerged condition i.e. a loading condition in which the marine structure has water on the impulse-side as well as the back-side.

Failure in the monolithic structure is in the form of shear-cracking in the matrix, fiber-matrix debonding and fiber-fracture. In sandwich-composite face-sheets, failure in the front-face (impulse-side) is primarily in the form of compressive buckling failure which causes instantaneous core-face debonding followed by front-face rupture. Failure in the back-face is identical to the failure observed in monolithic-composite, showing matrix-cracking and fiber-matrix debonding under large tensile stretching.

Sandwich structures outperform monolithic composite structures at all load intensities. The damage mechanisms in low-density cores are primarily in the form core-indentation, core-crushing and cracking due to bending-stresses while in high-density cores are primarily in the form of face-wrinkling under compressive loads, face-rupture, core-cracking and fragmentation and core-crushing, in that order. An important aspect of the dynamic response of high-density cores is the delayed core-compression - high-density cores undergo large-scale fracture and fragmentation *before* the onset of core-crushing. Low-density cores undergo fracture simultaneously with core-crushing and fracture is primarily due to tensile loads created by bending deformation. Experiments demonstrate that the dynamic behavior of PVC foams is significantly influenced by rate-effects when loads are complex and multi-axial. All these damage and deformation modes are captured by the finite-element simulations.

The midpoint deflections and reaction-forces transmitted to supports are used as metrics to evaluate blast-resistance of sandwich panels. The lower the deflections and reaction forces, the better is the blast resistance. Results show that low-density cores are superior to high-density cores or monolithic composite structures, consistently showing lesser deflections and transmitting lower impulses. The sandwich structure with the HP60 core is the only composite structure studied here that does not undergo complete rupture, maintaining better structural integrity than other structures at very high intensity loads. Provided that the dimensional constraints are satisfied, on a per-mass basis, a combination of thick, low-density cores and thin stiff faces provide better blast-mitigation in marine structures subjected underwater impulsive loads.

6. DYNAMIC RESPONSE OF SUBMERGED MARINE STRUCTURES

6.1 Introduction

As discussed previously, marine structures are often subjected to complex, multi-axial loads due to underwater blasts and impacts. The dynamic behavior of structural materials under these loads is complicated and prediction of the dynamic response is difficult. An important factor that influences the dynamic behavior of marine structures is the environment in which they are situated. There are several sections of the ship structure that are submerged and have water on both sides, namely the keel, hull, fins, rudders and turbine blades as illustrated in Figure 6.1. This condition is also observed in applications like water and oil-pipes, oil-tankers and so on.

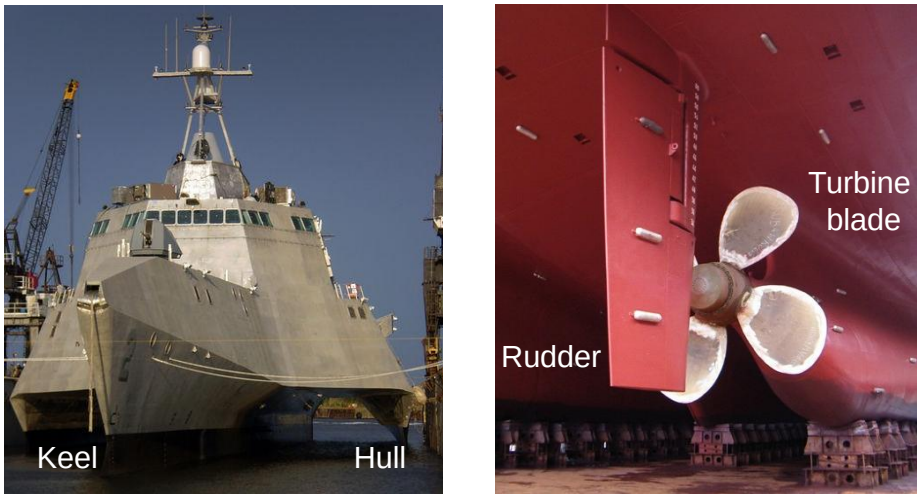

Figure 6.1 Sections of ships in a submerged environment including keel, hull, rudder and turbine blades. These sections are designed to withstand dynamic loads.

The objective of this computational study is to analyze the dynamic response of submerged or water-backed structures subjected to underwater impulsive loads. Finite

element simulations discussed in chapter 4 are extended to account for submerged conditions. Damage modes and failure mechanisms for air-backed as well as submerged structures are analyzed. Results show that the dynamic behavior of submerged structures is significantly different that those of air-backed structures. Submerged structures experience ~60% lesser deflections and damage in the core is much more extensive as compared to air-backed structures. Due to lower deflections, the composite faces absorb very little energy and the majority of total energy-absorption (~90%) occurs in the core.

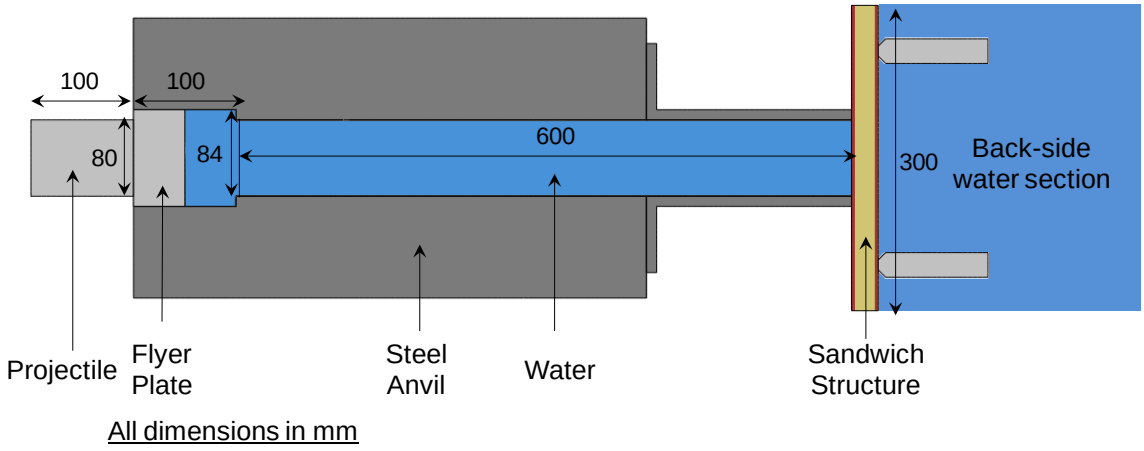

Figure 6.2 Sectional view of a simply-supported sandwich structure in water-backed conditions.

6.2 Finite-element simulations

The commercial code, Abaqus/Explicit, is used to carry out detailed, fully-dynamic finite element simulations accounting for deformation and damage in sandwich structures and fluid-structure interaction at the water-structure interface. Submerged environment is simulated by positioning a water-tank behind the composite structure. This water-tank is sufficiently large to prevent reflected waves from interacting with the

sandwich structure. Cohesive element based contact is implemented at the interfaces between the faces and core. The cohesive elements follow the bilinear traction-separation law. Non-penetrating, frictionless contacts are implemented at the water-structure interface, flyer-water interface, projectile-flyer interface and structure-supports interfaces. Components consisting of composites and PVC foams are meshed with 2-D 8-node brick elements with 5 integration points through the thickness. The constitutive and damage models for these materials – glass fiber composite, PVC foam, water and aluminum - are explained in detail in chapter 2.

6.3 Dynamic deformation and damage

The sandwich structures are designed such that mass remains constant in spite of variations in material properties. Four load intensities are considered as shown in Figure 5.2 (a-d). Figure 6.3 shows a comparison of sequential contour plots of damage in air-backed and water-backed composite sandwich structures with HP60 cores for a pressure pulse corresponding to Figure 5.2(c). Due to the dense water section behind the composite structure, the back-face is prevented from deflecting. Hence, deformation mechanisms in the core are highly-localized and primarily in the form of core-crushing. Inclined cracks are not observed for water-backed structures – instead, the core near the impulsively loaded region experiences permanent inelastic deformations. The front-face experiences intense compressive loads and wrinkles but is relatively undamaged.

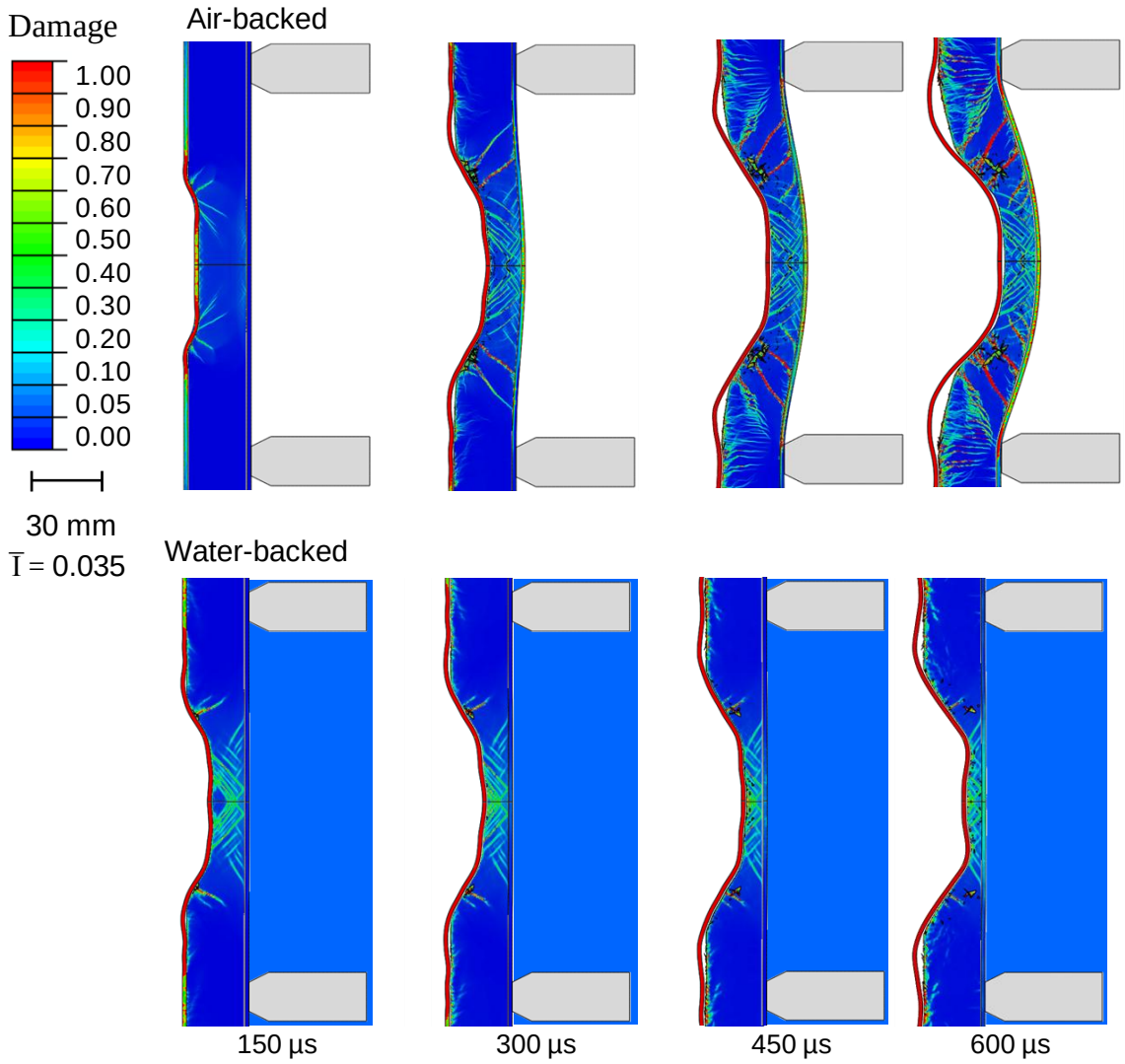

Figure 6.3 Comparison of deformations for a sandwich structure with HP60 core under air-backed and water-backed conditions. The dynamic response of the same sandwich structure in these two conditions is drastically different. In water-backed conditions, damage is highly localized and the faces are relatively undamaged due to lack of stretching.

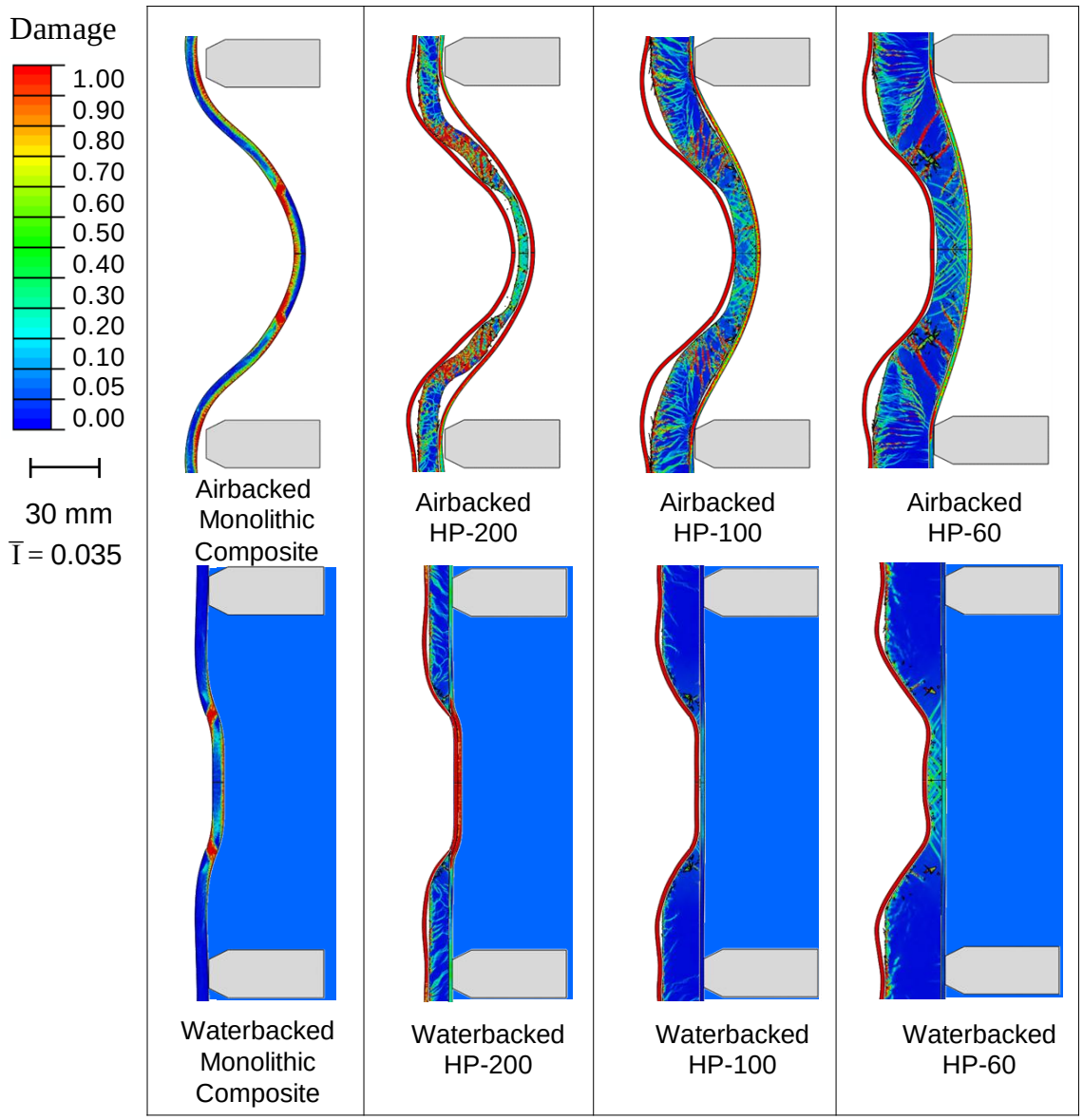

Figure 6.4 Comparison of damage contour plots for different composite structures subjected to underwater impulsive loads under air-backed and water-backed conditions (at $t = 1000\,\mu s$). The monolithic structure transmits the impulse instantaneously. As the core thickness *increases*, the magnitude and duration of transmitted impulse *decreases*.

Figure 6.4 shows contour plots of damage for different composite structures subjected to underwater impulsive loading shown in Figure 5.2(c). Clearly, for all structures, overall deflection under water-backed conditions is severely impeded due to

the presence of the back-side water-section. Damage is localized and the structure is relatively undamaged in regions that are away from the loading area. Flexural waves travel through the front-face and sever the core-face bonding. Since overall deflection is low, the stretching in the front and back faces is restricted. Consequently, damage in the form of matrix-cracking and rupture is negligible in both the faces. The dynamic response of water-backed sandwich structures is thus quite insensitive to face thickness and core-face bonds. In real applications, damage occurring in sandwich structures is largely invisible on the surface and can be severe inside the structure.

6.4 Deflection

Figure 6.5 shows a comparison of midpoint displacements as functions of peak pressure for composite structures subjected to underwater impulsive loads for both air-backed and water-backed conditions. Water-backed structures exhibit ~50% lesser deflection for all cores and impulse magnitudes in comparison to air-backed structures. For water-backed condition, in comparison to the monolithic composite structure (if monolithic composite deflection is 100%), sandwich structures with HP200 cores experience ~20% lesser deflection; those with HP100 cores experience ~70% less deflection and those with HP60 cores experience ~80% less deflection. Thick cores made of weaker material consistently outperform thin cores made of stronger material. As the dynamic deformation in water-backed sandwich structures is highly localized near the loading area, the reaction forces transmitted to the supports are insignificant. Consequently, reaction forces and transmitted impulses *measured at the supports* cannot

be used as metrics to determine blast-resistance. However, the transmitted impulses measured in the back-side water-section can be used to evaluate the blast-resistance of water-backed structures.

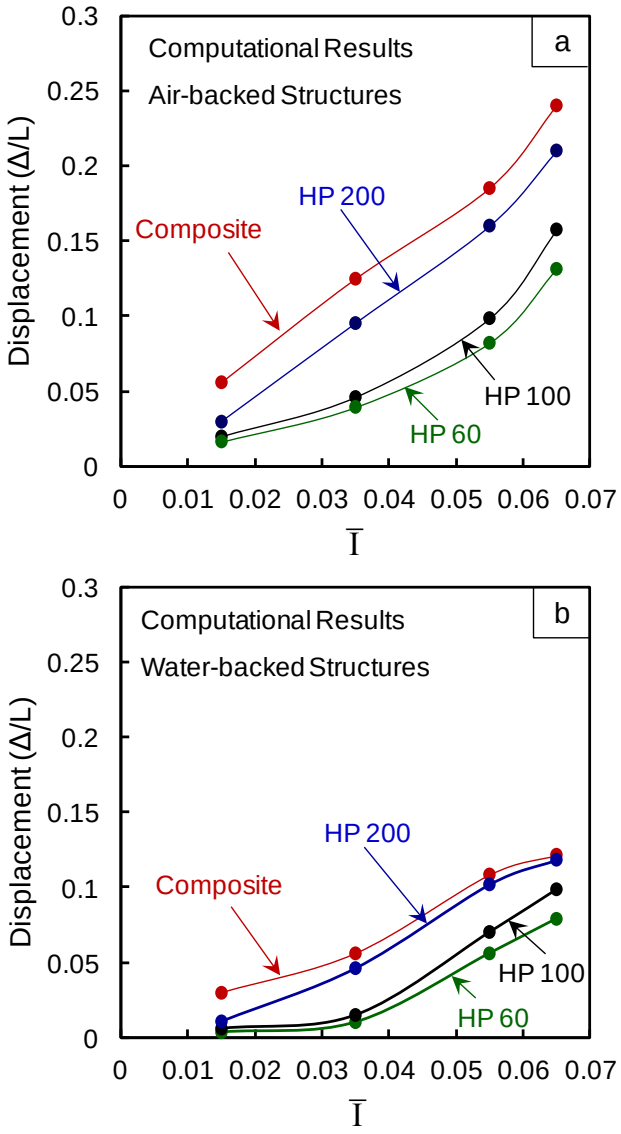

Figure 6.5 Midpoint displacements as functions of peak pressure for different composite structures under air-backed and water-backed conditions.

6.5 Transmitted impulses

The resistance of a water-backed structure to applied impulse can be quantified by how much of the applied impulse is transmitted into the water-backed section. Figure 6.6 shows the transmitted pressure histories for different sandwich structures subjected to an impulsive load corresponding to Figure 5.2 (c). The monolithic composite structure exhibits the least blast mitigation of all the structures studied – transmitting ~80% of the incident impulse into the back-side water-section. The HP200 core transmits ~40% of the incident impulse. In the core-compression regime, which is 100 μs, the impulse transmitted is very small. However, when the core fails completely, the front-face hits the back-face causing a pressure wave to be generated in the back-side water-section. The sandwich structure with the HP100 core transmits ~20% of the incident impulse with characteristics similar to HP200 – a low-pressure plateau followed by complete core failure and a rise in pressure magnitude. The sandwich structure with the HP60 core exhibits superior blast mitigation in comparison to all other composite structures – transmitting less than 5% of the incident impulse at the end of 1000 μs. Clearly, blast mitigation, while relatively insensitive to face thickness, is dependent on core-density. Weak, thick provide the highest blast mitigation on a per-weight basis.

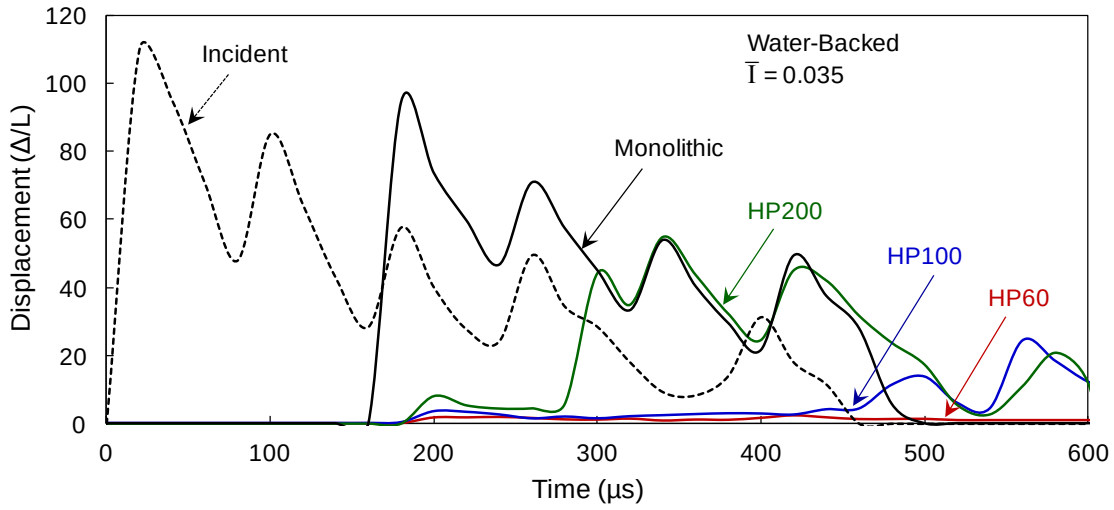

Figure 6.6 Transmitted pressure histories for water-backed composite structures.

6.6 Energy absorption

Energy dissipation in composite sandwich structures is a complex phenomenon because there are a multitude of inelastic deformations that can occur under high-strain-rate loading. The inelastic deformations commonly encountered in composite materials are delamination, matrix fracture, matrix-fiber debonding, fiber pullout, fiber-fracture. The inelastic deformations in the PVC foam core are core-ligament fracture, core-wall-collapse, core cracking and fragmentation. Inelastic deformations in composites as well as PVC foams have been shown using high-speed in-situ photography and post-mortem analysis. In finite-element simulations, all these energy dissipation mechanisms are amalgamated into a single scalar parameter called “internal energy”. Figure 6.7 shows the internal energy dissipation in a sandwich structure with HP60 core subjected to an impulsive load corresponding to Figure 5.2 (c) for both air-backed and water-backed conditions.

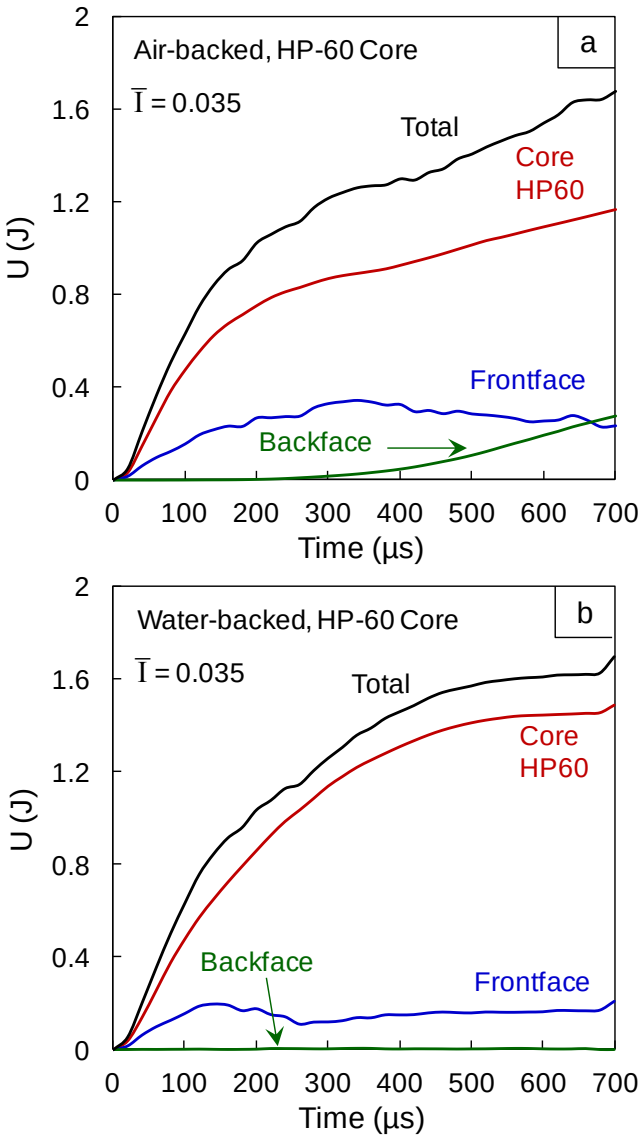

Figure 6.7 Energy dissipation in the form of inelastic deformations and damage as a function of time for different components of a sandwich structures with HP60 cores for (a) air-backed and (b) water-backed conditions.

In air-backed conditions, as a percentage of total energy dissipated, the core dissipates ~70%, the front-face ~15% and back-face ~15%. The same sandwich structure subjected to identical loads under water-backed conditions shows significantly different energy partitioning with the core dissipating ~90% of the total energy, the front-face

dissipating ~10% of the energy and negligible energy dissipation in the back-face. This indicates that the dynamic deformations in the core define the overall dynamic response of the sandwich structure – strong cores transmit large impulses, while weak cores transmit smaller impulses.

6.7 Structural Design for Water-Backed Structures

Figure 6.8 shows the normalized deflections (Δ/L) for all 16 unique configurations for the water-backed case as functions of impulse $(\bar{I})$ and relative density $(\bar{\rho})$. The relationship between overall deflection (Δ/L_{WB}) and $\bar{I}$ and $\bar{\rho}$ is given by

$$\Delta/L_{WB} = 19.43 \cdot \bar{\rho}^{(0.36)} \cdot \bar{I}^{(1.6)}. \tag{53}$$

The energy dissipation for all 16 configurations as a function of impulse $(\bar{I})$ and relative density $(\bar{\rho})$ is shown in Figure 6.9. Comparing Figure 6.9 and Figure 5.19 indicates that the trend in energy dissipation for the water-backed cases is opposite to that for the air-backed cases. Specifically, structures with low relative density absorb higher amounts of energy. The variation in energy dissipation in water-backed structures (E_{WB}) can be quantified using the non-dimensional measures $\bar{I}$ and $\bar{\rho}$ as,

$$E_{WB} = 74.48 \cdot \bar{\rho}^{(-0.12)} \cdot \bar{I}^{(1.02)}. \tag{54}$$

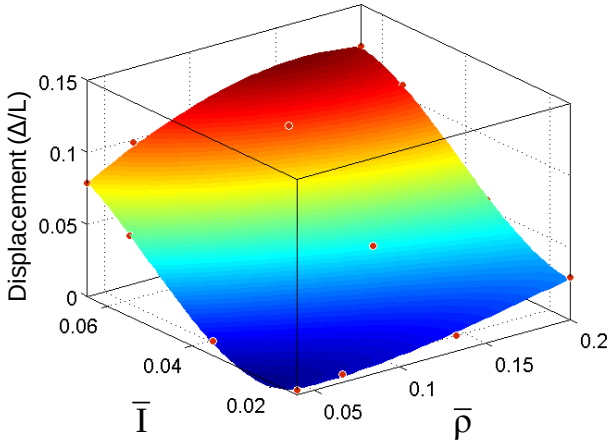

Figure 6.8 Normalized displacement in water-backed structures as a function of incident impulse $\bar{I}$ and core relative density $\bar{\rho}$.

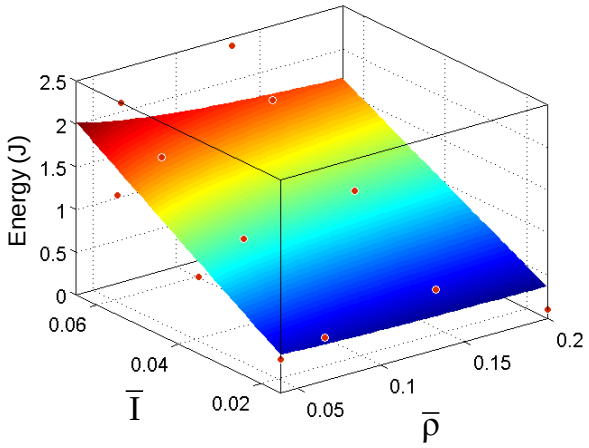

Figure 6.9 Energy dissipated due to inelastic deformation in water-backed structures as a function of incident impulse $\bar{I}$ and core relative density $\bar{\rho}$.

The impulse transmitted by all 16 configurations in the water-backed case is shown as a function of $\bar{I}$ and $\bar{\rho}$ in Figure 6.10. At all impulse magnitudes, the

magnitude of the transmitted impulse increases monotonically with the relative density. The relationship between transmitted impulse $\left(\bar{I}_T\right)$ and $\bar{I}$ and $\bar{\rho}$ is given by

$$\bar{I}_T = 7.40 \cdot \bar{\rho}^{(1.33)} \cdot \bar{I}^{(1.01)}. \tag{55}$$

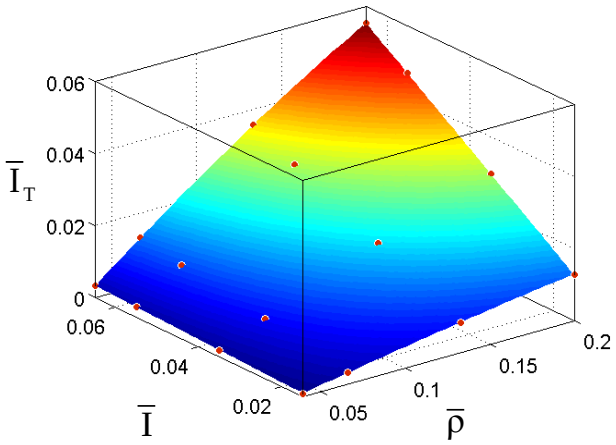

Figure 6.10 Transmitted impulses measured in the back side water for water-backed structures as a function of incident impulse $\bar{I}$ and core relative density $\bar{\rho}$.

6.7 Concluding remarks

Detailed finite element simulations are carried out to characterize the dynamic response of water-backed composite structures i.e. structures with water on both- the impulse-receiving face and the back-face. Results show that the dynamic response of such structures is drastically different than air-backed structures i.e. structures with water on the impulse-side and air on the back-side.

The monolithic composite structure experiences slight damage and transmits most of the impulse into the back-side water-section. Damage in the monolithic-composite is in the form of matrix compressive failure and shear-localization.

In sandwich structures, core-compression and crushing are highly localized near the loading region. Since large-scale bending is prevented due to water-backed condition, no inclined cracks originate at the loaded area and fragmentation is negligible. Damage is primarily in the form of core-crushing and core shear fracture. Large scale debonding is observed at the frontface-core interface. In the sandwich structures, since deflection is severely restricted, tensile stretching in the face sheets is negligible. In the front-face (impulse-side), wrinkling failure occurs under compressive loads but there is no rupture. The back-face experiences a "cushioning" effects, whereby it does not experience any deformation until the core is completely crushed and the front-face impacts the back-face. It is observed that high-density cores transmit a larger fraction of incident impulses in comparison to low-density cores.

Blast-mitigation is relatively insensitive to face properties and highly sensitive to core thickness and density. Weak cores allow a stress-saturated compressive-strain regime and greatly reduce the intensity of the incident impulse and consequently also the transmitted impulse.

The deflection and the magnitude of the pressure-wave transmitted to the back-side water-section are used as metrics to evaluate the blast-resistance. Water-backed structures, on average, undergo ~50% lesser deflection than air-backed structures. The

transmitted pressure waves show that the monolithic structures transmit ~80%, HP200 core transmits ~40%, HP100 core transmits ~20% and HP60 core transmits negligible pressure into the back-side water-section.

There are a number of instances in which water-backed loading conditions are observed. In some of these instances, it is more advantageous to *transmit* the largest possible fraction of incident impulse through the structure rather than absorbing the incident impulse. For example, in ship sections such as the keel, turbine-blades and rudders, the back-side region of the marine structure does not need protection because the transmitted wave has no effect on the ship. In these instances, strong, monolithic composite structures or sandwich structures with high-density cores are more effective, because they transmit a large fraction of the incident impulse and undergo less damage.

Contrary to that, there are also instances in which it is more advantageous to *absorb* the incident impulse and transmit the minimum possible fraction of incident impulse. For example, in ship sections such as underwater pipelines, protective structures and hull, the back-side sections needs to be protected against the incident wave. In these instances, sandwich structures with low-density cores are more effective, because they transmit the smallest fraction of incident impulse.

7. EFFECT OF FACE STIFFNESS ON DYNAMIC RESPONSE

7.1 Introduction

The objective of this study is to examine the effect of the ratio between facesheet thickness and core thickness on the dynamic response of composite sandwich structures. To this end, the core thickness and core density are kept constant and the thickness of the facesheets is varied. Under this condition, the total mass of the structure changes with the thickness of the facesheets. Another approach is to keep the total weight constant and vary the thicknesses of the core and the facesheets accordingly. The second approach can lead to unrealistic sandwich designs and, therefore, is not followed here. We quantify the response of the structures using fiber and matrix damage, facesheet deflections and energy absorbed. The results are analyzed in both normalized and non-normalized forms to gain insight into underlying trends that can be explored in the design of materials and structures.

7.2 Structures Analyzed

The load configuration analyzed consists of a sandwich plate subject to impulsive loading at its center. The plate can be regarded as a portion of a ship's hull. The exponentially decaying pressure pulse has an impulse consistent with what is first proposed by Taylor [105]. Figure 7.1 shows a schematic illustration of a square sandwich

plate 300 × 300 mm in size with a loading area of 76 mm in diameter at the center. The load area is 5% of the total area of the plate.

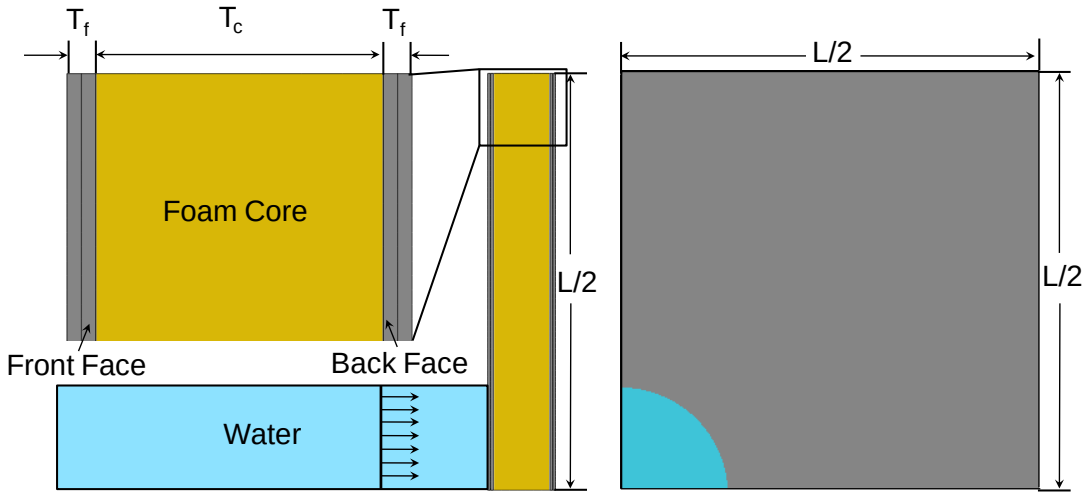

Figure 7.1 Configuration of planar sandwich structures subject to water-based impulsive

The outer boundaries of the plate are clamped. The symmetries of the plate and loading allow a quarter of the total plate to be considered in the simulations. All panels have a core thickness of M_c mm and a core density of 100 kg/m^3, giving a core unit areal mass of M_c = 2 kg/m^2. The side length of the plate is L = 300 mm. The facesheets, consisting of plies 0.25 mm in thickness each, are modeled with continuum shell elements. The total facesheet thickness T_f varies from 1 to 20 mm, giving rise to different areal mass values of the sandwich plates. The ratio between the facesheet thickness and the core thickness is $R = T_f / T_c$. All plates have the same material properties. Figure 7.2 illustrate the sandwich plates analyzed, the T_f / T_c value ranges from 0.05 to 0.4. The insets show magnified views of the plates. In the numerical

simulations, the plates are considered to be free of defects due to manufacturing variability and without any pre-stress.

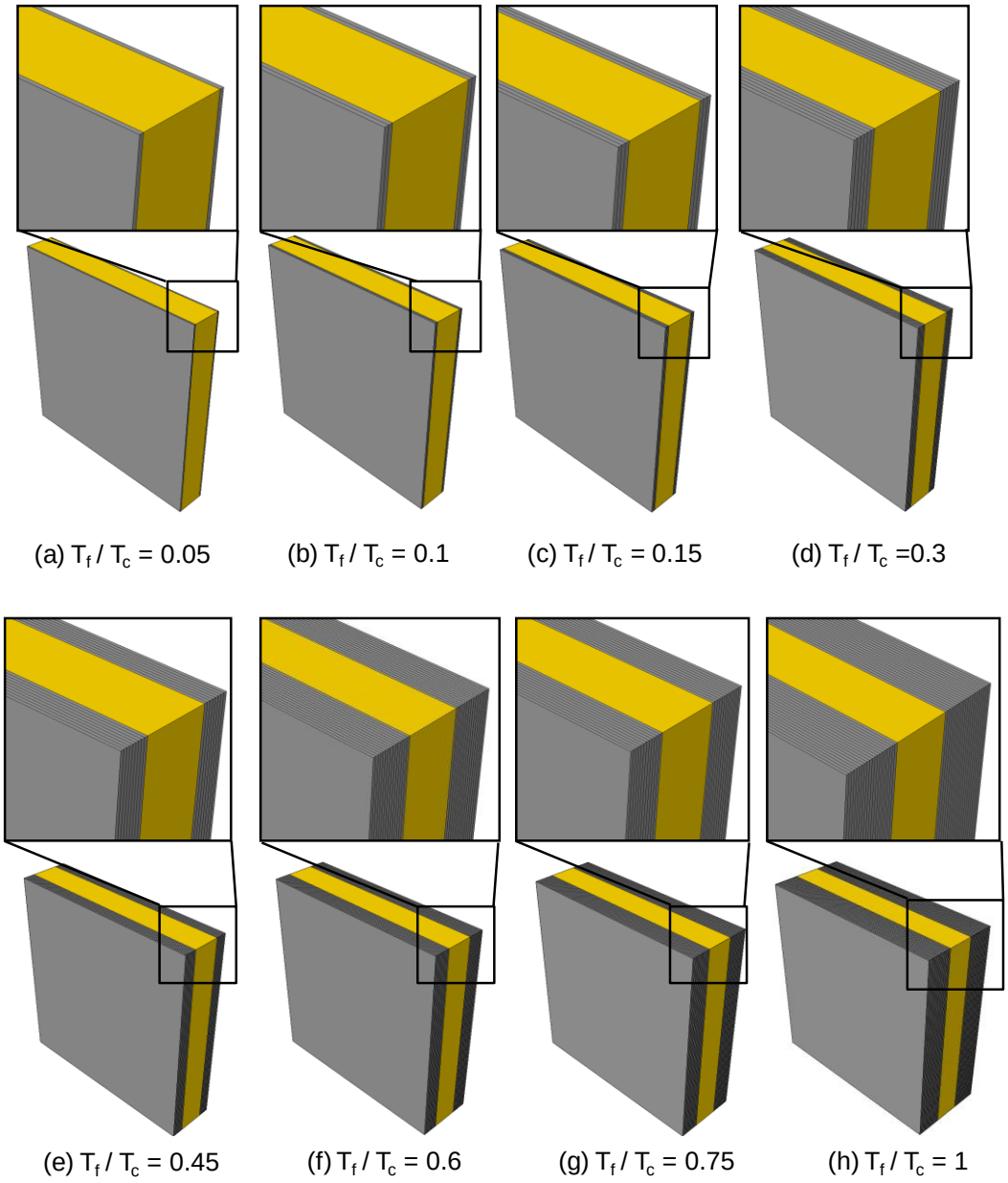

Figure 7.2 Configurations of composite sandwich structures with different facesheet thicknesses.

7.3 Finite Element Model

The numerical model explicitly accounts for the projectile, piston plate and water column in contact with the sandwich plate target. The projectile is prescribed with an initial velocity V_0. Simulations are carried out with a Lagrangian description for the water and target. Since the Lagrangian framework produces water-structure interactions and accurate pressures and impulses, this framework is used for the current set of calculations.

The projectile, piston, water and foam core are discretized with 8-node 3D brick elements while the composite facesheets are discretized with continuum shell elements. A $(0/90)_S$ layup is specified for each ply in the facesheets. For the composite material of the facesheets, an element is deleted if internal damage exceeds a pre-determined threshold. The constitutive and damage response of all materials considered in this analysis are given in chapter 2. A master-slave contact algorithm is used for interactions between the facesheets and core and a non-penetrating, general contact algorithm is implemented at projectile-piston, piston-water and water-sandwich structure interfaces. Cohesive elements are used at the core-facesheet interface to simulate core-facesheet debonding [101, 106]. A bilinear cohesive law is implemented accounting for mixed-mode failure at interfaces. Post-failure, the normal penalty-contact algorithm is enforced to prevent interpenetration. The following quantities are tracked to quantify and compare the responses of the sandwich plates:

1. the displacements at the center of facesheets 1 and 2;
2. core crushing rate and core crushing strain;

3. energy dissipated in the structure; and
4. compressive and tensile damages in the facesheets.

When an explosive detonates in a marine environment, the expanding chemical products compress the surrounding water and propagate outwards at high velocities. The shock wave can be described by the Rankine-Hugoniot jump equations which are derived from the conservation of mass, momentum and energy. At any distance from the point source, the blast pressure exponentially decays over time. Underwater blasts are much more harmful than air blasts because the impedance mismatch between water and sandwich structures is smaller than that between air and sandwich structures. Also, underwater blast waves propagate farther and maintain their magnitude over larger distances than air blast waves. The pressure wave can be described by the equation

$$p(t) = p_0 \exp\left(-\frac{t}{t_0}\right) \tag{56}$$

where p_0 is the peak pressure, t is time at which measurement is carried out and t_0 is the decay time. Impulse is calculated as

$$I = \int_0^t p(t)\,dt \tag{57}$$

A non-dimensional impulse is defined for dimensional analysis, such that

$$\bar{I} = \frac{I}{\rho_w c_w \sqrt{A}}, \tag{58}$$

where ρ_w is the density of water, c_w is the speed of sound water and A is the area under impulsive loading.

Different values of peak pressure and decay time are obtained by varying the initial velocity of the projectile. Apart from the projectile velocity, other factors that influence the pressure pulse are projectile mass, piston plate thickness, and the shape of the shock tube. All variables are varied to obtain impulses that best match analytical predictions from the Taylor analysis [105]. The pressure decays faster in the numerical data largely due to higher dissipation rates in the finite element description. Hence, the parameters in the equation of state for water are adjusted to obtain close matches between the numerical and analytical results.

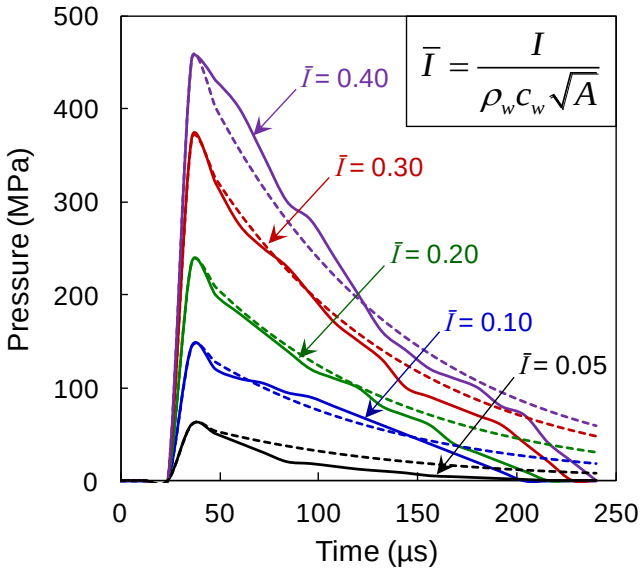

Figure 7.3 Pressure pulses measured in the water-chamber compared to theoretical pressure pulses.

7.4 Dynamic deformation and damage

To illustrate the process at hand, Figure 7.4 shows the distribution of particle velocity at different times after the projectile impact on the piston. The projectile velocity is 200 m/s (giving an impulse of $\bar{I} = 0.2$). The particular sandwich structure has thickness ratio of $T_f/T_c = 0.05$. The velocity is relatively uniform across the cross-section of the shock tube and the reflection of the pulse from the water-target interface can be seen. Cavitation occurs at the water-target interface when the pressure drops to zero.

The deformation of the core shows three distinct stages of response: (1) onset of core crushing, (2) onset of motion of back-face and (3) momentum transfer through the structure. Changes made to the facesheets affect all three stages. In general, all things being equal, structures with thicker facesheets are stronger in an absolute sense, since more material is used. To reveal trends on a per weight basis, we analyze the results in both normalized and non-normalized forms.

Five different impulse levels are considered. The impulses per unit area are $\bar{I} = 0.4, 0.3, 0.2, 0.1$ and 0.05 where $\bar{I} = \left[I \Big/ \left(\rho_w c_w \sqrt{A} \right) \right]$. We first consider the results for $\bar{I} = 0.2$ and then compare the results for different impulse levels. Facesheets with thicknesses less than 6 mm ($T_f/T_c < 0.3$) are classified as "thin facesheets" and facesheets with thicknesses greater than 6 mm ($T_f/T_c > 0.3$) are classified as "thick facesheets".

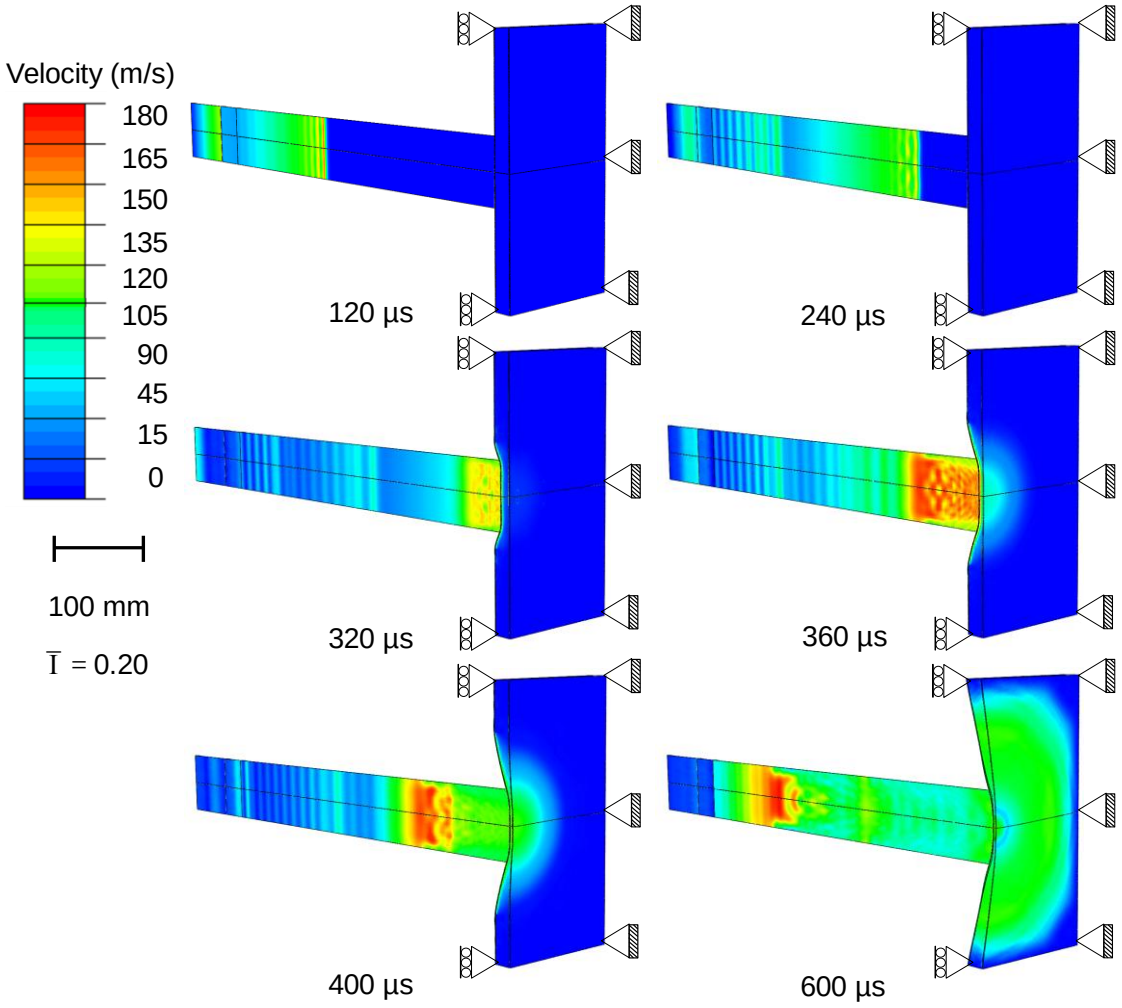

Figure 7.4 Sectional views of an impulsive loading process obtained by three-dimensional finite element simulation. The sequence of images show the distributions of particle velocity at different times. The impulsive loading intensity is $\bar{I} = 0.2$.

Figure 7.5 shows the distribution of tensile damage in the matrix for the last plies of the facesheets 600 µs after onset of deformation in a sandwich plate with a facesheet thickness of 1 mm ($T_f / T_c = 0.05$). The load intensity is $\bar{I} = 0.2$. Damage in the front sheet (front-face) is more severe and is dependent on fiber orientation. Maximum damage occurs close to the loading area and spreads outward in later stages of the loading event.

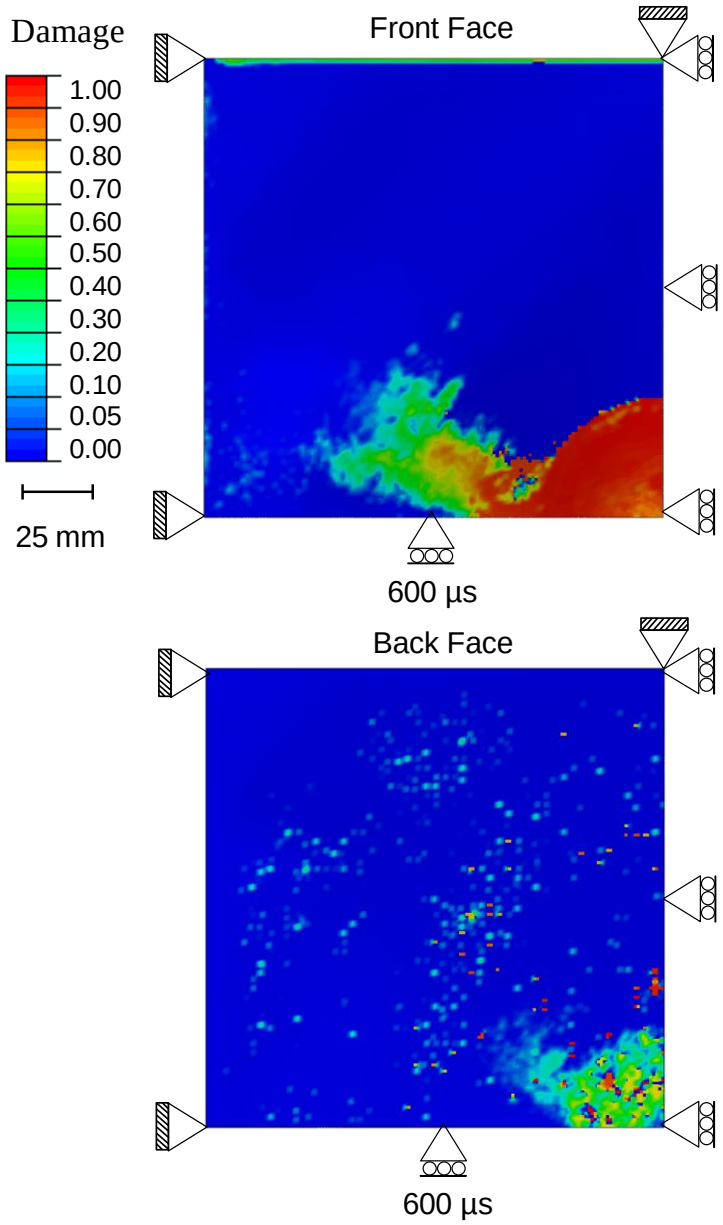

Figure 7.5 Distributions of tensile damage in the matrix of the facesheets at $t = 600\ \mu$s. $T_f / T_c = 0.05$ and $\bar{I} = 0.2$. The plies shown are oriented horizontally.

Figure 7.6 shows the corresponding distributions of equivalent plastic strain at three different times for this structure sandwich. The arrival of the load pulse at the target is taken as $t = 0$. Core compression occurs immediately after the onset of loading. Back-

face starts to deform at $t = 100\,\mu s$ and has acquired significant momentum by $t = 500\,\mu s$. Since the facesheets are thin, core crushing is highly localized and the rate of deformation is highly non-uniform in the core. Significant core-facesheet debonding is observed at late stages of the deformation.

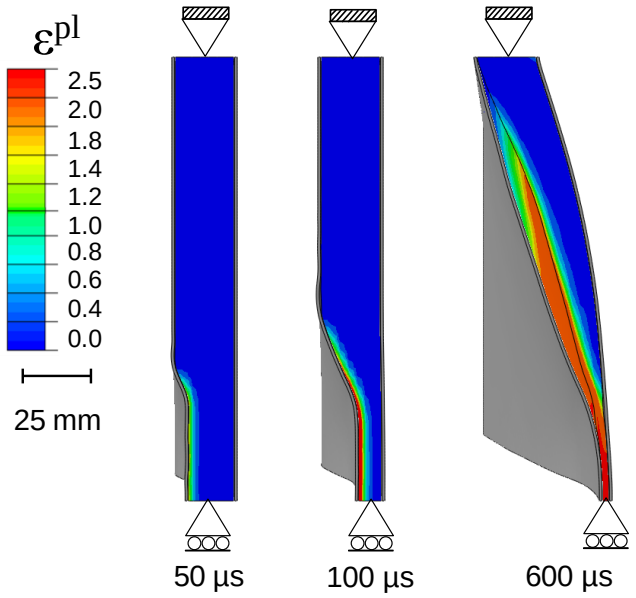

Figure 7.6 Distributions of equivalent plastic strain in the core at different times for $T_f / T_c = 0.05$ and $\bar{I} = 0.2$.

Figure 7.7 shows the tensile damage in the matrix for the last plies of the facesheets in a sandwich structure with a facesheet thickness of 8 mm ($T_f / T_c = 0.4$). While the damages in front-face for both $T_f / T_c = 0.05$ (Figure 7.5) and $T_f / T_c = 0.4$ (Figure 7.7) are similar, the damages in back-face are quite different, with the damage for $T_f / T_c = 0.4$ being much lower than that for $T_f / T_c = 0.05$. Beyond $T_f / T_c = 0.4$, there is

essentially no further improvement in damage resistance. This observation is supported by the analysis of deflections discussed in next section.

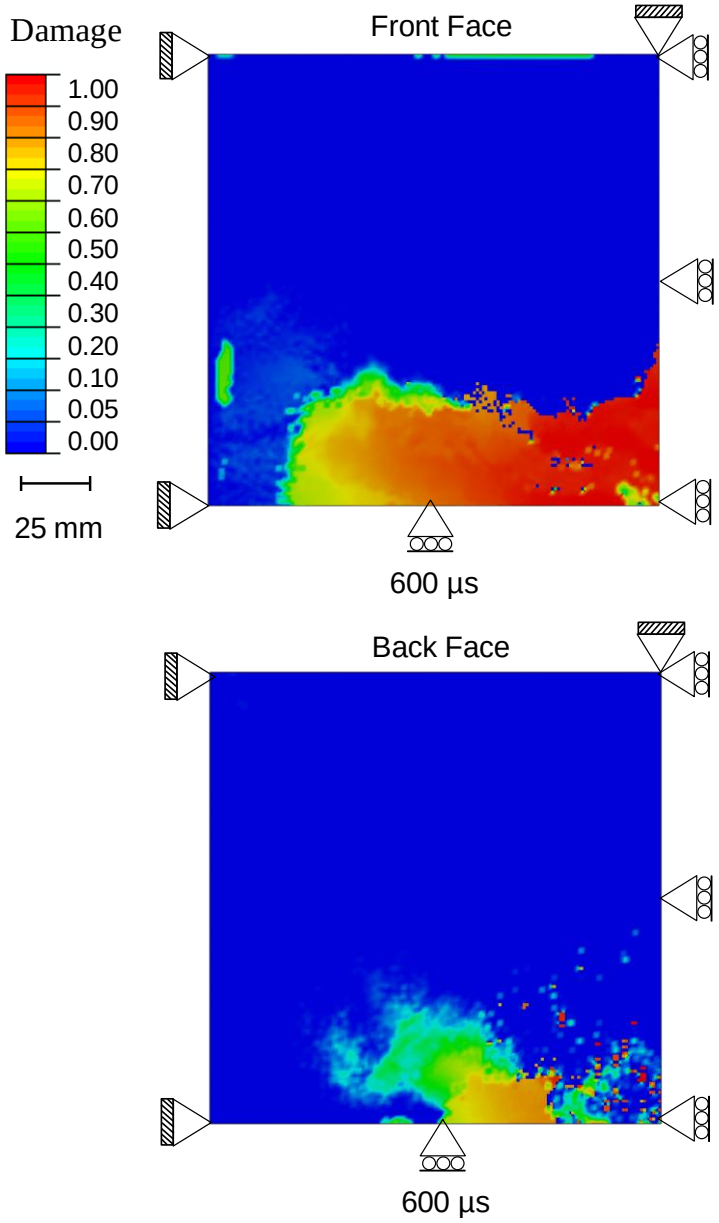

Figure 7.7 Distributions of tensile damage in the matrix of the facesheets at $t = 600\ \mu s$. $T_f / T_c = 0.4$ and $\bar{I} = 0.2$. The plies shown are oriented horizontally.

Figure 7.8 shows the corresponding distributions of equivalent plastic strain for the sandwich plate in Figure 7.7. Core deformation is more spread out relative to what is seen in Figure 7.6 (thinner facesheets) and the motion of back-face starts at a later time of $t = 140\,\mu s$ compared with what is seen in Figure 7.6. The back-face has acquired significant momentum by $t = 500\,\mu s$.

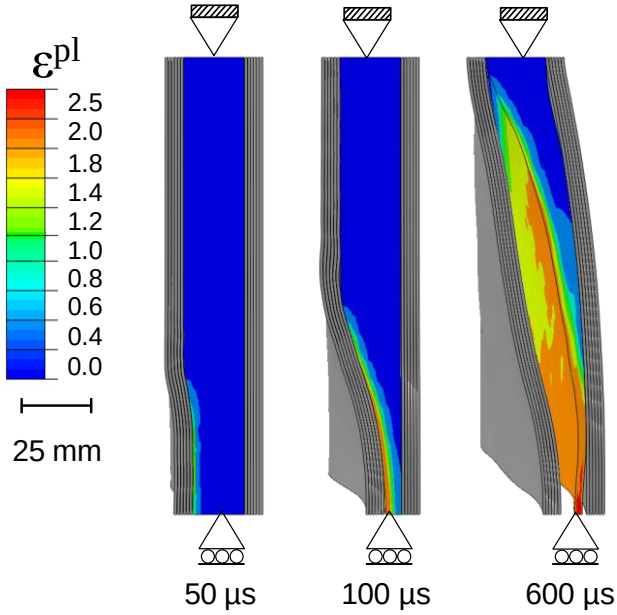

Figure 7.8 The distributions of equivalent plastic strain in the core at different times. $T_f / T_c = 0.4$ and $\bar{I} = 0.2$.

7.5 Deflection

The displacements at the center of the structures are used to quantify deflection and core compression. In particular, the displacements at the center of the front and back-facesheets (Δ) at 600 μs after the onset of loading are analyzed. The deflections are normalized with the side length (L) of the sandwich plates. Figure 7.9 (a) shows that Δ / L

increases with I and decreases with the ratio between the thickness of the facesheets and the thickness of the core (T_f/T_c) (and therefore decreases with the areal mass (M of sandwich plates). The deflection of back-face is generally lower than that of front-face, due to core compression. As T_f/T_c increases, the decreases in deflections are monotonic. At low impulse magnitudes ($\bar{I} < 0.1$), increasing facesheet thickness does not provide significant reductions in the deflections. As the impulse magnitude increases, the difference between the responses of structures with low T_f/T_c and the responses of those with high T_f/T_c becomes pronounced. For impulse magnitudes above 163 N·s, structures with high T_f/T_c values show markedly lower deflections. For example at $\bar{I} = 0.2, 0.3$ and 0.4, as T_f/T_c increases from 0.01 to 0.36, Δ/L decreases by approximately 56 %. If T_f/T_c increases from 0.6 to 1, Δ/L decreases by only ~5 %. At all impulse magnitudes, no appreciable reduction in the deflection of front-face is seen for $T_f/T_c > 0.6$.

The deflections of back-face shown in Figure 7.9 (b) are generally lower that the deflections of front-face but exhibit the same trend seen in Figure 13 (a). Overall, increasing the relative thickness of the facesheets up to a certain value ($T_f/T_c = 0.6$) can significantly decrease the deformation of the structures. Increases beyond this value yields no obvious benefit in terms of structural rigidity. Since the overall weight of the structures is one of the most important aspects in naval structural design, this finding points to a design criterion useful for relevant systems.

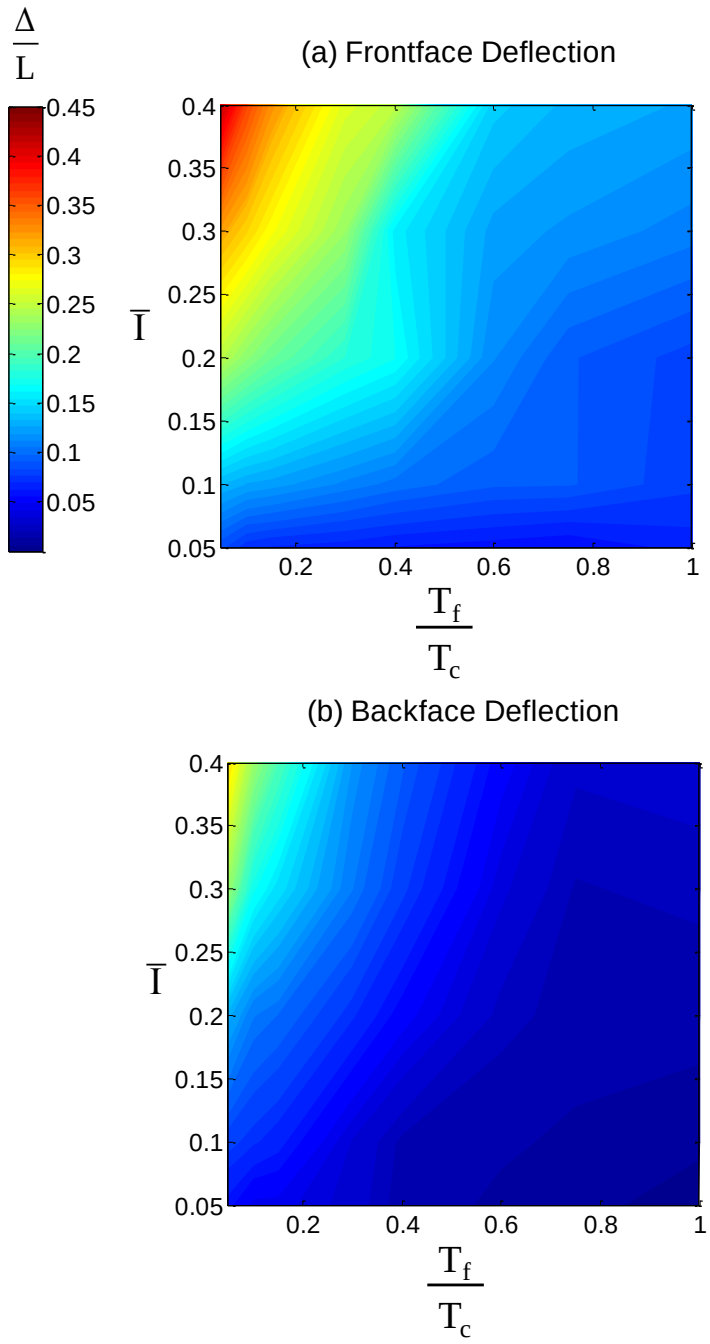

Figure 7.9 Normalized displacement as a function of T_f/T_c for (a) front-face and (b) back-face.

7.6 Energy Absorption

Energy dissipation in glass-fiber reinforced composites is in the form of matrix cracking, fiber breakage and delamination. In the current analysis, only matrix and fiber damages are considered. Energy absorption in the core is in the form of permanent core compression which accounts for the largest portion of overall energy dissipated. For the load conditions analyzed, the primary mode of core deformation is compression with very small amounts of stretching at the supports. Therefore, taking full advantage of core compression is important.

Figure 7.10 shows the total energy dissipated in the structure (U) as a function of T_f/T_c. For thin facesheets ($\mathrm{T_f/T_c} < 0.15$), the core compression is highly localized to the load area, leaving large portions of the core relatively intact or underused. For $0.15 < \mathrm{T_f/T_c} < 0.45$, the facesheets are rigid enough to distribute core compression over a larger area, whereby achieving maximum energy dissipation. For $\mathrm{T_f/T_c} > 0.6$, no further improvement in energy dissipation can be gained at all impulse magnitudes, since the core is already fully utilized. An interesting aspect of this plot is that U reaches a maximum at a certain value of T_f/T_c, indicating that there is an optimum thickness ratio (approximately $\mathrm{T_f/T_c} = 0.2 - 0.3$) for maximizing energy dissipation. This maximum becomes more obvious at higher load intensities.

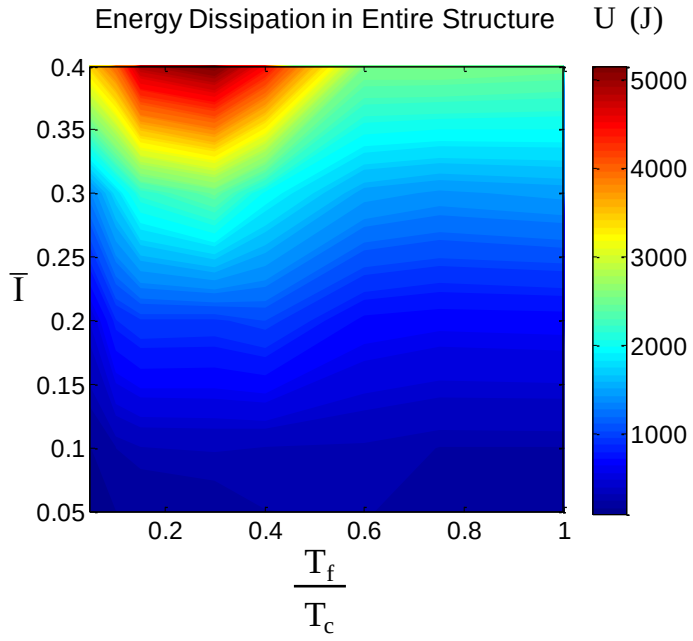

Figure 7.10 Energy dissipated in the entire structure as a function of T_f/T_c.

Figure 7.11 shows the energy dissipated per unit areal mass (U/M) as a function of T_f/T_c for different load intensities. As the T_f/T_c increases, U/M decreases significantly and eventually levels off at around $T_f/T_c = 0.6$. Clearly, the facesheets increase the weight of the structure and provides only limited capability for energy dissipation. This is not surprising as the primary function of the facesheets is to increase stiffness and strength of the structure.

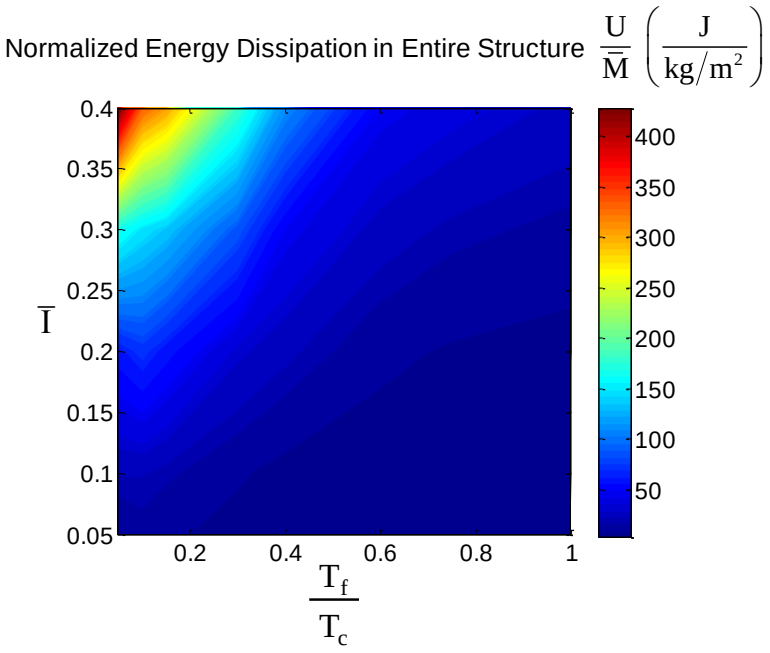

Figure 7.11 Energy dissipated per unit areal mass as a function of T_f/T_c.

7.7 Performance of Sandwich Core

By keeping the dimensions and material properties of the core the same for all cases, we can assess the performance of the core at different facesheet thicknesses. Figure 7.12 shows the energy dissipated per unit areal mass (U/M) in the core as a function of T_f/T_c at different impulse magnitudes. The results are in general agreement with those in Figure 7.10; the core is responsible for a significant amount of the energy dissipated in the structures.

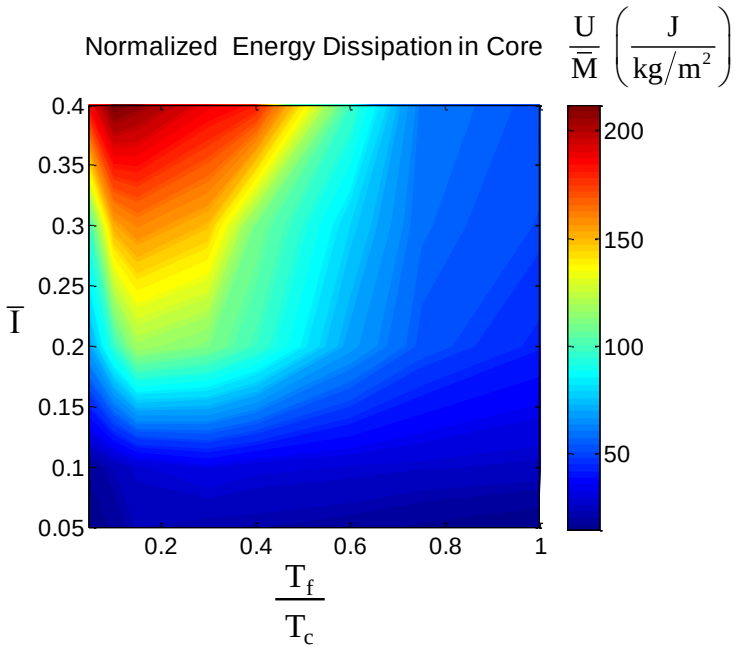

Figure 7.12 Energy dissipated per unit areal mass as a function of T_f/T_c for the Divinycell H100 foam core. Note that areal mass of core is the same in all calculations.

7.8 Desirable Structural Configurations

The desired attributes for a sandwich structure is high energy dissipation capacity and high stiffness (small deflections). For energy dissipation, we consider the energy dissipated per areal mass. For stiffness, we consider maximum deflection of the structure. Figure 7.9 and Figure 7.11 show that there is practically no performance benefit for structures with $T_f/T_c > 0.6$. Figure 7.11 and Figure 7.12 show that the highest energy dissipation capacity occurs for $0.15 < T_f/T_c < 0.4$. Figure 7.9 shows increases in facesheet thickness are most effective for $0.05 < T_f/T_c < 0.3$. Accounting for both

factors, the most desirable range for facesheet thickness is T_f/T_c between 0.15 and 0.4 for a given core configuration.

7.9 Concluding remarks

The responses to underwater impulsive loads of composite sandwich plates consisting of glass-fiber reinforced epoxy facesheets and PVC foam core with different facesheet-thickness-to-core-thickness ratios are analyzed. The configuration studied is that used in experiments being carried out in the Underwater Shocking Loading Simulator recently developed at Georgia Tech. For comparison purposes, all material properties and core dimensions are kept constant.

A fully dynamic 3D finite element model is developed for the experimental configuration, accounting for impulsive loading generation and the dynamic response processes of the structure and water. Deformation and failure mechanisms considered are core crushing, facesheet damage, and core-facesheet separation and contact. Calculations show the distinct response regimes of the structures, as measured by energy dissipated and the maximum deflection.

It is found that under the loading conditions and material systems analyzed, there is a range of facesheet thickness in which planar sandwich structures offer the best performance. Specifically, structures with facesheet-thickness-to-core-thickness ratios between $0.15-0.4$ provide the most efficient use of material in terms of both energy dissipation capacity and rigidity. The insight gained here provides guidelines for the

design of structures for which response to water-based impulsive loading is an important consideration.

It is important to note that the analysis reported here concerns only one structural configuration, one combination of core and facesheet materials, and one core size. More extensive analyses and experimental verification are needed to determine the applicability of the findings to sandwich structures of different geometries, sizes and materials.

8. CONCLUSIONS AND RECOMMENDATIONS FOR FUTURE WORK

8.1 Background and objectives

Recent investigations in this area have shown that sandwich-structures consistently outperform monolithic structures of identical mass. While metallic sandwich structures have been studied exhaustively, there is a significant dearth of knowledge pertaining to composite sandwich structures. This work is aimed at providing insights into the dynamic behavior of sandwich composites subjected to underwater impulsive loads. This thesis focuses on the dynamic deformation, damage and failure in sandwich composites comprising of fiber-reinforced composite facesheets and polymeric foam cores. Experiments and finite-element simulations are used to evaluate the blast resistance of these structures.

The objectives of the research work presented here are:

1. develop an experimental technique to accurately characterize the dynamic response of composite and metallic structures to underwater blasts;
2. develop high-speed digital diagnostics for in-situ characterization of deformation mechanisms in heterogeneous materials;
3. develop a numerical framework for modeling the dynamic deformation and failure of composite laminates that accounts for damage in the form of matrix-

cracking and rupture in composite materials and cracking and fragmentation in polymeric foam cores;

4. characterize time and space-resolved evolution response and failure of composite structures under impulsive underwater loading;
5. develop scaling laws and structure-performance relations for material and structural design; and
6. evaluate the blast-resistance of fiber-reinforced composite/PVC foam sandwich structures to develop material-structure-property relations and enhance blast-mitigation of naval structures.

8.2 Experimental technique and diagnostics

An underwater impulsive loading facility, the Underwater Shock Loading Simulator (USLS) has been designed and fabricated. The facility makes use of a gas-gun based projectile-impact mechanism to generate controlled, planar underwater impulsive loads which impinge on the target structure. Impulsive loads with peak pressures exceeding 500 MPa and wave-velocities exceeding the speed of sound in water $MPa \cdot s$ can be achieved using this technique. The USLS enables the generation of controlled, planar, uniform and repeatable underwater impulsive loads. A modular support system allows in-situ high-speed digital imaging of the dynamic deformations in marine structures.

An Imacon 200D high-speed camera is used to take photographs of the deformation occurring in composite structures. A frame rate of ~20000 FPS is used to

make measurements. Dynamic pressure-transducers are used to measure the impulse intensity. The facility can be modified to test oblique and curved structures.

8.3 Numerical framework

Experiments are supported by finite element simulations, accounting for FSI effects, damage in the form of core-cracking and fragmentation, matrix-cracking and core-face debonding. The dynamic response of panels is investigated using this computational model and shows that the experiments and simulations are in good agreement. The model is then extended to different loading configurations that include a water-backed/submerged condition i.e. a loading condition in which the marine structure has water on the impulse-side as well as the back-side.

8.4 Conclusions and implications for structural design

This analysis focused on the following aspects of marine structures:

1. Variations in materials properties: HP60, HP100 and HP200 and fiber-reinforced composites.
2. Variations in structures: monolithic and composite sandwich structures.
3. Variations in structural attributes: core-thicknesses and face-thicknesses.
4. Variations in loading intensities: from low-intensity impulses to high-intensity impulses.
5. Variations in environmental conditions: air-backed and water-backed structures.

The experiments and simulations reveal underlying trends in the dynamic response impulsively loaded composite structures. These trends can be used to design lighter and more efficient blast resistant structures.

For high loading intensities, light facesheets and low-density cores that are as thick as dimensional constraints allow, provide the highest blast mitigation. It is clear that high-density cores experience large scale fragmentation and rupture and are not significantly superior to monolithic structures. For low loading intensities, monolithic structures or sandwich structures with high-density cores can be used to save space and provide efficient blast resistance because they are significantly thinner than sandwich structures with low-density cores (on a per-weight basis). Provided that the dimensional constraints are satisfied, on a per-mass basis, a combination of thick, low-density cores and thin stiff faces provide better blast-mitigation in marine structures subjected underwater impulsive loads.

In the case of water-backed structures, sandwich structures with thick, low-density cores are suited for applications in which protection of the sub-structure is paramount because they *absorb* a large fraction of the incident impulse. Conversely, monolithic or sandwich structures with high-density cores are suited for applications in which there is no sub-structure because they *transmit* a large fraction of the incident impulse.

It is found that under the loading conditions and material systems analyzed, there is a range of facesheet thickness in which planar sandwich structures offer the best

performance. Specifically, structures with facesheet-thickness-to-core-thickness ratios between $0.15-0.4$ provide the most efficient use of material in terms of both energy dissipation capacity and rigidity. The insight gained here provides guidelines for the design of structures for which response to water-based impulsive loading is an important consideration.

It is important to note that the analysis reported here concerns only one structural configuration, one combination of core and facesheet materials, and one core size. More extensive analyses and experimental verification are needed to determine the applicability of the findings to sandwich structures of different geometries, sizes and materials.

8.5 Recommendations for future work

8.5.1 Laser diagnostics

While high-speed digital imaging of sandwich beams is a useful technique to track the deformations and deflections, Digital Image Correlation (DIC) can give a much more accurate quantification of dynamic response. An important goal in the future is to add this capability to the USLS.

DIC is a non-contact technique which can be used to measure in-plane and out-of-plane deformations and surface velocities. DIC enables the determination of the location and amplitude of maximum strain which can be used to quantify blast resistance. Strains are calculated using the gradients of deformation on the curved surface and the resolution is ~ 5 μm. In this research, the source of illumination is a 5 watt laser of wavelength 532 nm and the photographs are recorded by an Imacon 200D high-speed camera.

8.5.2 Exploiting the FSI effect

Recent assessments of the underwater blast response of marine structures by Hutchinson [105] and Kambouchev et al. [107-109] have shown that the FSI effect plays a major role in the dynamic behavior of materials as well as structures. By showing that marine structures subjected to impulsive loads have higher blast resistance than those subjected to transient, instantaneous loads; they propose that the FSI effect can be exploited to improve blast mitigation. Assessments of blast resistance (not reported here) carried out by this author also show that in sandwich structures, light front-faces and low dynamic-strength cores are beneficial in improving blast mitigation. These studies have focused on metallic sandwich structures and there have been no reported studies carried out on composite structures.

It seems possible that identical modifications in composite structures have the capability of improving blast mitigation. Additionally, composite materials can be designed to maximize the FSI effect. However, owing to the complex and competing deformation mechanisms in composite materials, there is a need to accurately quantify the effect of varying structural properties on dynamic response.

8.5.3 Novel materials and structures

Studies on the dynamic response of marine structures have focused on conventional materials like steel, aluminum, E-glass/epoxy and carbon-fiber/epoxy. However, novel ceramics, alloys and composite materials have great potential in applications that require blast mitigation. A demand for well-engineered structures has

led to improvements in ductility, fracture toughness, corrosion resistance and machinability of constituent materials. Microstructures of geomaterials like concrete and soil have been modified to improve their resistance to impacts and temperature changes. Polymers, glasses and foams have found use in structures to impede fragments and projectiles. Steel, aluminum and titanium alloys have been developed and are highly useful in protecting structures due to their inherent fracture toughness, strength and energy absorption capacities.

There is a need to develop new structures consisting of these novel materials to enhance the blast mitigation capabilities of marine structures.

8.5.4 Dynamic response of hybrid metal-composite structures

A large number of existing naval and marine structures consist of steel or aluminum. With improved understanding of dynamic deformations in marine structures subjected to underwater blasts, new strategies can be employed to retrofit existing infrastructure to improve blast resistance. Thin, stiff composite structures and foams affixed to the impulse receiving side of a pre-existing marine structure has the potential to drastically improve the blast resistance of metallic structures. This strategy can be used to prevent the superposition of pressures at the metal-water interface and reflect the incoming wave before it reaches the underlying metallic structure. This approach to improving the blast resistance of pre-existing infrastructure merits research.

8.5.5 Effect of naval mines

Results presented here and in literature show that light structures subjected to impulsive loads attain lower momentum than heavier structures and consequently cause lesser damage to the substructure. However, marine structures are often exposed to combined impulsive and projectile loads. An example of this is underwater naval mines, which release projectiles in addition to a shock wave. In this situation, the marine structure is subjected to an impulsive load caused by the shock wave as well as impact loads caused due to projectile impact. Naturally, a marine structure designed exclusively to sustain impulsive loads cannot withstand impact loads.

It is therefore necessary to analyze the combined effect of impulsive and impact loads on sandwich structures. This will lead to significant improvement in resistance of marine structures to a range of service loads.

8.5.6 Dynamic response of obliquely loaded and curved structures

The loading angle of an impulsive wave on a marine structure is an engineering problem that has not been studied previously. When oblique impulses interact with a marine structure, deformation is dominated by shear effects. The same structure responds differently when subjected to oblique loads as opposed to normal loads.

Ship hulls, turbine blades and underwater pipelines are all curved structures which experience complex dynamic deformations due to oblique impulsive loads. The analysis of dynamic response of marine structures subjected to oblique underwater impulsive loads merits research.

REFERENCES

1. Cole, R.H., *Underwater Explosions.* Princeton University Press, Princeton, NJ, 1948.

2. Swisdak, M.M., *Explosion Effects and Properties: Part II--Explosion Effects in Water.* NSWC/WOL TR 76-116 1978.

3. Taylor, G.I., *The pressure and impulse of submarine explosion waves on plates.* . The scientific papers of G I Taylor, vol. III, pp. 287–303. Cambridge: Cambridge University Press, 1941

4. Taylor, G.I., *The Scientific Papers of G I Taylor.* Cambridge University Press, Cambridge, 1963.

5. Hutchinson, J.W. and Z.Y. Xue, *Metal sandwich plates optimized for pressure impulses.* International Journal of Mechanical Sciences, 2005. **47**(4-5): p. 545-569.

6. *USS Tripoli, http://www.navsource.org/archives/10/11/1110.htm, Retrieved 04/15/2012.*

7. *USS Cole, http://www.navsource.org/archives/05/01067.htm, Retrieved 04/15/2012.*

8. *USS Princeton, http://upload.wikimedia.org/wikipedia/commons/8/8d/ USS_Princeton_(CG-59)_hull_crack.jpg, Retrieved 04/15/2012.*

9. Taylor, G.I., *The distortion under pressure of a diaphragm which is clamped along its edge and stressed beyond its elastic limit.* Underwater Explosion Research, Vol. 3, The Damage ProcessOffice of Naval Research (1950), pp. 107–121 originally written 1942, 1942.

10. Travis, F.W. and W. Johnson, *Experiments in the dynamic deformation of clamped circular sheets of various metals subject to an underwater explosive charge.* Sheet Metal Indust., 39 (1961), pp. 456–474, 1961.

11. Johnson, W., et al., *Experiments in the underwater explosive stretch forming of clamped circular blanks.* Int. J. Mech. Sci., 8 (1966), pp. 237–270, 1966.

12. Williams, T., *Some metallurgical aspects of metal forming.* Sheet Metal Indust., 39 (1962), pp. 487–494, 1962.

13. Finnie, T.M., *Explosive forming of circular diaphragms.* Sheet Metal Indust., 39 (1962), pp. 391–398, 1962.

14. Bednarski, T., *The dynamic deformation of a circular membrane.* Int. J. Mech. Sci., 11 (1969), pp. 949–959, 1969.

15. Symonds, P.S. and N. Jones, *Impulsive loading of fully clamped beams with finite plastic deflections and strain-rate sensitivity.* Int. J. Mech. Sci., 14 (1972), pp. 49–69 1972.

16. Bodner, S.R. and P.S. Symonds, *Experiments on dynamic plastic loading of frames.* Int. J. Solids Struct., 15 (1979), pp. 1–13, 1979.

17. Bodner, S.R. and P.S. Symonds, *Experiments on viscoplastic response of circular plates to impulsive loading.* J. Mech. Phys. Solids, 27 (1979), pp. 91–113, 1979.

18. Richardson, R.M. and J.G. Kirkwood, *Theory of the plastic deformation of thin plates by underwater explosions.* Underwater Explosion Research, Vol. 3, The Damage ProcessOffice of Naval Research, pp. 305–421, 1950.

19. Hudson, G.E., *A theory of the dynamic plastic deformation of a thin diaphragm.* J. appl. Phys., 22 (1951), pp. 1-11, 1951.

20. Frederick, D., *A simplified analysis of circular membranes subjected to an impulsive loading producing large plastic deformations.* Proc. 4th Annual Conf. Solid Mechanics, University of Texas (1959), pp. 18–35, 1959.

21. Griffith, J. and H. Vanzant, *Large deformation of circular membranes under static and dynamic loading.* 1st Int. Cong. Exp. Mech. Paper No. 702 (1961), 1961.

22. Hopkins, H.G. and W. Prager, *On the dynamics of plastic circular plates.* ZAMP (J. appl. Math. and Phys.), 5 (1954), pp. 317–330, 1954.

23. Wang, A.J. and H.G. Hopkins, *The plastic deformation of built-in circular plates under impulsive load.* J. Mech. Phys. Solids, 3 (1954), pp. 22–37, 1954.

24. Florence, A.L., *Circular plates under a uniformly distributed impulse.* Int. J. Solids Struct., 2 (1966), pp. 37–47, 1966.

25. Hopkins, H.G., *On the plasticy theory of plates.* Proc. Soc. Lond., A241 (1957), pp. 153–179, 1957.

26. Shapiro, G.S., *On a rigid-plastic annular plate under impulsive loading.* J. appl. Math. Mech. (Pnk. Mat. i Mek), 23 (1959), pp. 234–241, 1959.

27. Jones, N., *Recent progress in the dynamic plastic behaviour of structures. Part I, II and III.* Shock Vib. Dig., 1978, 1978 and 1981.

28. Nurick, G.N. and J.B. Martin, *Deformation of Thin Plates Subjected to Impulsive Loading - a Review .1. Theoretical Considerations.* International Journal of Impact Engineering, 1989. **8**(2): p. 159-170.

29. Nurick, G.N. and J.B. Martin, *Deformation of Thin Plates - Subjected to Impulsive Loading - a Review .2. Experimental Studies.* International Journal of Impact Engineering, 1989. **8**(2): p. 171-186.

30. Zenkert, D., *An introduction to sandwich construction.* Engineering Materials Advisory Service, 1995.

31. Plantema, F., *Sandwich construction.* New York: Wiley, 1996.

32. Allen, H., *Analysis and design of structural sandwich panels.* Oxford: Pergamon Press, 1969.

33. Fleck, N.A. and V.S. Deshpande, *The resistance of clamped sandwich beams to shock loading.* Journal of Applied Mechanics-Transactions of the Asme, 2004. **71**(3): p. 386-401.

34. Cote, F., et al., *The out-of-plane compressive behavior of metallic honeycombs.* Materials Science and Engineering a-Structural Materials Properties Microstructure and Processing, 2004. **380**(1-2): p. 272-280.

35. Qiu, X., V.S. Deshpande, and N.A. Fleck, *Dynamic response of a clamped circular sandwich plate subject to shock loading.* Journal of Applied Mechanics-Transactions of the Asme, 2004. **71**(5): p. 637-645.

36. Deshpande, V.S. and N.A. Fleck, *One-dimensional response of sandwich plates to underwater shock loading.* Journal of the Mechanics and Physics of Solids, 2005. **53**(11): p. 2347-2383.

37. Kazemahvazi, S., et al., *Dynamic failure of clamped circular plates subjected to an underwater shock.* Journal of Mechanics of Materials and Structures, 2007. **2**(10): p. 2007-2023.

38. McMeeking, R.M., et al., *An analytic model for the response to water blast of unsupported metallic sandwich panels.* International Journal of Solids and Structures, 2008. **45**(2): p. 478-496.

39. McShane, G.J., V.S. Deshpande, and N.A. Fleck, *Dynamic Compressive response of stainless-steel square honeycombs.* Journal of Applied Mechanics-Transactions of the Asme, 2007. **74**(4): p. 658-667.

40. Wei, Z., F.W. Zok, and A.G. Evans, *Design of sandwich panels with prismatic cores.* Journal of Engineering Materials and Technology-Transactions of the Asme, 2006. **128**(2): p. 186-192.

41. Wei, Z., M.Y. He, and A.G. Evans, *Application of a dynamic constitutive law to multilayer metallic sandwich panels subject to impulsive loads.* Journal of Applied Mechanics-Transactions of the Asme, 2007. **74**(4): p. 636-644.

42. Wei, Z., et al., *Analysis and interpretation of a test for characterizing the response of sandwich panels to water blast.* International Journal of Impact Engineering, 2007. **34**(10): p. 1602-1618.

43. Wei, Z., et al., *The resistance of metallic plates to localized impulse.* Journal of the Mechanics and Physics of Solids, 2008. **56**(5): p. 2074-2091.

44. Xue, Z.Y. and J.W. Hutchinson, *A comparative study of impulse-resistant metal sandwich plates.* International Journal of Impact Engineering, 2004. **30**(10): p. 1283-1305.

45. Valdevit, L., J.W. Hutchinson, and A.G. Evans, *Structurally optimized sandwich panels with prismatic cores.* International Journal of Solids and Structures, 2004. **41**(18-19): p. 5105-5124.

46. Wicks, N. and J.W. Hutchinson, *Performance of sandwich plates with truss cores.* Mechanics of Materials, 2004. **36**(8): p. 739-751.

47. Xue, Z.Y. and J.W. Hutchinson, *Preliminary assessment of sandwich plates subject to blast loads.* International Journal of Mechanical Sciences, 2003. **45**(4): p. 687-705.

48. Vaziri, A., Z.Y. Xue, and J.W. Hutchinson, *Performance and failure of metal sandwich plates subjected to shock loading.* Journal of Mechanics of Materials and Structures, 2007. **2**(10): p. 1947-1963.

49. Vaziri, A. and J.W. Hutchinson, *Metal sandwich plates subject to intense air shocks.* International Journal of Solids and Structures, 2007. **44**(6): p. 2021-2035.

50. Spuskanyuk, A.V. and R.M. McMeeking, *Sandwich panels for blast protection in water: simulations.* International Journal of Materials Research, 2007. **98**(12): p. 1250-1255.

51. Deshpande, V.S. and N.A. Fleck, *Isotropic constitutive models for metallic foams.* Journal of the Mechanics and Physics of Solids, 2000. **48**(6-7): p. 1253-1283.

52. Xue, Z.Y. and J.W. Hutchinson, *Constitutive model for quasi-static deformation of metallic sandwich cores.* International Journal for Numerical Methods in Engineering, 2004. **61**(13): p. 2205-2238.

53. Dharmasena, K.P., et al., *Mechanical response of metallic honeycomb sandwich panel structures to high-intensity dynamic loading.* International Journal of Impact Engineering, 2008. **35**(9): p. 1063-1074.

54. Wadley, H.N.G., et al., *Dynamic compression of square honeycomb structures during underwater impulsive loading.* Journal of Mechanics of Materials and Structures, 2007. **2**(10): p. 2025-2048.

55. Liang, Y.M., et al., *The response of metallic sandwich panels to water blast.* Journal of Applied Mechanics-Transactions of the Asme, 2007. **74**(1): p. 81-99.

56. Deshpande, V.S. and N.A. Fleck, *Collapse of truss core sandwich beams in 3-point bending.* International Journal of Solids and Structures, 2001. **38**(36-37): p. 6275-6305.

57. Lee, S., et al., *Dynamic failure of metallic pyramidal truss core materials - Experiments and modeling.* International Journal of Plasticity, 2006. **22**(11): p. 2118-2145.

58. Mori, L.F., et al., *Deformation and fracture modes of sandwich structures subjected to underwater impulsive loads.* Journal of Mechanics of Materials and Structures, 2007. **2**(10): p. 1981-2006.

59. Queheillalt, D.T. and H.N.G. Wadley, *Pyramidal lattice truss structures with hollow trusses.* Materials Science and Engineering a-Structural Materials Properties Microstructure and Processing, 2005. **397**(1-2): p. 132-137.

60. Rathbun, H.J., et al., *Structural performance of metallic sandwich beams with hollow truss cores.* Acta Materialia, 2006. **54**(20): p. 5509-5518.

61. Wicks, N. and J.W. Hutchinson, *Optimal truss plates.* International Journal of Solids and Structures, 2001. **38**(30-31): p. 5165-5183.

62. Yungwirth, C.J., et al., *Impact response of sandwich plates with a pyramidal lattice core.* International Journal of Impact Engineering, 2008. **35**(8): p. 920-936.

63. Symons, D.D., R.G. Hutchinson, and N.A. Fleck, *Actuation of the Kagome Double-Layer Grid. Part 1: Prediction of performance of the perfect structure.* Journal of the Mechanics and Physics of Solids, 2005. **53**(8): p. 1855-1874.

64. Wang, J., et al., *On the performance of truss panels with Kagome cores.* International Journal of Solids and Structures, 2003. **40**(25): p. 6981-6988.

65. Wicks, N. and J.W. Hutchinson, *Sandwich plates actuated by a Kagome planar truss.* Journal of Applied Mechanics-Transactions of the Asme, 2004. **71**(5): p. 652-662.

66. Mouritz, A.P., *The effect of underwater explosion shock loading on the flexural properties of GRP laminates.* International Journal of Impact Engineering, 1996. **18**(2): p. 129-139.

67. Mouritz, A.P., D.S. Saunders, and S. Buckley, *The Damage and Failure of Grp Laminates by Underwater Explosion Shock Loading.* Composites, 1994. **25**(6): p. 431-437.

68. Steeves, C.A. and N.A. Fleck, *Collapse mechanisms of sandwich beams with composite faces and a foam core, loaded in three-point bending. Part II: experimental investigation and numerical modelling.* International Journal of Mechanical Sciences, 2004. **46**(4): p. 585-608.

69. Tagarielli, V.L., V.S. Deshpande, and N.A. Fleck, *The dynamic response of composite sandwich beams to transverse impact.* International Journal of Solids and Structures, 2007. **44**(7-8): p. 2442-2457.

70. Kleun, B.J.K. and A.W. Van der Wart, *Misspecification in infinite-dimensional Bayesian statistics.* Annals of Statistics, 2006. **34**(2): p. 837-877.

71. Raftenberg, M.N. and M.J. Scheidler, *Gap Formations in Simulations of Shpb Tests on Elastic Materials Soft in Shear.* Shock Compression of Condensed Matter - 2009, Pts 1 and 2, 2009. **1195**: p. 715-718.

72. Raftenberg, M.N., *A shear banding model for penetration calculations.* International Journal of Impact Engineering, 2001. **25**(2): p. 123-146.

73. DIAB Inc., S.D., DeSoto, Texas 75115, USA http://www.diabgroup.com/europe/literature/e_pdf_files/man_pdf/H_man.pdf Accessed 5 May 2011.

74. Mines, R.A.W., C.M. Worrall, and A.G. Gibson, *The Static and Impact Behavior of Polymer Composite Sandwich Beams.* Composites, 1994. **25**(2): p. 95-110.

75. J. L. Abot, I.M.D., *Composite sandwich beams under low velocity impact.* Proc. of AIAA Conf. , Seattle, 2001.

76. Tagarielli, V.L., V.S. Deshpande, and N.A. Fleck, *The high strain rate response of PVC foams and end-grain balsa wood.* Composites Part B-Engineering, 2008. **39**(1): p. 83-91.

77. Qiao, P.Z., M.J. Yang, and F. Bobaru, *Impact mechanics and high-energy absorbing materials: Review.* Journal of Aerospace Engineering, 2008. **21**(4): p. 235-248.

78. Lee, S., et al., *Deformation rate effects on failure modes of open-cell Al foams and textile cellular materials.* International Journal of Solids and Structures, 2006. **43**(1): p. 53-73.

79. Tekalur, S.A., A.E. Bogdanovich, and A. Shukla, *Shock loading response of sandwich panels with 3-D woven E-glass composite skins and stitched foam core.* Composites Science and Technology, 2009. **69**(6): p. 736-753.

80. Tekalur, S.A., A. Shukla, and K. Shivakumar, *Blast resistance of polyurea based layered composite materials.* Composite Structures, 2008. **84**(3): p. 271-281.

81. LeBlanc, J., et al., *Shock loading of three-dimensional woven composite materials.* Composite Structures, 2007. **79**(3): p. 344-355.

82. Grogan, J., et al., *Ballistic resistance of 2D and 3D woven sandwich composites.* Journal of Sandwich Structures & Materials, 2007. **9**(3): p. 283-302.

83. Wang, E.H., N. Gardner, and A. Shukla, *The blast resistance of sandwich composites with stepwise graded cores.* International Journal of Solids and Structures, 2009. **46**(18-19): p. 3492-3502.

84. LeBlanc, J. and A. Shukla, *Dynamic response and damage evolution in composite materials subjected to underwater explosive loading: An experimental and computational study.* Composite Structures, 2010. **92**(10): p. 2421-2430.

85. Latourte, F., et al., *Failure mechanisms in composite panels subjected to underwater impulsive loads.* Journal of the Mechanics and Physics of Solids, 2011. **59**(8): p. 1623-1646.

86. Rathbun, H.J., et al., *Performance of metallic honeycomb-core sandwich beams under shock loading.* International Journal of Solids and Structures, 2006. **43**(6): p. 1746-1763.

87. Zok, F.W., et al., *Structural performance of metallic sandwich panels with square honeycomb cores.* Philosophical Magazine, 2005. **85**(26-27): p. 3207-3234.

88. Qiu, X., V.S. Deshpande, and N.A. Fleck, *Impulsive loading of clamped monolithic and sandwich beams over a central patch.* Journal of the Mechanics and Physics of Solids, 2005. **53**(5): p. 1015-1046.

89. Radford, D.D., V.S. Deshpande, and N.A. Fleck, *The use of metal foam projectiles to simulate shock loading on a structure.* International Journal of Impact Engineering, 2005. **31**(9): p. 1152-1171.

90. Espinosa, H.D., S. Lee, and N. Moldovan, *A novel fluid structure interaction experiment to investigate deformation of structural elements subjected to impulsive loading.* Experimental Mechanics, 2006. **46**(6): p. 805-824.

91. Mori, L.F., et al., *Deformation and Failure Modes of I-Core Sandwich Structures Subjected to Underwater Impulsive Loads.* Experimental Mechanics, 2009. **49**(2): p. 257-275.

92. Horacio D. Espinosa , D.G., Félix Latourte and Ravi S. Bellur-Ramaswamy *Failure Modes in Solid and Sandwich Composite Panels Subjected to Underwater Impulsive Loads.* 9th International Conference on Sandwich Structures, ICSS9, 2010.

93. Wadley, H., et al., *Compressive response of multilayered pyramidal lattices during underwater shock loading.* International Journal of Impact Engineering, 2008. **35**(9): p. 1102-1114.

94. *VARTM, http://www.compositesworld.com/articles/ddg-1000-zumwalt-stealth-warship, Retrieved 04/15/2012.*

95. Minnaar, K. and M. Zhou, *A novel technique for time-resolved detection and tracking of interfacial and matrix fracture in layered materials.* Journal of the Mechanics and Physics of Solids, 2004. **52**(12): p. 2771-2799.

96. Hashin, Z., *Failure Criteria for Unidirectional Fiber Composites.* Journal of Applied Mechanics-Transactions of the Asme, 1980. **47**(2): p. 329-334.

97. Puck, A. and H. Schürmann, *Failure analysis of FRP laminates by means of physically based phenomenological models.* Composites Science and Technology, Volume 62, Issues 12–13, September–October 2002, Pages 1633–1662, 1999.

98. Schubel, P.M., J.J. Luo, and I.M. Daniel, *Low velocity impact behavior of composite sandwich panels.* Composites Part a-Applied Science and Manufacturing, 2005. **36**(10): p. 1389-1396.

99. Kiel, A.H., *The Response of Ships to Underwater Explosions.* Department of the Navy, 1961.

100. Deshpande, V.S. and N.A. Fleck, *High strain rate compressive behaviour of aluminium alloy foams.* International Journal of Impact Engineering, 2000. **24**(3): p. 277-298.

101. Hibbit, Karlsson, and Sorensen, *Abaqus/Explicit User's Manual, Version 6.9.* 2009.

102. Hooputra, H., et al., *A comprehensive failure model for crashworthiness simulation of aluminium extrusions.* International Journal of Crashworthiness, 2004. **9**(5): p. 449-463.

103. D'Alembert, J.R., *Recherches sur la courbe que forme une corde tenduë mise en vibration (Researches on the curve that a tense cord forms [when] set into vibration).* Histoire de l'académie royale des sciences et belles lettres de Berlin, vol. 3, pages 214-219, 1747.

104. Graff, K.F., *Wave Motion in Elastic Solids.* Oxford Universiy Press, 1975.

105. Hutchinson, J.W., *Energy and Momentum Transfer in Air Shocks.* Journal of Applied Mechanics-Transactions of the Asme, 2009. **76**(5).

106. Reid, W.D., *The Response of Surface Ships to Underwater Explosions.* DSTO Aeronautical and Maritime Research Laboratory, PO Box 4331, Melbourne, Victoria, Australia 3001, 1993.

107. Kambouchev, N., R. Radovitzky, and L. Noels, *Fluid-structure interaction effects in the dynamic response of free-standing plates to uniform shock loading.* Journal of Applied Mechanics-Transactions of the Asme, 2007. **74**(5): p. 1042-1045.

108. Kambouchev, N., L. Noels, and R. Radovitzky, *Numerical simulation of the fluid-structure interaction between air blast waves and free-standing plates.* Computers & Structures, 2007. **85**(11-14): p. 923-931.

109. Kambouchev, N., L. Noels, and R. Radovitzky, *Nonlinear compressibility effects in fluid-structure interaction and their implications on the air-blast loading of structures.* Journal of Applied Physics, 2006. **100**(6): p. -.